



UNIVERSITY OF SALERNO
DEPARTMENT OF PHARMACY



PhD course in
Scienza e Tecnologie per l'Industria Chimica, Farmaceutica e Alimentare
XI course NS (XXV)
2009-2012

“Molecular dynamics investigations of drug-cell membrane interactions”

Tutor

Prof. Stefano Piotto Piotto

PhD Student

Federica Campana

Coordinators

Prof. Paolo Ciambelli

Prof.ssa Nunziatina De Tommasi

List of publications:

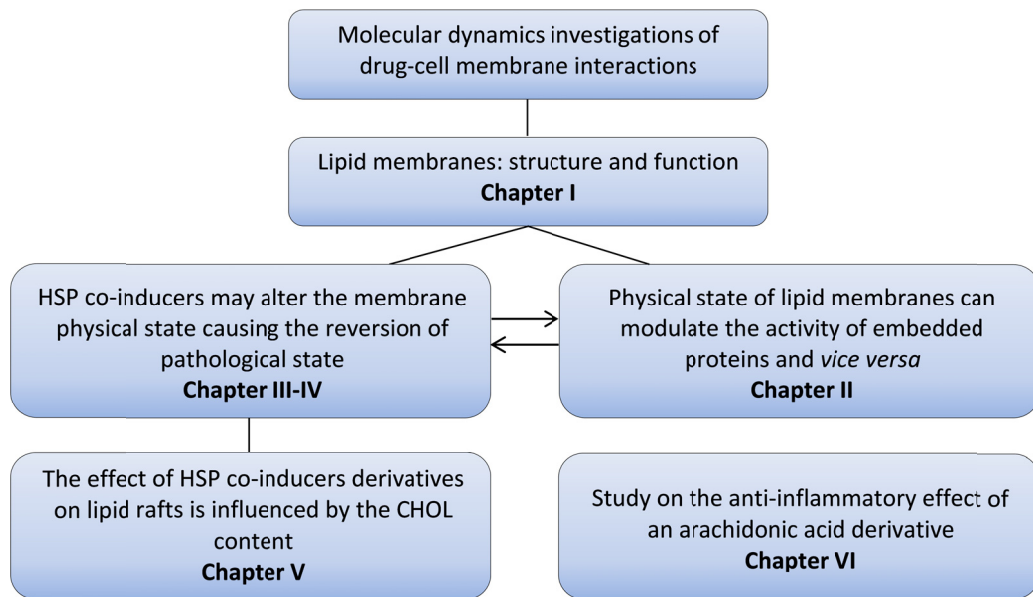
- I. Casas, J., Álvarez, R., Terés, S., Lladó, V., Campana, F., Piotto, S., Escribá P. V. Effect of G protein lipids on membrane structure and G protein-membrane interactions. *BBA Biomembranes*. Submitted.
- II. Gombos, I., Crul, T., Piotto, S., Gungor, B., Torok, Z., Balogh, G., Peter, M., Slotte, J.P., Campana, F., Pilbat, A.M., Hunya, A., Toth, N., Literati-Nagy, Z., Vigh L. Jr., Glatz, A., Brameshuber, M., Schutz, G.J., Hevener, A., Febbraio, M.A., Horvath, I., Vigh L. 2011. Membrane-Lipid Therapy in Operation: The HSP Co-Inducer BGP-15 Activates Stress Signal Transduction Pathways by Remodeling Plasma Membrane Rafts. *PLoS ONE* 6(12): e28818. doi:10.1371/journal.pone.0028818
- III. Crul, T., Toth, N., Piotto, S., Literati-Nagy, P., Tory, K., Haldimann, P., Kalmar, B., Greensmith, L., Torok, Z., Balogh, G., Gombos, I., Campana, F., Concilio, S., Gallyas, F., Nagy, G., Berente, Z. Gungor, B., Peter, M., Glatz, A., Hunya, A., Literati-Nagy, Z., Vigh, L. Jr., Hoogstra-Berends, F., Heeres, A., Kuipers, I., Loen, L., Seerden, J. P., Zhang, D., Meijering, R. A., Henning, R. H., Brundel, B. J., Kampinga, H. H., Koranyi, L., Szilvassy, Z., Mandl, J., Sumegi, B., Febbraio, M. A., Horvath, I., Hooper, P. L., Vigh, L. 2013. Hydroxamic Acid Derivatives: Pleiotropic Hsp Co-Inducers Restoring Homeostasis and Robustness. *Curr Pharm Des* 19(3), pp. 309-346(38).
- IV. Lopez, D. H., Fiol-de Roque, M. A., Noguera-Salva, M. A., Teres, S., Campana, F., Piotto, S., Castro, J. A., Mohaibes, R. J., Escribá P. V., Busquets, X. 2-Hydroxy Arachidonic Acid: A New Non-Steroidal Anti-Inflammatory Drug. *British Journal of Pharmacology*. Submitted.

Contents:

Overview	3
1. The structure of cell membranes	7
1.1 Biological membranes	7
1.2 Phospholipids	9
1.3 Lipid composition of biomembranes.....	12
1.4 Lipid polymorphism	16
2. Proteins modulated by the membrane physical state	21
2.1 G Protein-Coupled Receptors	21
2.2 G proteins	22
2.3 Lipid modification of G proteins	26
2.3.1 Myristoylation and palmitoylation: G α subunit lipid modifications.....	26
2.3.2 Isoprenylation of G γ subunit.....	28
2.4 Interactions of lipid membranes with G proteins	30
2.5 Materials and methods.....	30
2.6 Analysis	33
2.6.1 Binding energy	33
2.6.2 Lateral pressure (stress) profile	33
2.7 Results	37
2.7.1 Binding energies.....	37
2.7.2 Lateral pressure profile.....	39
2.8 Conclusions.....	41
3. The HSP co-inducers remodel plasma membrane rafts.....	45
3.1 Introduction.....	45
3.2 Membranes construction and equilibrations	49
3.3 Results and discussion	50
3.3.1 Density profile.....	50
4. Effect of hydroxylamines in modulating membrane physical state.....	53

4.1	Membranes construction	54
4.2	Results and discussion:	56
4.2.1	Radial distribution function.....	58
4.2.2	Charge distribution.....	61
4.2.3	Density profile	62
4.3	Conclusions	64
5.	Cholesterol removal upregulates specific HSP's	65
5.1	Systems construction.....	65
5.2	Results and discussion	67
5.2.1	Binding energy	67
5.2.2	Atomic energy contribution	70
5.2.3	Radial distribution function.....	72
5.2.4	Dynamical Cross-Correlation Matrix	76
5.2.5	Membrane fluidity	78
5.3	Conclusions	80
6	Hydroxy arachidonic acid, a new potential non steroidal anti-inflammatory drug ..	82
6.1	The COX system	82
6.2	Molecular Docking on COX enzymes	89
6.3	Results and discussion	93
6.3.1	Binding energy	94
6.3.2	The Fukui analysis	96
7	Appendix – Computational methods	100
7.1	Introduction to molecular dynamics	100
7.1.1	Minimization	102
7.2	Production	105
7.3	Principles of flexible docking	107
7.4	Fukui function	108
	Bibliography	113

Overview



This thesis is about lipid membranes. In short, the work is organized with an introductory description of lipid membranes, with a special attention to their physical state (**Chapter 1**). Membranes represent an additional level of signal control, since the particular organization of lipids can significantly modify the conformation, and therefore the function, of membrane proteins.

One of my aims was to understand how the physical state of lipid membranes can modulate the activity of embedded proteins and *vice versa*. To this end, I studied the mechanisms underlying the interaction between lipid moieties of G protein subunits and membranes with different phospholipid composition (**Chapter 2**).

The physical state of membranes can also be modulated by fluidizers. I have taken into account a group of extremely active anticancer drugs belonging to the class of hydroxylamine, which artificially alter the membrane physical state of stressed cells and restore homeostasis (**Chapters 3-4**). In **Chapter 5** I consider the importance of sphingomyelin/cholesterol ratio in tuning the bilayer fluidity.

During the three years of my work I have dealt to several fatty acid molecules. Among others, I have studied the effect of lipid chain polyunsaturation on the membrane fluidity (data not reported). A molecule that proved high *in vivo* anti-inflammatory effect was a derivative of arachidonic acid (AAOH). Since this acid is the natural substrate of cyclooxygenases, in **Chapter 6** I show some results of docking and quantum mechanical calculations of the interaction AAOH–COX-1/2.

During the last two decades, evidence has been gathered showing that the plasma membrane lipid composition and structure play key roles, as a medium for proteins to function and as structural scaffolding for cells.

At the same time, the protein activity is influenced and, in some cases, modulated by the physical state of membranes. The interest of computational biologists has recently focused on the active roles of phospholipids in affecting the behavior of membrane proteins [1, 2], the assembly of protein-lipid arrays [3, 4] and the mediation of protein-protein interactions [3, 4].

Several essential cellular activities depend on proper membrane function. Thus, membrane lipid composition and membrane physical state have received significant attention in the past years [5, 6]. Membranes have fluidity properties that permit the cell to sense changes in temperature, pH, osmotic and atmospheric pressure. Abrupt changes in the environment can cause modifications of membrane structure and, consequently, loss of physiological functions [7].

Moreover, multiple changes in membrane lipid composition occur during pathological conditions (such as cancer [8] or degenerative diseases [9]) or alterations in diet [10] and ageing processes [11, 12]. Each of these changes leads to membrane remodeling and to alterations in the organization and dynamic properties of membrane lipids. As a consequence, the activities of many membrane-associated proteins and transporters also change dramatically [13-15].

Despite the obvious involvement of lipids in human pathologies, therapies and drugs currently used or in development are not usually focused on membranes.

Therefore, it is conceivable that molecules capable of interacting with membrane lipids may induce modifications in membrane composition, protein function or gene expression and reversion of the pathological state. Most current clinical drugs are designed to interact with proteins, so that they are usually referred to as chemotherapy (cure with chemical compounds) agents. Membrane-lipid therapy is a relatively novel approach involving regulation of the membrane lipid structure/composition [16]. The overall strategy of this approach is similar to conventional chemotherapy in that the final effect of the drug is modulation of activity of a protein and subsequent regulation of gene expression to produce changes in the cell's function to reverse the pathological malfunction. Far from being applicable only to rare or infrequent diseases, lipid therapy could potentially be used alone or combined with other therapies in the treatment of some major pathologies.

1. The structure of cell membranes

1.1 Biological membranes

The biological membranes, or biomembranes, carry out the function of “barrier” that not only divide the cell from the environment, but also the internal cell volume into comparably isolated compartments such as nuclei, mitochondria, chloroplasts, endoplasmic reticulum and the Golgi apparatus [17].

Membranes are built of a double layer (often called “bilayer”) of phospholipid molecules practically impermeable for ions and polar molecules. The lipid bilayer includes numerous intrinsic protein molecules and molecular complexes, involved in transport processes across membranes, like pumps and channels for ions and molecules.

The thickness of a membrane is about 5nm, extremely thin compared to the typical dimensions of cells (several 10 μm). Such membranes are flexible and heterogeneous, and their properties depend on temperature, pressure, electrical field, pH, salt concentration, but also the presence of proteins and protein conformation. For this reason, the physical state of a biological membrane depends on all thermodynamic variables.

Our understanding of the structure and properties of biomembranes has increased steadily since 1895 when Ernest Overton first described the cell membrane as a covering structure made up of lipid molecules. Years later, in 1925, Gorter and Grendel concluded that the erythrocyte membranes were formed by two lipid layers [18] and, in 1972, Singer and Nicolson’s fluid mosaic

model represented a qualitative leap in our understanding of the membrane structure and functionality [19]. Nowadays, the lipid membrane is no longer defined as just a passive film that blocks the passage of water and solutes, and in which the 'truly' regulatory elements (proteins) are inserted. The development of novel biophysical techniques has made it possible to attribute new properties to membranes not previously defined in Singer and Nicolson's model [20, 21].

The complex dynamics of the plasma membrane goes far beyond the basic functions, since it also participates in lipid-lipid and lipid-proteins interactions. These interactions modify the lipid bilayer itself, influencing protein activity. In turn, the presence of proteins also affects the structure of membranes.

The protein density seems to be higher than was originally thought, and lipids and proteins are clearly not homogeneously distributed since lipid-lipid, lipid-protein and protein-protein interactions induce the formation of domains of specific lipid and protein compositions.

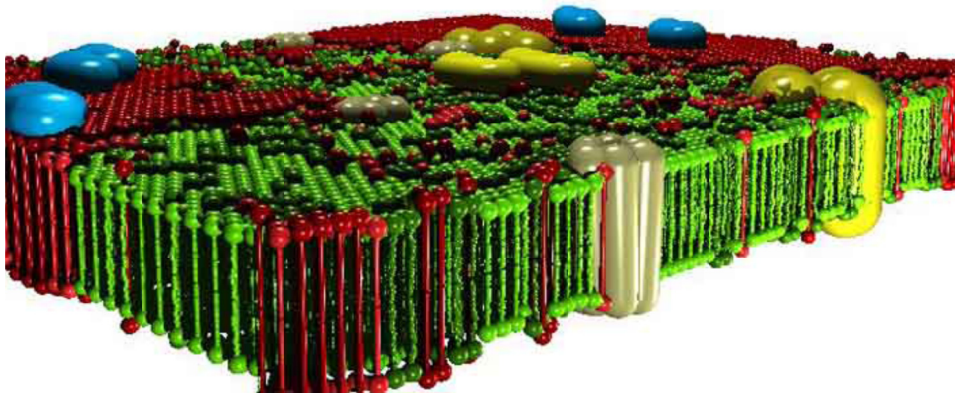


Figure 1: Schematic representation of a biological membrane with various lipids in different physical states and embedded or adsorbed proteins [6].

In addition, interactions between different molecules and cytoskeletal proteins also play an important role in defining membrane microdomains.

Singer-Nicolson's model did not contemplate the existence of transmembrane proteins with a hydrophobic region thicker than that of the phospholipid bilayer. The currently accepted model postulates that proteins are not the elements that adapt to the thickness of the membrane but rather, lipids have certain flexibility to accommodate proteins with different sized hydrophobic transmembrane regions. Thus, the bilayer thickness may vary over the entire surface of the membrane.

1.2 Phospholipids

Phospholipids are an important class of biomolecules which represent the fundamental building blocks of cellular membranes. Their structure consists of two fatty acyl chains, each typically having an even number of carbon atoms between 14 and 20, esterified at the sn-1 and sn-2 positions of glycerol, and contains a polar or charged head group linked by a phosphate residue at the sn-3 position.

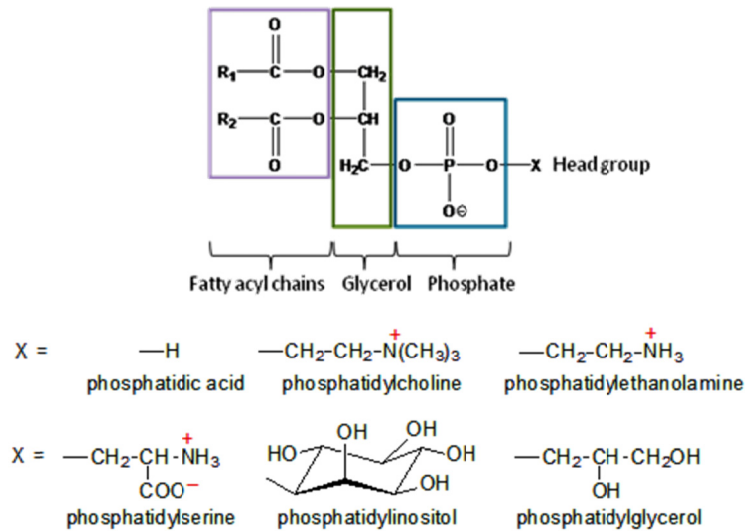


Figure 2: Structure and principal classes of phospholipids.

The head group forms a hydrophilic region and determines the type of phospholipid. The fatty acyl side chains are hydrophobic; this amphipathic property of phospholipids provides the basis for the compartmentalization of cells.

Common phospholipids, widely distributed in nature, are produced by further reaction of the phosphate group in phosphatidate with an alcohol, such as serine, ethanolamine, choline, glycerol or inositol. The resulting lipids may be charged, for example phosphatidylserine (PS), phosphatidylinositol (PI) and phosphatidylglycerol (PG); or dipolar (having separate positively and negatively charged regions), for example phosphatidylcholine (PC) and phosphatidylethanolamine (PE).

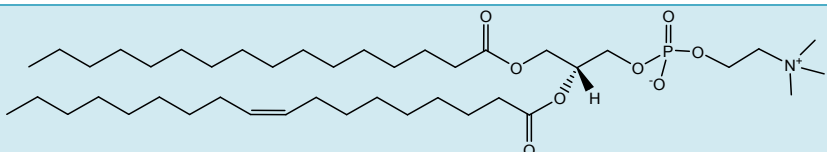
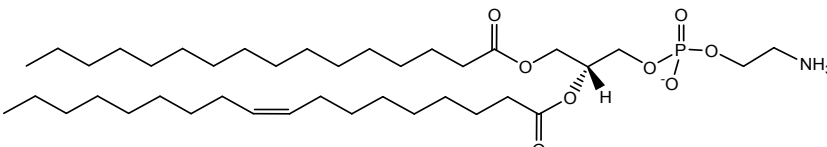
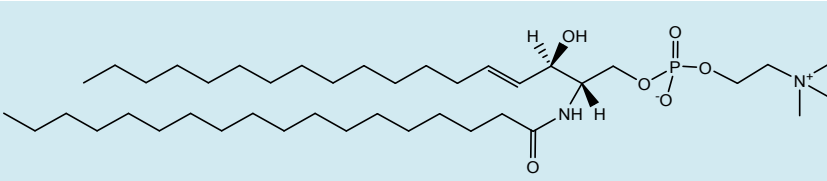
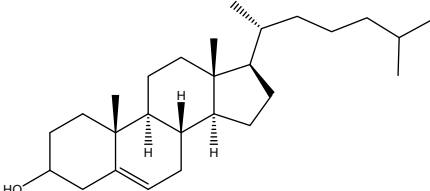
A typical phospholipid arrangement is the presence of a saturated fatty acid, such as palmitic or stearic acid, at the sn-1 position, and an unsaturated or

polyunsaturated fatty acid, such as oleic (18:1) or arachidonic (20:6) acid, at sn-2 position.

Sphingolipids constitute another class of phospholipids. A sphingolipid molecule has the phosphatidyl-based head group structure but, in contrast to a common phospholipid molecule, contains a single fatty acid and a long-chain alcohol as its hydrophobic components. Additionally, the backbone of the sphingolipid is sphingosine, an amino alcohol, rather than glycerol.

The structures of phospholipids used to prepare model membranes in Chapters 2-5 are shown in Table 1:

TABLE 1: PHOSPHOLIPID STRUCTURES OF SIMULATED MEMBRANES

STRUCTURE	NAME
	1-palmitoyl-2-oleoyl-sn-glycero-3-phosphocholine (POPC)
	1-palmitoyl-2-oleoyl-sn-glycero-3-phosphoethanolamine (POPE)
	Brain Sphingomyelin N-(octadecanoyl)-sphing-4-enine-1-phosphocholine (BSM)
	Cholesterol (CHOL)

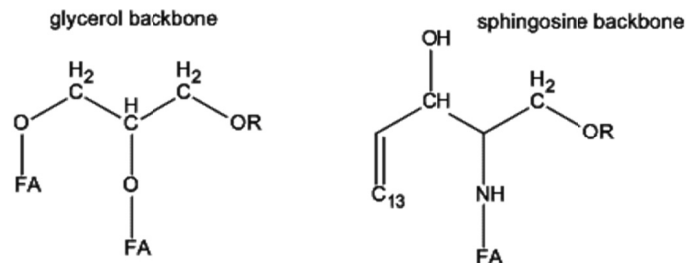


Figure 3: Comparison of glycerol and sphingosine head group structure.

The size, shape, charge and chemical composition of different phospholipid classes play a role in the formation and maintenance of the plasma membrane of cells, as well as membranes surrounding subcellular organelles and vesicles. An asymmetric distribution of phospholipid types within the membrane imparts different functional characteristics between the inner and outer leaflets.

Phospholipids are essential for the absorption, transport and storage of lipids. They are involved in stabilizing proteins within the membrane, facilitating the active conformational structure of proteins and as cofactors in enzymatic reactions.

1.3 Lipid composition of biomembranes

When talking about the composition of biological membranes, one has to distinguish proteins that are encoded in the genome and the lipid composition that is not encoded in the genome. The latter rather adapts to the environmental conditions, partially by the control of membrane active proteins that display an activity depending on the physical state of the membrane.

The composition of membranes is complex. There are hundreds or even thousands of different lipid species and further thousands of different membrane proteins. The composition of membranes is different not only between different species, but also between different cell types of the same organism, and even between the membranes of different organelles within the same cell [17].

Proteins act, e. g., as catalysts and the importance of their role seems intuitively clear, while the role of the lipid membrane and the range of different lipid compositions are less obvious and there is no agreement in the biophysical community yet on what the purpose of the heterogeneity of the lipids precisely is. Moreover, the lipid composition of the inner and the outer leaflet of some membranes may also be asymmetric. For example, while phospholipids are distributed equally in both monolayers of the endoplasmic reticulum, the lipid distribution of the major membrane lipids in the inner and outer leaflets of the erythrocyte membrane is completely different and is presented in Fig. 3. The choline-containing phospholipids, SM and PC, are localized predominantly in the outer monolayer of the plasma membrane. The aminophospholipids PS and PE, by contrast, are enriched in the cytoplasmic leaflet of the membrane due to the action of various enzymes [22-26].

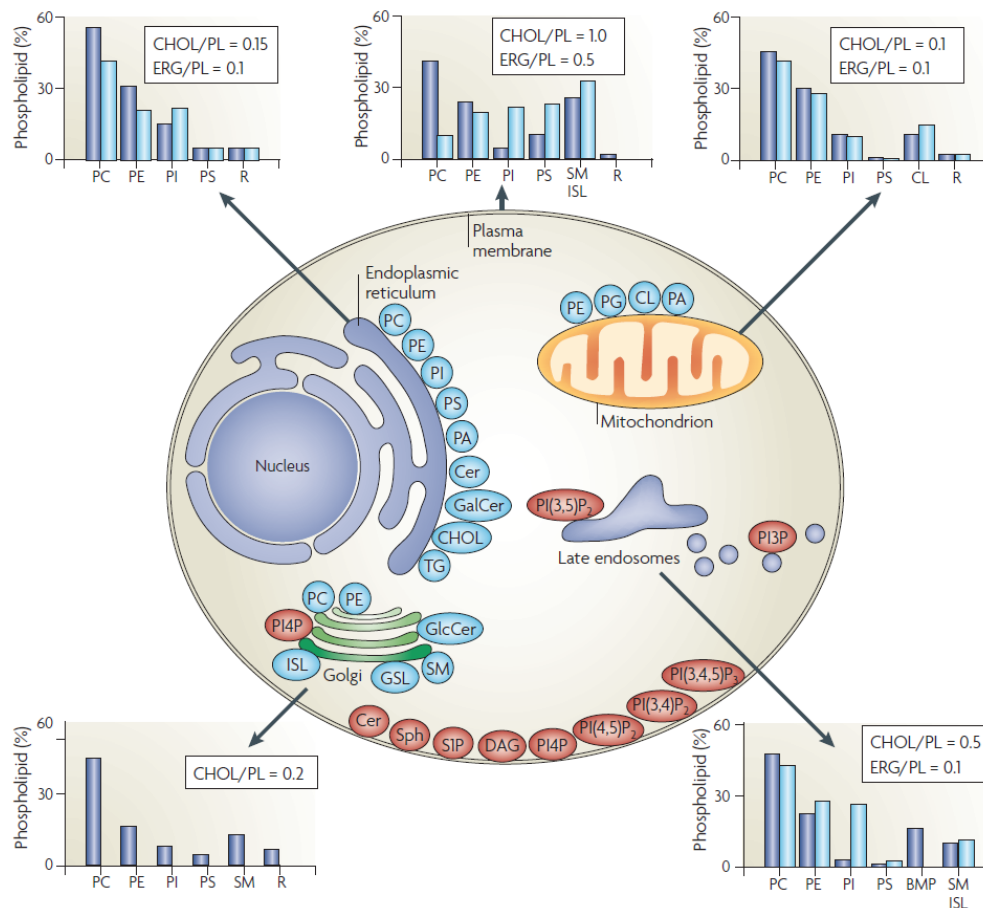


Figure 4: Lipid synthesis and steady-state composition of cell membranes. The lipid composition of different membranes varies throughout the cell. The lipid compositional data (shown in graphs) are expressed as a percentage of the total phospholipid (PL) in mammals (blue) and yeast (light blue). As a measure of sterol content, the molar ratio of cholesterol (CHOL; in mammals) and ergosterol (ERG; in yeast) to phospholipid is also included. The figure shows the site of synthesis of the major phospholipids (blue) and lipids that are involved in signaling and organelle recognition pathways (red).

It should be appreciated that the levels of signaling and recognition lipids are significantly below 1% of the total phospholipid, except for ceramide (Cer). The major glycerophospholipids assembled in the endoplasmic reticulum (ER) are phosphatidylcholine (PC), phosphatidylethanolamine (PE), phosphatidylinositol (PI), phosphatidylserine (PS) and phosphatidic acid (PA). In addition, the ER synthesizes Cer, galactosylceramide (GalCer), cholesterol and ergosterol. Both the ER and lipid droplets participate in steryl ester and triacylglycerol (TG) synthesis. The Golgi lumen is the site of synthesis of sphingomyelin (SM), complex glycosphingolipids (GSLs) and yeast inositol sphingolipid (ISL) synthesis. PC is also synthesized in the Golgi, and may be coupled to protein secretion at the level of its diacylglycerol (DAG) precursor. Approximately 45% of the phospholipid in mitochondria (mostly PE, PA and cardiolipin (CL)) is autonomously synthesized by the organelle. BMP (bis(monoacylglycero)phosphate) is a major phospholipid in the inner membranes of late endosomes [27] (not shown). PG, phosphatidylglycerol;

PI(3,5)P₂, phosphatidylinositol-(3,5)-bisphosphate; PI(4,5)P₂, phosphatidylinositol-(4,5)-bisphosphate; PI(3,4,5)P₃, phosphatidylinositol-(3,4,5)-trisphosphate; PI₄P, phosphatidylinositol-4-phosphate; R, remaining lipids; S1P, sphingosine-1-phosphate; Sph, sphingosine.

Besides this cross-sectional asymmetry, many membranes also show an important lateral asymmetry.

Microdomains called “lipid rafts”, primarily occurring in nervous tissue, coexist in a single membrane and maintain their own special biophysical properties by restricting or impairing the intermixing of their lipid and protein components [28].

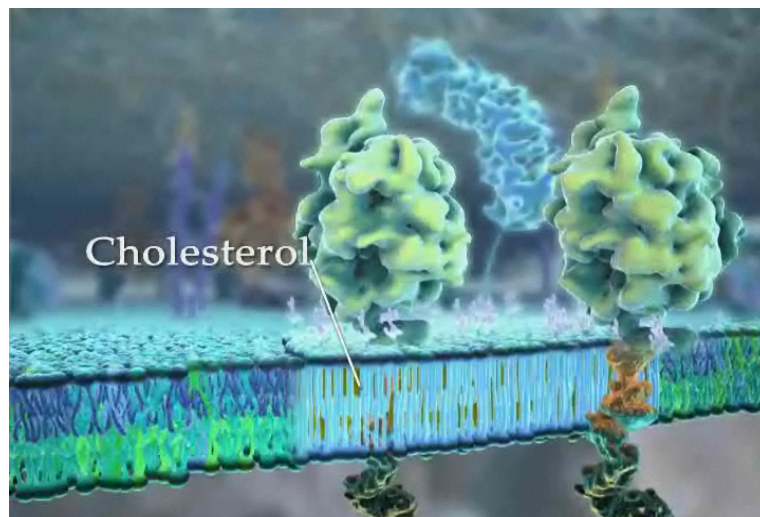


Figure 5: Lipid Rafts enriched in sphingomyelin and cholesterol.

Such domains have gained increasing interest due to their implication in many cellular processes such as signal transduction, vesicular trafficking and viral infection. Over a decade ago, the lipid raft was first defined as a detergent-resistant transient microdomain composed of cholesterol (CHOL), SM, glycosphingolipids and different proteins that attach to the lipid structure via a

glycosylphosphoinositol (GPI) anchor, a fatty acid modification or a hydrophobic aminoacid sequence [29]. The carbonyl group of sphingolipids forms a hydrogen bond with the 3 β -OH of CHOL, forming a rigid structure with the phospholipid acyl chains fully extended, but with certain rotational and bending mobility.

Cholesterol appears to be a key player in the formation of lipid rafts. It is planar and inflexible and would pack better with saturated fatty acid chains and could also induce them to elongate to form lower energy zig-zag structures in which all the methylene groups are anti. This liquid-ordered (L_o) structure is more fluid than the gel lamellar phase (L_β), although it is more rigid than the liquid crystalline phase (L_α). By contrast, a liquid-disordered phase (L_d) contains a small amount of cholesterol with unsaturated PCs, producing a less compact structure that resembles the L_α structure. In L_d regions, the surface packing is looser than in L_o regions; it is especially loose in regions with high PE content, where proteins with bulky membrane anchors (e.g. isoprenyl moieties) can find an appropriate docking space for their membrane binding.

1.4 Lipid polymorphism

When dispersed in aqueous solutions, lipids can organize in different ways depending on their molecular structure, water concentration, pH, ionic strength or system pressure [30, 31]. Such polymorphism among lipids is important in cell processes such as membrane fusion and fission, vesicular trafficking, macromolecule transport through the membrane and the stabilization of protein complexes in the lipid bilayer [32, 33]. Moreover, the way in which lipids are

organized affects their interactions with membrane proteins, thereby modulating their activity [34, 35].

A lipid phase is a thermodynamic concept that defines each of the different structural stages of matter, like water in the solid or liquid state. A lipid phase refers to a specific conformation adopted by lipids in an aqueous solution (i.e. how lipids organize into supramolecular structures). Lipid phases may be classified according to three criteria: (i) the type network; (ii) the packing of the acyl chains; and (iii) the curvature of the whole structure.

The most widely used nomenclature for their designation involves the use of a letter and a subscript, as proposed by Luzzati [36]. The type of network may be: unidimensional, as a lamellar (L) or micellar structures; bidimensional, like in hexagonal (H) phases, or cubic (Q) and crystalline three-dimensional (C) structures. The subscript indicates the degree of acyl chain packing: “ α ” refers to disordered hydrocarbon chains (fluid); “ β ”, ordered (gel); “ β' ”, rippled-ordered; and “c”, crystalline. In addition, the lipid structure may adopt a positive curvature with the phospholipid acyl chains facing inward (type I), or a negative curvature where the acyl chains are outwards (type II or inverted). The most relevant lipid structures from a biological point of view are the lamellar, micellar, inverted hexagonal (H_{II}) and inverted cubic (Q_{II}) phases (Figure 6). Lamellar phases include L_{β} , L_{α} , L_o and L_d .

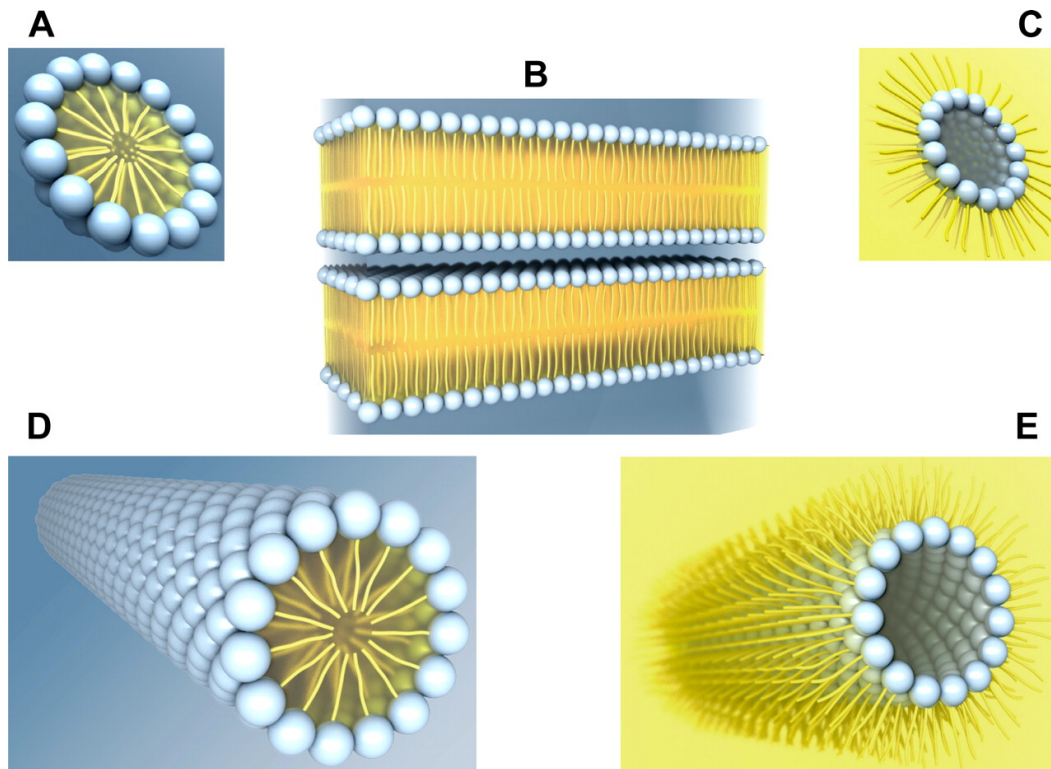


Figure 6: Lipid polymorphism. (A) Normal micelle (type I). (B) Lamellar structure. (C) Inverted micelle (type II). (D) Normal hexagonal phase (H_I). (E) Inverted hexagonal phase (H_{II}). Each phospholipid molecule consists of a hydrophilic (water-loving) head group (blue spheres) facing an aqueous environment (blue background) and 1 or 2 hydrophobic (water-fearing) carbon tails (yellow) facing a lipid environment (yellow background) [37].

The coexistence of large amounts of CHOL (over 20 mol%), SM and glycerophospholipids (e.g. PC) leads to the formation of L_o structures, like lipid rafts, where CHOL and SM molecules are tightly packed.

The macroscopic lipid organization within a membrane in part depends on the monomeric structure of its lipids [38] (Figure 7). Lipids with a cylindrical shape, like SM and PC, form lamellar structures with a global curvature of zero. Other lipids, such as PE, CHOL or diacylglycerol, form membranes with negative curvature strain due to their truncated cone shape. These molecules induce the

formation of inverted hexagonal phases in vitro. Finally, molecules whose hydrophilic region occupies a larger area than the hydrophobic moiety (e.g. detergents and lysophospholipids) possess an inverted cone shape and they induce a positive curvature in the lipid structure.

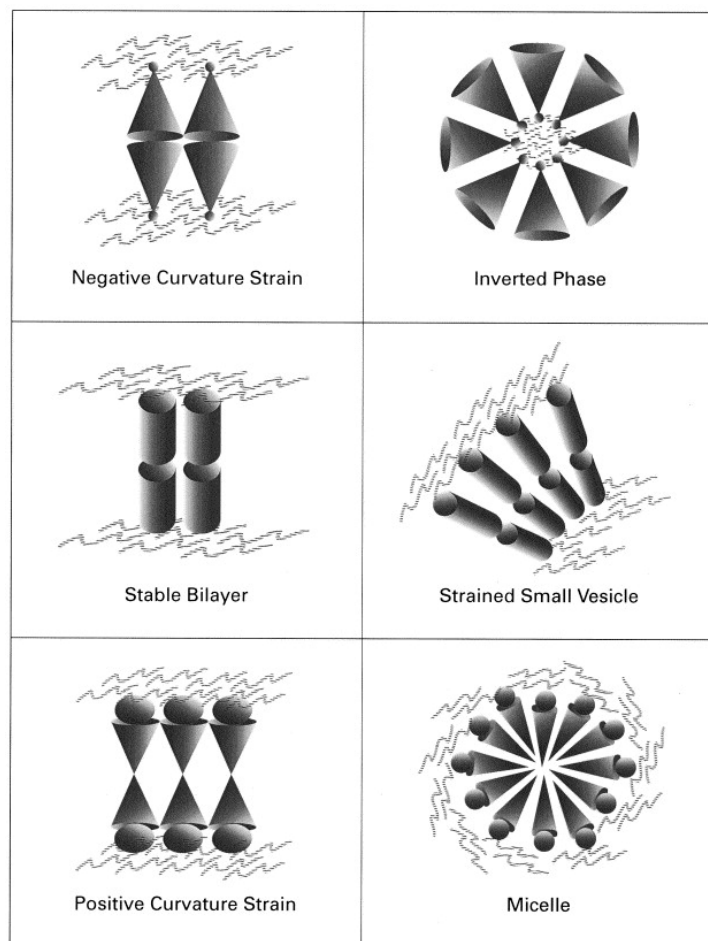


Figure 7: In the left-hand column of this figure are schematically represented three alternative bilayer motifs. Representations of the ‘shapes’ of the lipids packed in a bilayer have been exaggerated in order to emphasize the consequences of packing into a flat structure phospholipids that have an effectively small head group (negative curvature strain), a head group of size comparable to the cross-section of the acyl chains (stable bilayer) or a phospholipid with a large head group (positive curvature strain). The right-

hand panels indicate the types of curved structures that the corresponding types of lipids can form. Wavy lines indicate the location of the water [34].

On the whole, biological membranes adopt a lamellar structure, though certain transient regions with a high concentration of specific lipids may exist that induce a local curvature other than zero. This modulation in membrane lipid composition is essential to many cell processes including membrane fusion-fusion [39], the formation of proteolipidic pores [40] or the binding of membrane proteins to the lipid bilayer [35, 41].

2. Proteins modulated by the membrane physical state

2.1 G Protein-Coupled Receptors

The ability of cells to communicate with and respond to their external environment is critical for their continued existence. A universal feature of this communication is that the external signal must in some way penetrate the lipid bilayer surrounding the cell. In most cases of such signal acquisition, the signaling entity itself does not directly enter the cell but rather transmits its information to specific transmembrane proteins, which communicate with additional proteins associated with the intracellular face of the membrane. Membrane localization and function of many of these proteins are dependent on their covalent modification by specific lipids.

According to the human genome sequence, transmembrane proteins may account for 30% of the total pool of proteins in the cell [42]. Among such proteins, G protein-coupled receptors (GPCRs) represent by far the largest family of membrane proteins involved in cell signaling. Indeed, their importance is highlighted by the fact that these proteins are encoded by around 950 genes [43] and that they currently constitute the main target for rational drug design [44].

GPCRs are integral membrane proteins with seven transmembrane α -helices that are associated with three extracellular and three intracellular loops. The N-terminal extracellular region of the protein may contain glycosylated moieties, as well as highly conserved cysteines that form disulfide bonds to stabilize the receptor structure. The first crystal structure of mammalian GPCR to be resolved

was that of bovine rhodopsin [45] and, in 2007, the β_2 -adrenergic receptor was the first human GPCR to be crystallized [46].

These receptors bind extracellular molecules and activate signal transduction pathways, ultimately regulating many cellular responses. GPCRs are only found in eukaryotes and are mostly involved in biological cell functions. This almost ubiquitous presence in cell signaling events is due to their wide distribution in different cell types, the diversity of agonists that they may bind (e.g. light-sensitive compounds, chemokines, pheromones, hormones, small molecule neurotransmitters, etc.), and the variety of downstream effector they modulate.

2.2 G proteins

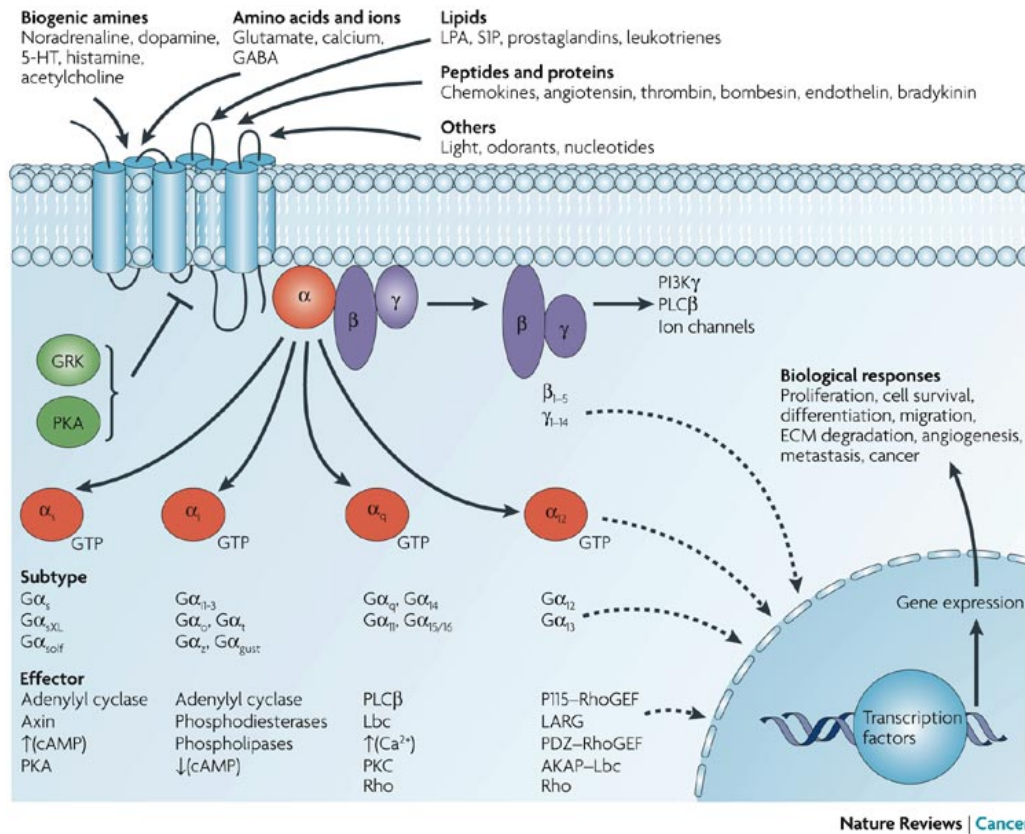
Heterotrimeric G proteins, composed of α , β and γ subunits, function to transduce signals from GPCRs to intracellular effector proteins: they are thus responsible for the initial amplification of the signals triggered through GPCRs by a variety of messengers.

G protein signaling pathways mediate a vast number of physiological responses, and dysregulation of these pathways contributes to many diseases, including cancer, heart disease, hypertension, endocrine disorders, and blindness [47-51].

It is known that GPCRs bind to the membrane at defined sites in the bilayer. When an extracellular signal mediated by an agonist ligand induces a conformational change in the receptor, the heterotrimeric G protein bound to the GPCR becomes activated.

For G proteins, the accepted mechanism of action is visualized as a continuous cycle of activation and inactivation of the G protein α subunit ($G\alpha$). Agonist

binding to a GPCR at the extracellular cell surface induces a conformational change in the GPCR that allows it to directly promote GDP release from the inactive $G\alpha$, which is in the heterotrimeric ($\alpha\beta\gamma$) complex. Next, GTP binds to $G\alpha$, and $G\alpha$ and the $\beta\gamma$ dimer ($G\beta\gamma$) dissociate, giving rise to signaling-competent GTP-bound $G\alpha$ and free $G\beta\gamma$. With the exception of the β_5 subunit [52], β subunits ($G\beta$) and γ subunits ($G\gamma$) appear to irreversibly associate and exist as $\beta\gamma$ dimers, whether as free $G\beta\gamma$ or $G\beta\gamma$ bound to $G\alpha$. To complete the G protein cycle, $G\alpha$ hydrolyzes its bound GTP and then GDP-bound $G\alpha$ reassociates with $G\beta\gamma$ [47]. The overall process amplifies the original signal in a cascade, whereby a single agonist-activated receptor can activate several G proteins, each of which can interact with effector proteins that in turn can produce thousands of second messenger molecules to regulate downstream proteins. The first amplification step whereby several G proteins are activated by a single receptor molecule is produced through the presence of a large number of inactive (pre-active) heterotrimeric G proteins in the receptor vicinity.



Nature Reviews | Cancer

Figure 8: Various ligands use G-protein-coupled receptors (GPCRs) to stimulate membrane, cytoplasmic and nuclear targets. GPCRs interact with heterotrimeric G proteins composed of α , β and γ subunits that are GDP bound in the resting state. Agonist binding triggers a conformational change in the receptor, which catalyses the dissociation of GDP from the α subunit followed by GTP-binding to $G\alpha$ and the dissociation of $G\alpha$ from $G\beta\gamma$ dimer [53]. The α subunits of G proteins are divided into four subfamilies: $G\alpha_s$, $G\alpha_i$, $G\alpha_q$ and $G\alpha_{12}$, and a single GPCR can couple to either one or more families of $G\alpha$ proteins. Each G protein activates several downstream effectors [54]. Typically $G\alpha_s$ stimulates adenylyl cyclase and increases levels of cyclic AMP (cAMP), whereas $G\alpha_i$ inhibits adenylyl cyclase and lowers cAMP levels, and members of the $G\alpha_q$ family bind to and activate phospholipase C (PLC), which cleaves phosphatidylinositol bisphosphate (PIP₂) into diacylglycerol and inositol triphosphate (IP₃). The $G\beta$ and $G\gamma$ subunits function as a dimer to activate many signaling molecules, including phospholipases, ion channels and lipid kinases. Besides the regulation of these classical second-messenger generating systems, $G\beta\gamma$ and $G\alpha$ subunits such as $G\alpha_{12}$ and $G\alpha_q$ can also control the activity of key intracellular signal-transducing molecules, including small GTP-binding proteins of the Ras and Rho families and members of the mitogen-activated protein kinase (MAPK) family of serine-threonine kinases, including extracellular signal-regulated kinase (ERK), c-jun N-terminal kinase (JNK), p38 and ERK5, through an intricate network of signaling events that has yet to be fully elucidated [53, 55, 56]. Ultimately, the integration of the functional activity of the G-protein-regulated signaling networks control many cellular functions, and the aberrant activity of G proteins and their downstream target molecules can contribute to cancer progression and metastasis.

5-HT, 5-hydroxytryptamine; ECM, extracellular matrix; GABA, gamma-aminobutyric acid; GEF, guanine nucleotide exchange factor; GRK, G protein receptor kinase; LPA, lysophosphatidic acid; PI3K, phosphatidylinositol 3-kinase; PKA and PKC, protein kinase A and C; S1P sphingosine-1-phosphate. Adapted from [57].

GPCRs and G proteins are regulated by co- and post-translational modifications. Some such modifications have a relevant influence on protein-lipid interactions and on GPCR-associated signaling such as myristoylation, palmitoylation and isoprenylation- all of which have been observed in GPCRs [58], G proteins [59], their effector proteins [60] and receptor kinases [61]. These lipid modifications involve the covalent binding of acyl or isoprenyl groups of the amino acid backbone, and they modulate the membrane structure, protein activity and trafficking across the membrane.

As previously mentioned, the structure of lipid bilayer affects cell signaling transduction by modulating the binding of signaling proteins to the membrane, as well as their activity. The heterogeneous biophysical properties of lipids leads to the generation of microdomains with specific compositions, giving rise to membrane regions with singular physical characteristics in terms of the degree of fluidity and curvature. Membrane proteins have a preference for different environments in the membrane, in part since the localization and activity of proteins is influenced by the chemical nature of membrane lipids [62, 63]. In turn, both integral and peripheral proteins may change the lipid environment where they are localized by modulating the degree of mobility of the surrounding lipids, thereby modifying the properties and organization of the plasma membrane [64, 65].

In summary, the lipid-protein interactions related to G protein-associated signaling are not fortuitous events, but rather they are defined processes with important implications in signal transduction.

2.3 Lipid modification of G proteins

Both small monomeric G proteins like Ras, and heterotrimeric G proteins ($G\alpha\beta\gamma$), undergo lipidation co- or post-translationally. Lipid modifications participate in G protein-lipid interactions and they are involved in the translocation of G proteins to membranes and further mobilization to different microdomains. Lipid modifications of heterotrimeric G proteins involve the covalent binding of three different types of hydrophobic molecules to the signaling protein, namely myristic acid (MA, C14:0), palmitic acid (PA, C16:0) and isoprenyl groups (i.e. farnesyl or geranylgeranyl (GG)).

2.3.1 Myristoylation and palmitoylation: $G\alpha$ subunit lipid modifications

Myristoylation is a co-translational modification that involves the covalent attachment of the saturated fatty acid myristate to a glycine residue of the protein via an amide bond (N-myristoylation) [66]. This lipid modification is irreversible due to the chemically stable structure of the amide bond. Myristoylation is catalysed by the enzyme N-myristoyltransferase and takes place on glycine-2 (Gly-2) in the N-terminus of the mature $G\alpha$ subunit. However, a free N-terminal glycine residue alone is not sufficient to guarantee

myristoylation, because substrate recognition also depends on the subsequent amino acid sequence. In particular, the nature of the sixth amino acid seems to be important and myristoylated proteins usually contain a serine or threonine residue at this position [67]. Nevertheless, the presence of a myristoyl moiety is not sufficient for stable membrane attachment [68] and moreover the majority of $G\alpha$ subunits are not myristoylated. Therefore, it is clear that this sort of lipid modification must also have another function besides simply enhancing the membrane affinity of a protein. For the G_i family myristoylation is a precondition for palmitoylation [69, 70], the secondary lipid modification found on $G\alpha$ subunits. In this context, the role of the myristoyl group is to facilitate an initial contact with the membrane and to direct the $G\alpha$ subunit to the palmitoylation compartment.

Protein palmitoylation is a post-translational modification which affects most mammalian $G\alpha$ subunits. It consists in a covalent attachment of the saturated fatty acid palmitate to cysteine-3 (Cys-3) via a thioester bond (S-acylation). This reaction is catalysed by a palmitoyltransferase, a specific enzyme for $G\alpha$ mammalian Ras [71]. In contrast to N-myristoylation, palmitoylation is a more dynamic modification due to its chemically labile bond, which favours the rapid turnover of palmitoylation in the cell [72, 73]. This lipid modification occurs at one or several cysteine residues within the first 20 amino acids of the N-terminal domain of $G\alpha$ subunits, but the specific amino acid sequence required to facilitate palmitoylation has not yet been defined in detail. Although no consensus signal for this lipidation has been identified, the presence of myristic acid (in the case of myristoylated $G\alpha$ subunits) or an interaction with $G\beta\gamma$ subunits seems to be required for G protein palmitoylation.

Besides S-palmitoylation, a palmitate molecule can also be bound covalently to Gly-2 via an amide bond (N-palmitoylation) [74].

2.3.2 Isoprenylation of G γ subunit

Isoprenylation is a multistep post-translational process that affects all 12 known mammalian G γ subunits. This lipidation involves the formation of a covalent thioether bond between a farnesyl, consisting of 3 isoprene repeats with a total of 15 carbon atoms, or geranylgeranyl group of 4 isoprenes and a cysteine in a CAAX motif at the C-terminus [35]. This motif determines the substrate specificity for a farnesyl or geranylgeranyl transferase. It consists of a cysteine to be thioesterified (C), two aliphatic amino acids (AA) and one amino acid (X) that determines the type of isoprenyl group to be bound to C. If the last residue of the conserved motif is serine or methionine, the cysteine is farnesylated whereas, if the last residue is leucine, a geranyltransferase modifies the protein and a geranylgeranyl moiety is attached.

Isoprenylation of G γ subunits is an irreversible process that takes place in the cytosol and the G $\beta\gamma$ then translocates to the endoplasmic reticulum (ER) where the three terminal -AAX amino acids are hydrolysed by the Ras-converting enzyme (Rce) [75] and the isoprenylated cysteine is methylated by the isoprenylcysteine carboxyl methyltransferase (Icmt) [76]. The addition of an extra methyl group to the peptide structure seems to increase the hydrophobicity of the protein, and consequently, its binding to the lipid bilayer. However, these modifications are not sufficient for translocation of the G $\beta\gamma$ dimer from the ER to the plasma membrane. Palmitoylation has been

determined as a key signal for the trafficking of these proteins to the membrane: indeed, the G $\beta\gamma$ dimer can localize to the plasma membrane upon palmitoylation [77].

G $\beta\gamma$ dimers need a G α palmitate signal for their correct trafficking, while G α also needs to bind G $\beta\gamma$ for its palmitoylation and correct translocation to the plasma membrane. In this context, G α_s and G α_q subunits lacking the N-terminal region involved in the binding to the G $\beta\gamma$ dimer are neither palmitoylated nor translocated to the plasma membrane [78].

2.4 Interactions of lipid membranes with G proteins

Isoprenyl and/or fatty acid moieties in G proteins and GPCRs are not the only lipid-protein interactions in GPCR-associated signaling. The regions of lipid membranes to which these proteins are bound also constitute a meeting point between lipids and proteins. The regulatory effect of these lipid-protein interactions are bidirectional and as such, both the activities of G proteins and GPCRs can be modulated by the lipid environment in which they are localized, while these proteins are also capable of modulating the lipid structure and the organization of the membrane [79].

Since the regulatory influence of these lipids on the binding of G proteins to bilayers has not yet been studied [80-83], the first part of the present work was designed to study the effect of the lipids bounded to G proteins on the structural properties of membranes to model membranes with lamellar and non-lamellar prone lipid structures.

In particular I studied the effects of palmitic alcohol (POH), myristic alcohol (MOH), PA, MA and GG on two all-atom lipid bilayer used as symmetric membrane models.

2.5 Materials and methods

The first membrane was made of POPC and it was a model of a lamellar prone bilayer. The second membrane contained POPC and POPE in a 6:4 proportion,

similar to that found at the inner leaflet of the plasma membrane. Five molecules were added to both membranes: GG, MOH, MA, POH and PA.

GG, MOH and POH had zero charge, while MA and PA were negatively charged at pH 7.4. The POPC membrane was made of 98 POPC molecules. The box dimensions were $X=149,16 \text{ \AA}$, $Y=56,61 \text{ \AA}$ and $Z=55,85 \text{ \AA}$. 33 Na^+ , 33 Cl^- counter ions and 11301 water molecules were added to reach the density of 0,997g/mL.

The POPC-POPE membrane was made of 58 POPC and 40 POPE molecules. The box dimensions were $X=148,10 \text{ \AA}$, $Y=53,09 \text{ \AA}$ and $Z=51,52 \text{ \AA}$. 28 Na^+ , 28 Cl^- counter ions and 9825 water molecules were added.

The simulations were performed using the program YASARA [84] under NPT ensemble at 298K and 1 atm by coupling the system with a Berendsen thermostat [85] and by controlling the pressure in the manometer pressure control mode.

The AMBER03 force field was used. The geometry of the molecules was optimized by semi-empirical AM1 method using the COSMO salvation model [86]. Partial atomic charges were calculated using the same level of theory by the Mulliken point charge approach [87]. Electrostatic interactions were calculated with a cutoff of 10.48 \AA , and the long-range electrostatic interactions were handled by the Particle Mesh Ewald (PME) algorithm [88] using a sixth-order B-spline interpolation and a grid spacing of 1 \AA . The leap-frog algorithm was used in all simulations with a 1.25 fs time step for intramolecular forces and 2.5 fs time step for intermolecular forces.

The lipid bilayers were assembled and relaxed reducing the box dimension until the Van der Waals energy of the system started to increase and the structural parameters of the membranes compared with experimental data [89].

The time required for a drug to cross the membrane can be a few μs , much larger than the 50 ns afforded by the present simulations. As a consequence, the energy evaluation of trajectories of few tens of nanoseconds cannot guarantee that we are observing the system at equilibrium.

In order to calculate the free energy of binding across the membrane, I generated, for each system fatty acid/membrane, 160 initial conformations different in orientation and penetration of the molecules inside the membrane. In order to avoid bumps and to avoid abnormal non-covalent interactions, I downsized the added molecules to 20% of the original size and I reduced the non-covalent interactions to 10% of the normal value. The molecules were then placed at different position across the membrane. The size and the energy constants were gradually brought back to normal values through cycles of steepest descent minimization, and a cycle of annealing until the speed of the fastest atom dropped below 500 m/s. The membranes were then heated to 310K and an equilibration dynamics of 2 ns completed. After completion, free energies were calculated on the last 100 ps of the 160 molecular dynamics (MD) and the conformation with higher binding energy was chosen as initial structure for a longer and more accurate MD run of 50 ns. The whole process to create a free energy of binding profile was performed on a newly designed grid for scientific calculation [www.yadamp.unisa.it/grimd2].

The binding energies of fatty acids were calculated after minimization and averaging the last 30 structures spanning 10 ns. The lateral pressure profile was calculated as described in [90].

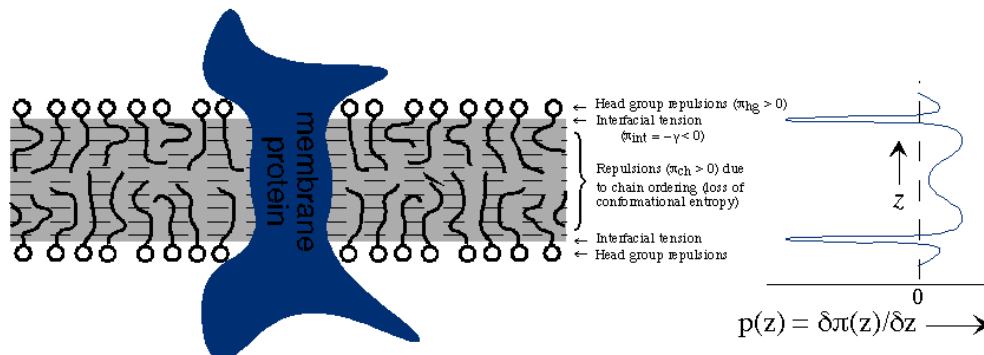
2.6 Analysis

2.6.1 Binding energy

The binding energy is obtained by calculating the energy at infinite distance (between the selected molecule and the rest of the system, i.e. the unbound state) and subtracting the energy of the system (i.e. the bound state). The more positive the binding energy, the more favorable the interaction in the context of the chosen force field. In some other programs like AutoDock, more negative energies indicate better binding. The reason is that these programs do not report 'binding energies' (the energy required to disassemble a whole into separate parts, usually positive), but instead 'energies of binding' or 'free energies of binding' (the energy change upon binding, usually negative).

2.6.2 Lateral pressure (stress) profile

In a "self-assembled" membrane, i.e., in the absence of any lateral constraints, the bilayer is free to adjust its molecular area (expand or contract laterally) so as to minimize its free energy. In other words, once equilibrium is reached, the sum of the forces acting in the plane of the bilayer (lateral pressures) is essentially zero.



Total pressure must be zero, so $\pi_{hg} + \pi_{ch} = \gamma$

Equivalently: divide up the bilayer into thin layers of thickness δz

each layer has pressure $\delta\pi(z)$

$$\sum_z \delta\pi(z) = \int_z p(z) dz = 0$$

Figure 9: Distribution profile of lateral pressure.

However, since the bilayer is of finite thickness, the various contributions to the total lateral pressure will in general act at different depths; positive lateral pressures occurring at some depth must therefore be balanced by negative pressures (tensions) elsewhere. To be more explicit, we should imagine dividing up the bilayer into thin planar slices. Within a slice centered at a depth z in the bilayer, a nonzero local lateral pressure $\pi(z)$ may exist, constrained only insofar as the sum of the pressures over the thickness of the entire bilayer gives the total lateral pressure, which must be zero: $\sum_z \pi(z) = 0$. While there is as yet no direct measurement of these localized lateral pressures, there is both experimental and theoretical evidence of their magnitude and distribution with respect to depth in the bilayer. For example, the curvature elastic properties (spontaneous curvature and curvature elastic moduli) of bilayers are integral

moments of the pressure "profile" (i.e., its depth-dependence) and its curvature derivatives, as discussed below.

The nonzero lateral pressure profile $\pi(z)$ arises in large part from the competition between contributions of opposite sign: a tension (negative pressure) largely localized near the interfaces, and more broadly distributed positive pressures arising predominantly from chain conformational entropy, as well as from head group repulsions. The interfacial tension derives from the large free energy cost of contact between hydrocarbon and water at each of the two hydrophilic/hydrophobic interfaces. This contribution to the free energy is approximately proportional to the area of interfacial contact, the constant of proportionality being roughly 0.5 J per m² of interface (equivalently, a constant interfacial tension of $g = 0.5 \text{ N/m} = 50 \text{ dyn/cm}$), using a typical value for fluid hydrocarbon/water interfaces. Acting alone, this contribution would induce the bilayer to minimize the area per molecule, e.g., for saturated chains, to align the chains in their all-trans configuration. However, the chain conformational entropy, which reflects the degree of chain conformational disorder, also makes a large contribution to the free energy of the bilayer. In contrast to the interfacial free energy, the chain conformational contribution to the pressure depends sensitively on molecular area. This pressure is very large at small molecular areas (when the acyl chains are necessarily very orientationally ordered, so even a small increase in molecular area allows for a large increase in conformational freedom), but at larger areas per molecule, at which the chains are already quite conformationally disordered, the change in entropy upon lateral expansion is much smaller. (The entropy eventually goes through a maximum with increasing area, beyond which the conformational freedom of the chains is reduced). It is

important to note that upon lateral expansion, the volume occupied by the lipids changes very little, since the energetic cost of creating free volume (the increase in Van der Waals energy among the hydrocarbon chains) would be enormous; rather, the bilayer thins as it expands laterally, the chains becoming increasingly bent and intertwined, thus able to sample more of the enormous number of their configurational states, while filling up all the space in the bilayer interior at roughly constant bulk density.

The free energy minimum that defines the bilayer equilibrium derives from the compromise between these opposing forces, at which the pressures arising from interfacial tension and chain conformational (and head group) interactions are just balanced.

A rough estimate of the magnitude of the lateral pressures in the bilayer interior is readily obtained by noting that the sum of the lateral stresses distributed over the hydrophobic interior of the fluid bilayer (ignoring head group contributions) must balance the pair of interfacial tensions at the interfaces. Using $g = 0.5 \text{ N/m}$ as the tension of each interface, the chains must generate an opposing lateral pressure of equal magnitude distributed over the hydrophobic interior of the bilayer, of thickness $(2h)$ somewhere in the range of 25 \AA to 30 \AA . The lateral pressure density (force per unit area), i.e., the lateral pressure (force per unit length) per unit thickness of the bilayer is thus on average roughly $2g/2h \approx 350 \text{ atm}$. While other contributions to the lateral pressure will alter this number somewhat, it nonetheless provides a measure of the magnitude of the lateral pressure densities acting upon an inclusion such as a protein or peptide aggregate that passes through the bilayer interior. The actual pressure profile

will be nonuniform, in a manner that depends sensitively upon the molecular composition of the bilayer.

2.7 Results

2.7.1 Binding energies

I have calculated the free energy of binding of GG, PA, POH, MA and MOH inserted in membranes of POPC and POPC-POPE. Since MA and PA are negatively charged at pH = 7.4, they exhibit binding energies larger than GG, POH and MOH. In the computational analysis, I decided to overcome this problem by comparing the corresponding alcohols MOH and POH with GG. This was done for two main reasons: GG is a neutral molecule and the comparison between molecules with charged head groups would unavoidably overlook the differences between the branched tail of GG and the linear chains of myristic and palmitic acids. Secondly, the carboxylic group of MA and PA experiments a strong pKa shift when moved from water into membrane surface. As consequence, MA and PA become partially or totally protonated depending on their concentration.

I decided to measure the effect of the addition of a single molecule, posing the accent on the capability of different tails to alter the physical state of membranes. In Fig. 10 the differential free energies of binding of GG, MOH, POH are shown.

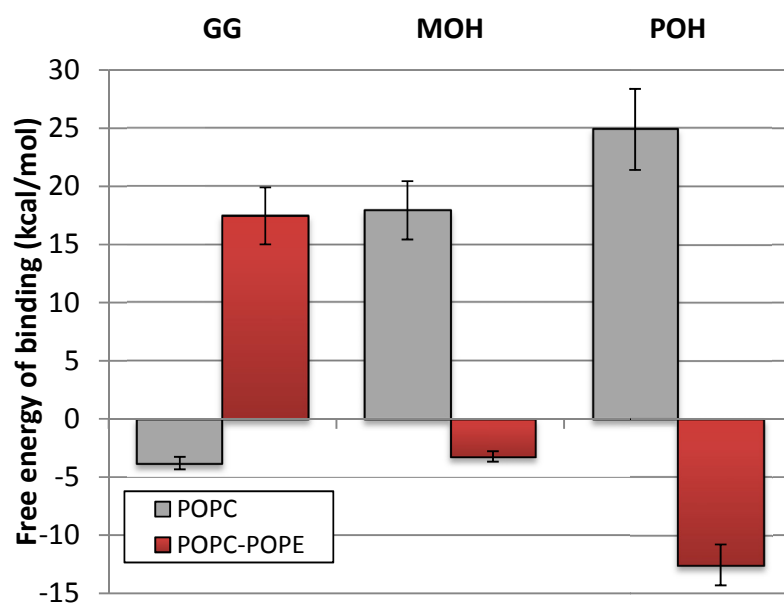


Figure 10: Differential free energy of binding.

The difference in free energy of binding, calculated in water and in membrane, gives an indication of the propensity of a molecule toward a lamellar prone or H_{II}-prone (PE-rich) membranes. GG shows a high propensity for PE-rich membrane. The free energy difference is of circa 20 kcal/mol, high enough to suggest a segregation of GG moieties in H_{II}-prone domains.

The binding of GG with POPC membrane is slightly negative. The hydroxyl group of GG prefers the aqueous phase where it can hydrogen bonds better than with the membrane surface, whereas the isoprenylated chain prefers the membrane core: therefore the two effects are opposite and quite similar in the absolute value.

The free energy difference of MOH between the two membranes is roughly equal to GG, but MOH has preference for POPC membrane. Even higher propensity for lamellar membranes is shown by POH.

These results suggested that a mixture of GG and POH or MOH should rapidly segregate in different membranes.

2.7.2 Lateral pressure profile

The addition of fatty acids can also substantially change the membrane organization. The lateral pressure profile, arising from the inhomogeneous nature of lipid bilayer, can be capable to regulate membrane protein functionalities.

I have calculated the lateral pressure profile for POPC and POPC-POPE membranes after addition of the examined fatty acids.

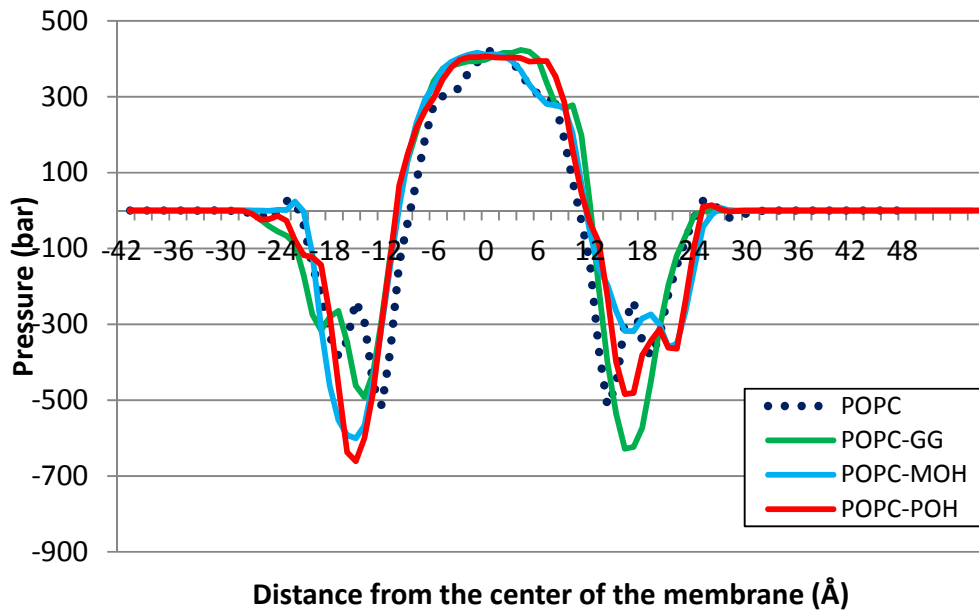


Figure 11: Lateral pressure profile of POPC membrane, pure and after FAs addition.

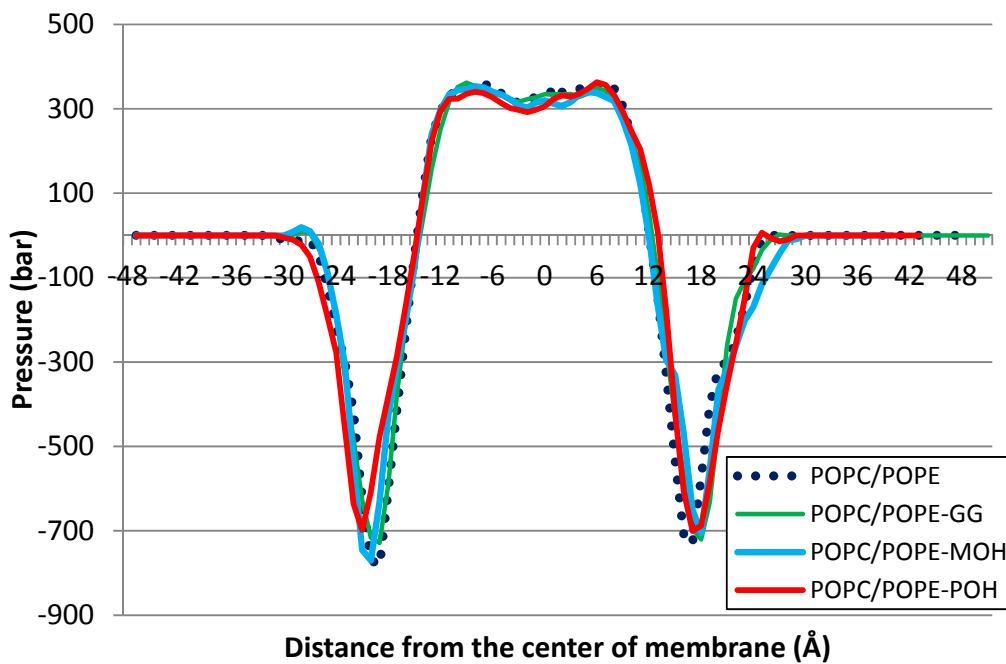


Figure 12: Lateral pressure profile of POPC-POPE membrane, pure and after FAs addition.

In Fig. 11-12 the pressure profiles of POPC and POPC-POPE membranes without fatty acid addition is indicated with blue dots. The integral of the profile is zero, corresponding to a relaxed membrane with zero surface tension. The comparison of the two diagrams suggests that the addition of only one molecule is not capable to alter the pressure profile of H_{II}-prone membranes.

The POPC membrane has an altered stress profile after addition of a single molecule. The alteration induced by GG is more evident and involves also the membrane core and the inner layer organization. The asymmetry in pressure profile can induce a spontaneous curvature in the membrane.

H_{II}-prone membranes seem to resist better than lamellar-prone membranes to the perturbation of a fatty acid, regardless its nature, or its ramification.

2.8 Conclusions

The binding energies and the lateral stress profiles suggest that the addition of GG to a membrane consisting of two domains, respectively lamellar-prone and H_{II}-prone, would prefer the second one where it would induce only a minor perturbation. Contrarily, MOH or POH tend to accumulate in lamellar-prone domains, and to alter the domain physical state.

All these data are in agreement with the results obtained by the group of Prof. Escribá. They used membranes containing 100% PC as a model of a lamellar-prone membrane. In addition, they also examined other situations that may resemble the bulk of the inner leaflet of the membrane (PC:PE, 6:4, mole:mole) or discrete membrane regions or microdomains with different non-lamellar phase propensity (different PE content). They found that an increase in the

proportion of PE gradually decreases $G\alpha$ monomer binding to model membranes. By contrast, heterotrimeric $G\alpha\beta\gamma$ subunits have a greater affinity for non-lamellar (H_{II}) phases. This behavior is most likely due to the $G\beta\gamma$ dimer, which exhibits a greater affinity for membranes containing PE. Thus, the $G\beta\gamma$ dimer would be responsible for the approach of the $G\alpha$ monomer to the receptor molecule in a H_{II} -prone membrane environment.

Considering that certain $G\alpha$ subunits only translocate to lipid rafts upon activation, lipid rafts represent platforms whose specific biophysical properties are able to enhance the effectiveness of the second step of the signaling cascade, trapping activated $G\alpha$ subunits and augmenting the spatial proximity between them and their effectors. On the other hand, dissociated $G\beta\gamma$ dimers still maintain a high affinity for membranes with a hexagonal propensity [91], which may also influence their distribution in native membranes. The general observation that prenylated proteins are normally not localized to lipid rafts [92] has also been confirmed for $G\beta\gamma$ subunits, which are excluded from synthetic lipid rafts [93]. This indicates that the $G\beta\gamma$ dimer most probably determines the lipid preference of heterotrimeric G proteins. In other words, the $G\beta\gamma$ dimer determines the preference of complete $G\alpha\beta\gamma$ heterotrimers for the hexagonal-phase, thereby masking the lamellar membrane affinity of the $G\alpha$ subunit. Therefore, one of the functions of the $G\beta\gamma$ dimer could be to transport $G\alpha$ subunits to the vicinity of the receptor, making them available for immediate activation (Fig. 13).

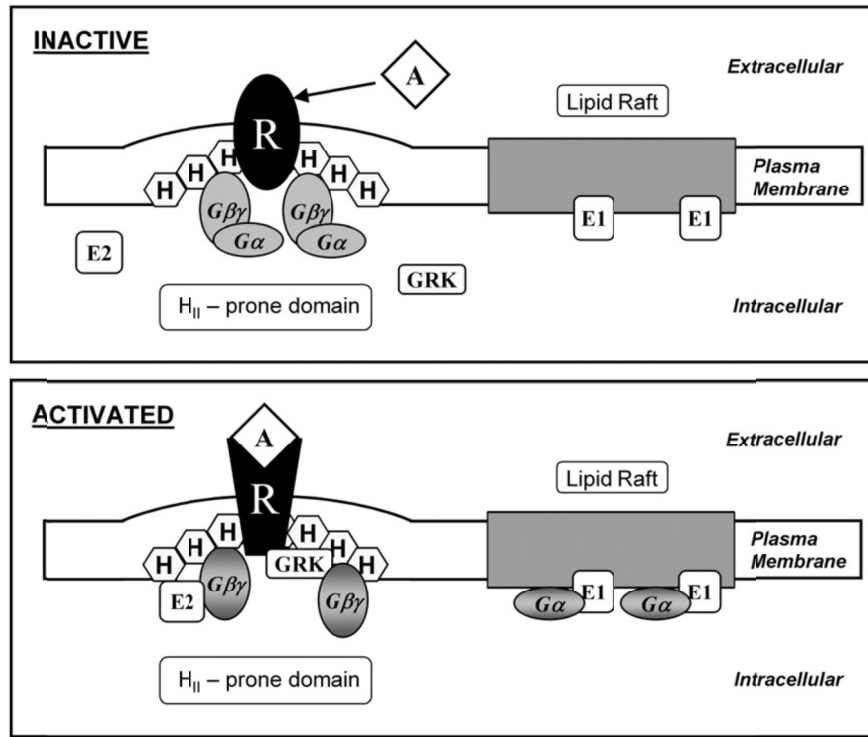


Figure 13: Membrane structure and GPCR-associated signaling. (Upper panel) GPCRs (R) induce the formation of hexagonal-phases (H_{II}) in their vicinity and these non-lamellar membrane regions attract heterotrimeric (inactive) G proteins, driven by the G $\beta\gamma$ -subunit. (Lower panel) Upon agonist (A) binding, several heterotrimeric G proteins are activated by one GPCR (R) molecule. Thus, G α subunits dissociate from the G $\beta\gamma$ dimers and they are targeted to special regions of the plasma membrane, such as lipid rafts, due to their greater affinity for bilayers with highly lamellar organized lipids. There, they may activate their corresponding effector proteins (E1). G $\beta\gamma$ dimers remain in non-lamellar-prone regions, where they can interact with their specific effectors (E2) and guide GRKs directly to the receptors. The latter would promote GPCR phosphorylation leading to receptor inactivation. Adapted from [35].

G protein lipid modifications (fatty acid and/or isoprenyl moieties) are probably involved in this effect, through which the different forms of G proteins are sorted into different membrane domains.

There is considerable evidence that the biophysical properties of the lipid bilayer modulate the activity of membrane proteins. The specific localization of membrane proteins is crucial for cell signaling because, in each membrane

microdomain, a given molecular entity (e.g. GPCRs, G proteins, etc.) may interact productively with different upstream and downstream signaling proteins. By extension, drugs targeted to membrane lipids can be used to regulate membrane structure and to reverse pathological malfunctions whose etiology is associated with alterations in membrane protein signaling. This approach has been called **Membrane-lipid therapy** and it has been successfully applied to the development of drugs for the treatment of cancer, obesity, hypertension, neurodegeneration, inflammation, metabolic diseases, etc. [94, 95].

3. The HSP co-inducers remodel plasma membrane rafts

OPEN ACCESS Freely available online

PLOS one

Membrane-Lipid Therapy in Operation: The HSP Co-Inducer BGP-15 Activates Stress Signal Transduction Pathways by Remodeling Plasma Membrane Rafts

Imre Gombos^{1,2}, Tim Crul^{1,2}, Stefano Piotto², Burcin Güngör¹, Zsolt Török¹, Gábor Balogh¹, Mária Péter¹, J. Peter Slotte³, Federica Campana², Ana-Maria Pilbat¹, Ákos Hunya⁴, Noémi Tóth¹, Zsuzsanna Literati-Nagy¹, László Vigh Jr.¹, Attila Glatz¹, Mario Brameshuber⁵, Gerhard J. Schütz⁵, Andrea Hevener⁶, Mark A. Febbraio⁷, Ibolya Horváth¹, László Vigh^{1*}

3.1 Introduction

For decades, sensing temperature changes in eukaryotes have exclusively been attributed to the formation of unspecified thermolabile proteins, whose unfolding recruits inhibitory chaperones (HSP90, HSP70) in the cytoplasm activating chaperone-repressed heat shock factors (HSFs) [96]. However, increasing evidence now shows that many stress events cause HSP induction without commensurate protein denaturation. That recognition has led to the “membrane sensor” hypothesis where the membrane’s physical properties and microdomain organization play an initiating role in the heat shock response (HSR).

Recent studies reveal the central importance of dynamic remodeling of membrane lipid domains in response to stress sensing and signaling in both plant and animal cells.

Clinical conditions are associated with specific changes in the physical state and lipid composition of cellular membranes, as well as the alteration of HSP levels in cells. Typically, an aberrantly high level of HSPs is characteristic in cancer, and the converse situation applies for ageing, type-2 diabetes or neurodegeneration. Cell membranes physical state is determined by composition, temperature and external conditions. It regulates the activity of all embedded proteins, as well as the expression of genes involved in stress responses to keep homeostasis.

It is known that molecules capable of inducing destabilization of sterol-rich domains formed by SM and CHOL in artificial bilayers [97, 98] may affect the activity of certain membrane proteins. Hence, the ability of some lipophilic drugs to affect the activity of certain membrane proteins could depend on the lateral localization of the proteins within a membrane. Since small molecules can interact with lipid membranes, they may also perturb the proteins contained within the membrane [94, 99-103].

There is a growing evidence that links the production of HSPs to changes in the lipid composition and in the architecture of membranes [104-106]. This “membrane sensor” hypothesis predicts that, besides protein denaturation or alteration in nucleic acid conformation, stress protein signals may originate from the cellular membranes [106, 107].

The idea proposed is that, rather than the overall changes in the physical state of membranes *per se*, the remodeling of specific microdomains and/or changes in the composition of specific lipid-protein interactions, are potentially and equally able to furnish stimuli for the activation or attenuation of heat shock genes. A plasma membrane-associated HSP response-refining signal can be related to the

altered operation of various membrane-localized receptor proteins, transmitters, lipases or other molecules [95, 108].

Lipid rafts can be considered the scaffolds of the HSR. In supporting this concept is the observation that HSF-1 activation upon heat shock requires cholesteryl glucoside. Importantly, cholesteryl glucoside synthetase is localized on lipid rafts [109].

Such observations not only emphasize the importance of membranes and their lipids in the “quality control” of the HSR, but also provide a new rationale for the introduction of novel HSP-chaperone modulating drug candidates.

A chaperone co-inducer is a substance that cannot induce HSPs by itself, but can enhance HSP induction in combination with other mild stresses. A chaperone co-inducer also has the ability to lower the temperature threshold of the heat shock response [110]. Hydroxylamine (HA) derivatives, such as Bimoclomol, BGP-15 and NG-094, represent one of the first chemical families of HSR co-inducers and may provide suitable therapeutic candidates for many disease states since they are capable of affecting stressed rather than unstressed cells and, therefore, unlikely to have major side effects as is the case with many classes of current drugs.

To determine their mechanism of action, a potential receptor interaction profile was extensively researched, although no significant specific candidate could be identified (α - or β -adrenergic, serotonergic receptors, various ion channels, etc.) however, the fact that the observed physiological activity of HA derivatives appeared exclusively in disease conditions suggested that they might have a novel biological target that was primarily accessible in disease or stress

conditions. Further biochemical analysis revealed that HA derivatives were able to facilitate the stress response and the expression of several HSPs [110].

The interaction and the subsequent function is dependent on the presence of specific lipid species in the membrane. As such, it was suggested that they might modify the domains of membrane-lipid phase where the thermally or chemically induced perturbation of lipid phase is sensed and transduced into a cellular signal, ultimately leading to an enhanced activation of heat shock genes.

In this chapter, I focus on the interactions between a HA derivative, BGP-15, with membrane rafts of sphingomyelin-cholesterol.

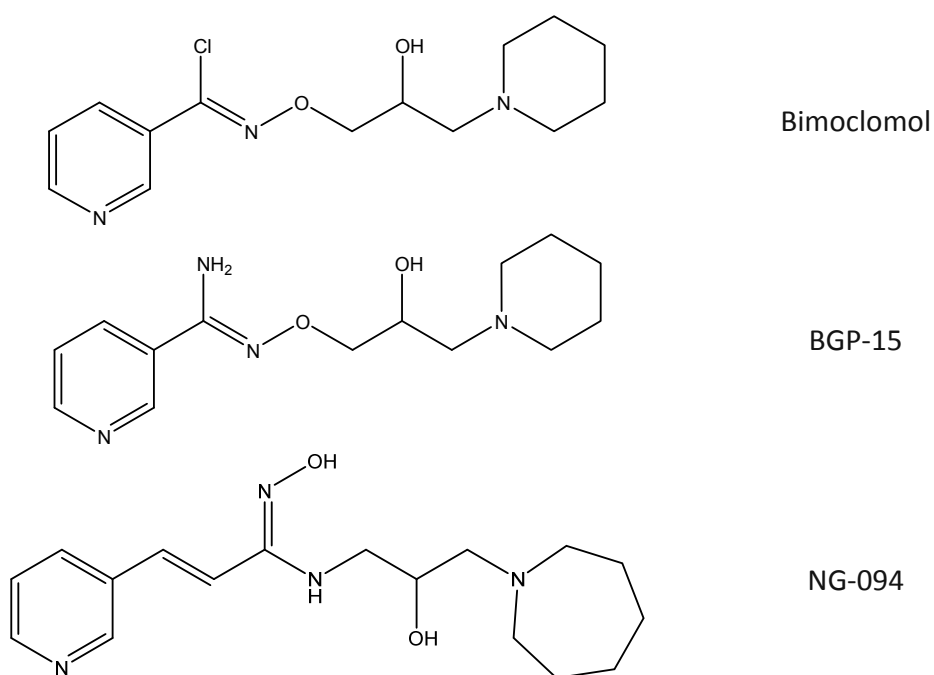


Figure 14: Hydroxylamine derivatives structures.

3.2 Membranes construction and equilibrations

The system studied was an asymmetric membrane made of brain BSM (N-octadecanoyl-D-erythro-sphingosylphosphorylcholine) and CHOL with/without BGP-15 at pH=7. The BSM/CHOL membrane was made of 30 BSM and 23 CHOL molecules in one leaflet, and of 19 BSM and 26 CHOL molecules in the other. 5 BGP-15 molecules were added on both layers. The simulation box dimensions were X=101.27 Å, Y= 6.66 Å and Z =46.26 Å. 4080 molecules of water to reach the density of 0.997 g/mL have been added. The simulations were carried out with the program YASARA.

Membrane was built and equilibrated as described in Paragraph 2.4.1.

To study the distribution and favorable localization of BGP-15 in a lipid membrane, I applied unconstrained atomistic MD simulations based on passive distribution between bulk water and bilayers. I placed 10 molecules of BGP-15 at random locations and orientations in bulk solution at the vicinity of 5-8 Å from the bilayer surface. The molecules of BGP-15 that were placed at random distances docked to the membrane in the first nanosecond of all simulations.

3.3 Results and discussion

3.3.1 Density profile

In characterizing the average structure of the membrane at different regions along its normal axis probably the most important tool is the density profile of various atoms or atomic groups. The calculation of density profiles is a rather straightforward task: the average occurrence of the atoms of interest per conformation has to be counted in different lateral slices of the membrane and divided by the volume of the slice.

As highlighted in the Fig. 15, which represents the asymmetric BSM-CHOL model membrane, it has been observed the docking of the drug at the water-lipid interface. BGP-15 interference with the membrane could modify the relative spatial positioning of its constituents as shown by the changes of density profile (Fig 16). Docking of BGP-15 is induced by high cholesterol level and its permeation is mildly influenced by the membrane composition. In addition, the docking of BGP-15 on the membrane triggers a reorganization of cholesterol and sphingomyelin with an increase of order of BSM in the outer layer. Furthermore, the slight movement of cholesterol toward the surface permits an increase of fluidity in the mid-section of the membrane (not reported).

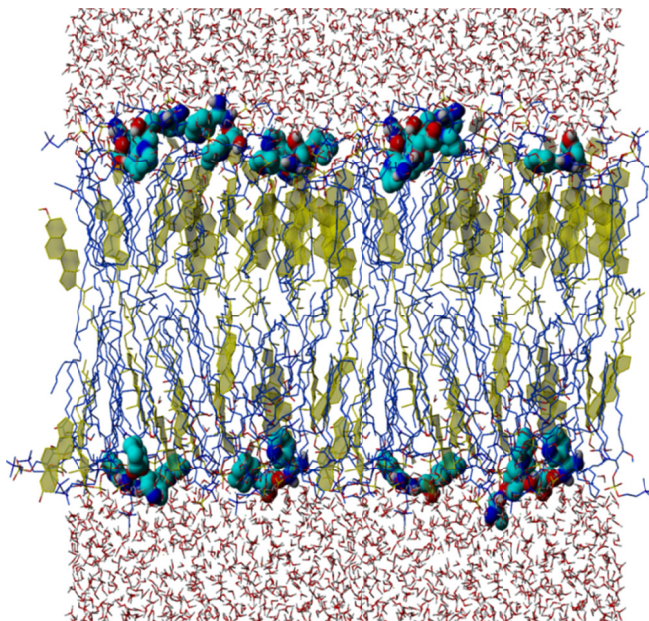


Figure 15: BSM/CHOL membrane after 5ns of MD. BSM is blue, cholesterol in yellow and BGP-15. All other atoms are colored using the CPK scheme.

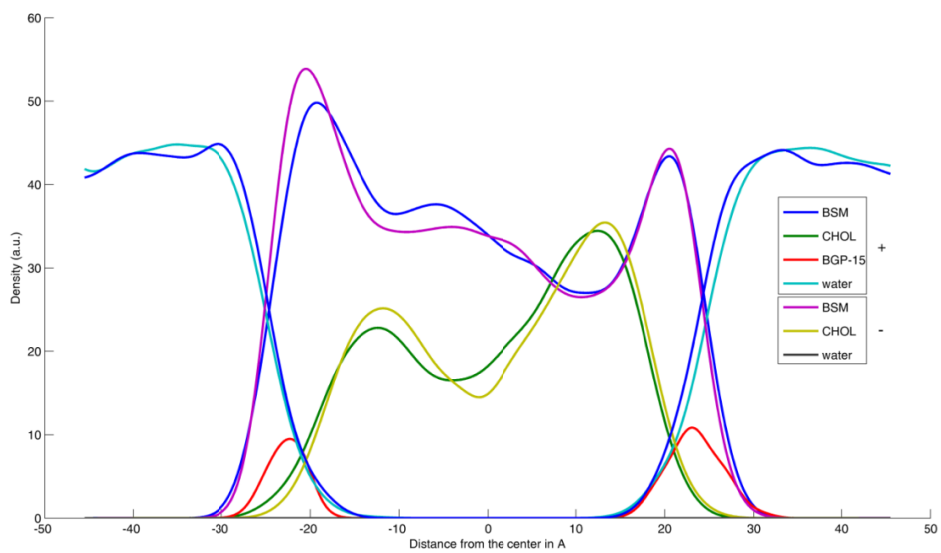


Figure 16: Position of BGP-15 molecules (in red) and structural changes of BSM/CHOL membranes after addition of BGP-15. The control membrane is indicated with -; the membrane upon addition of BGP-15 is indicated with +.

The BGP-15 molecules reach, by diffusion, the bilayer within 1 ns and snorkel just under the level of BSM phosphorous in the subsequent 5 ns. The permeation of BGP-15 is mildly influenced by the composition. Since the model membrane was built with a certain degree of asymmetry, with a higher cholesterol ration of the outer side, it has been have observed that the docking of BGP-15 is induced by high cholesterol level. The docking of BGP-15 molecules on the membrane triggers a reorganization of cholesterol and sphingomyelin with an increase of order of BSM in the outer layer. The slight movement of cholesterol toward the surface permits an increase of fluidity in the mid-section of the membrane.

This study, in collaboration with Prof. Laszlo Vigh (Institute of Biochemistry, Biological Research center, Hungarian Academy of Sciences, Szeged), indicates that BGP-15 is able to permeate into the surface membranes and to associate preferentially to CHOL-enriched lipid platforms.

4. Effect of hydroxylamines in modulating membrane physical state



For decades, protein denaturation has been thought to act as a major trigger for HSP induction. However, increasing evidence now shows that many stress events cause HSP induction without commensurate protein denaturation. That recognition, already described in Chapter 3, has led to the “membrane sensor” hypothesis where the membrane physical properties and microdomain organization play an initiating role in the heat shock response.

I hypothesize that the linkage between membrane state and HSPs is not coincidental, but casual, as “membrane defects” are known to cause suboptimal hsp-gene expression. I here address the effect of BGP-15, NG-094 and BMC on cholesterol-rich distribution patterns.

4.1 Membranes construction

The systems studied are 4 symmetric membranes made of 35 molecules of BSM and 14 molecules of CHOL in each leaflet. Three membranes were doped with BGP-15, NG-094 and BMC, respectively (5 molecules on both layers) to generate four different systems: BSM/CHOL, BSM/CHOL/BGP-15, BSM/CHOL/NG-094 and BSM/CHOL/BMC.

The BSM/CHOL membrane had simulation box dimensions of $X=100.29 \text{ \AA}$, $Y=47.36 \text{ \AA}$ and $Z=46.78 \text{ \AA}$ with 3764 H_2O molecules, 10 Na^+ and 10 Cl^- .

The BSM/CHOL/BGP-15 membrane had simulation box dimensions of $X=99.99 \text{ \AA}$, $Y=47.22 \text{ \AA}$ and $Z=46.64 \text{ \AA}$ with 3835 H_2O molecules, 11 Na^+ and 11 Cl^- .

The simulation box dimensions of BSM/CHOL/NG-094 were $X=103.44 \text{ \AA}$, $Y=47.59 \text{ \AA}$, and $Z=47.14 \text{ \AA}$. 3777 molecules of H_2O , 11 Na^+ and 11 Cl^- have been added.

The simulation box dimensions of BSM/CHOL/BMC were $X=99.99 \text{ \AA}$, $Y=47.22 \text{ \AA}$ and $Z=46.63$. 3835 molecules of H_2O , 11 Na^+ and 11 Cl^- have been added.

Membranes were built and equilibrated as described in Paragraph 2.4.1.

All the simulations were carried out with the program YASARA at pH 7.4.

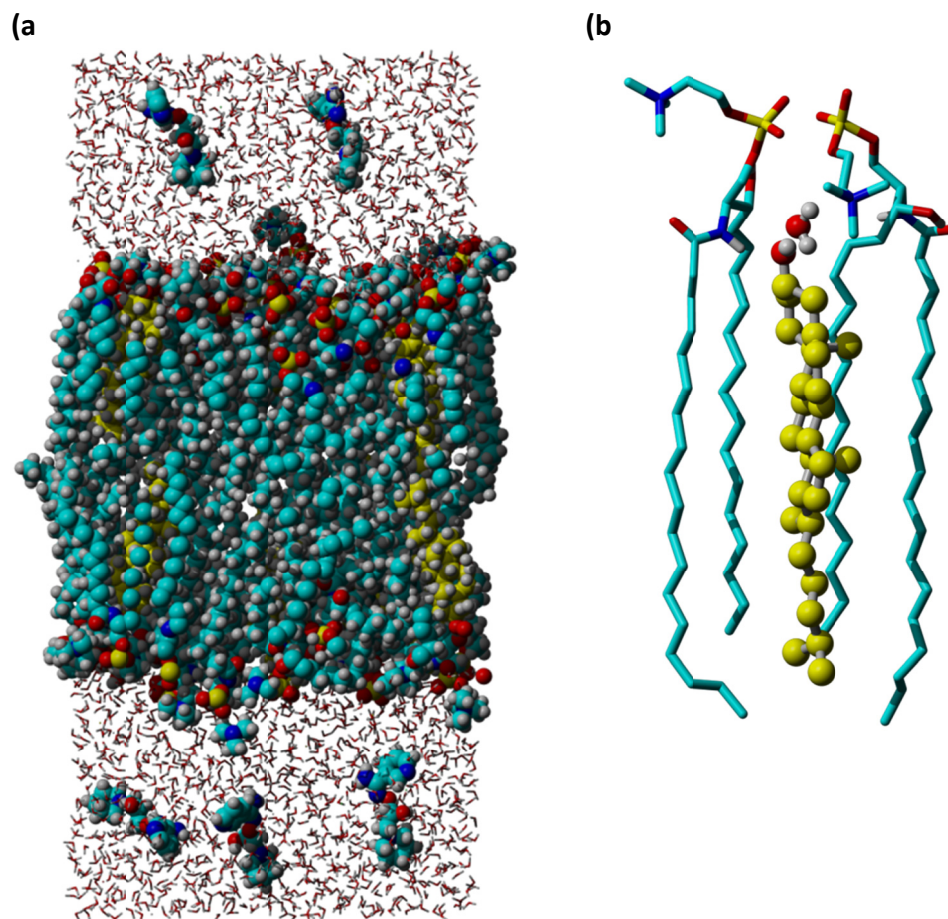


Figure 17: Figure (a) represents a slice of 10 nm of the simulation box at time $t=0$. BGP-15 molecules are visible in the water. The local organization of a molecule of CHOL is shown in (b) after 20 ns. The BSM head groups are influenced by the addition of BGP-15 and permit water molecules to reach cholesterol molecules. Cholesterol carbons are represented in yellow, carbon in cyan, oxygen, nitrogen and hydrogen in red, blue and grey respectively.

4.2 Results and discussion:

In a complex membrane, the BSM-CHOL domain is in a liquid-ordered phase where the hydrocarbon chains are largely in the all *trans* state. Hence, one would expect the bilayer to have a greater thickness in this region. Atomic force microscopy experiments indeed report a larger thickness of the raft-like domains [111]. A method to calculate the average membrane thickness is the peak-to-peak separation of an electron density profile, as the peaks represent the location of electron-rich PO_4^{2-} groups. The addition of HA molecules induced a reduction of the thickness of the BSM-CHOL membranes, though only NG-094 was capable to thin the bilayer of circa 0.3 nm, while BGP-15 and BMC maintained the thickness and the lipid packing substantially unaltered. Interestingly, though the latter two molecules reduced the global energy of the system resulting in the stabilization of the membranes, this was not true for NG-094, probably because it is a slightly bulkier molecule than BGP-15 and BMC (of circa 30 \AA^3).

The thinning of the membrane is probably responsible for the tilting of cholesterol molecules observed in NG-094 (Fig. 19). BMC molecules do not alter the orientation of cholesterol molecules. This is a strong indication that BMC, similarly to BGP-15 and more than NG-094, does not alter the overall order of the bilayer.

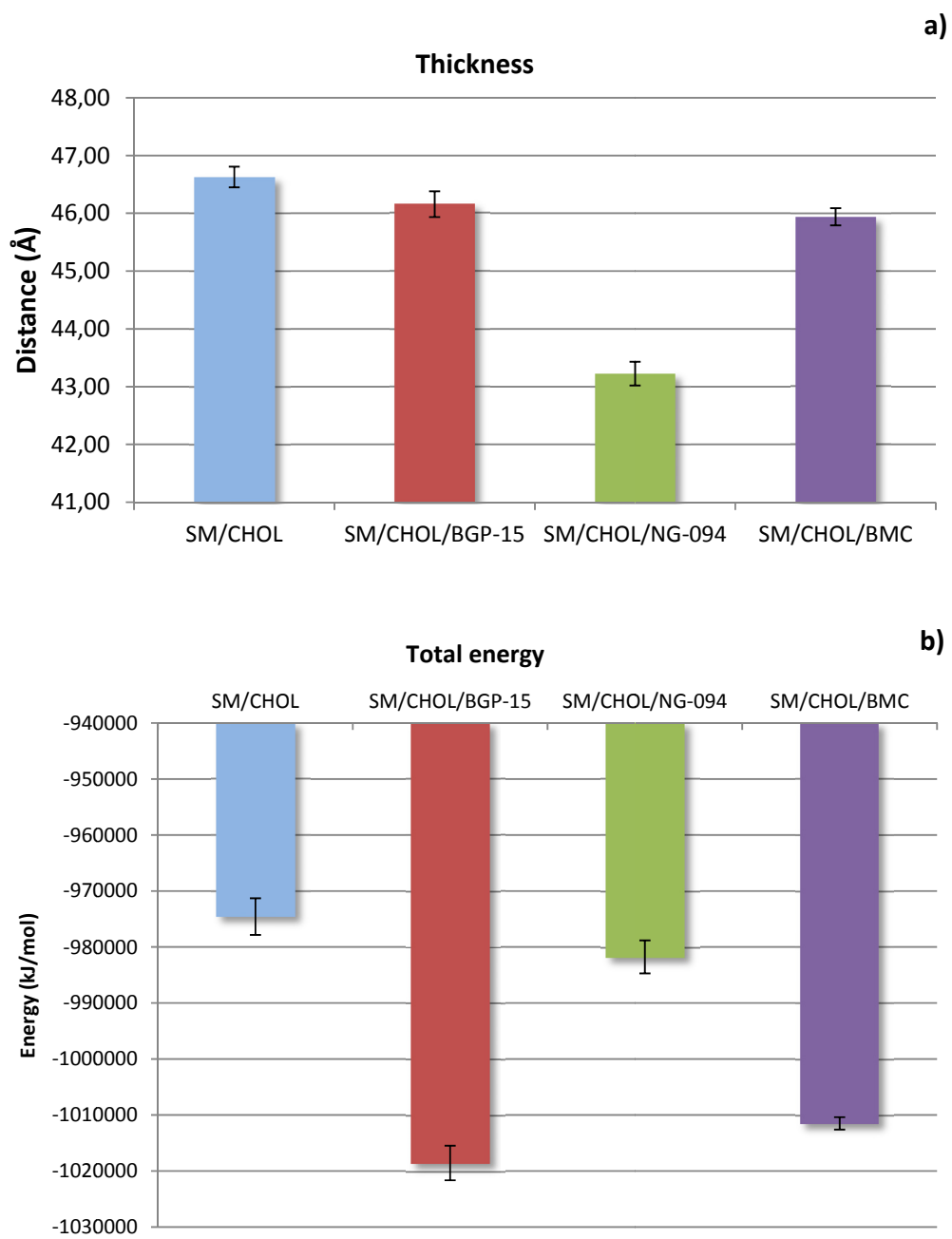


Figure 18 Thickness (Å) (a) and total potential energy (kJ/mol) (b) of the membranes BSM/CHOL. The error bars were calculated on 20 snapshots over the last 5 ns of simulation.

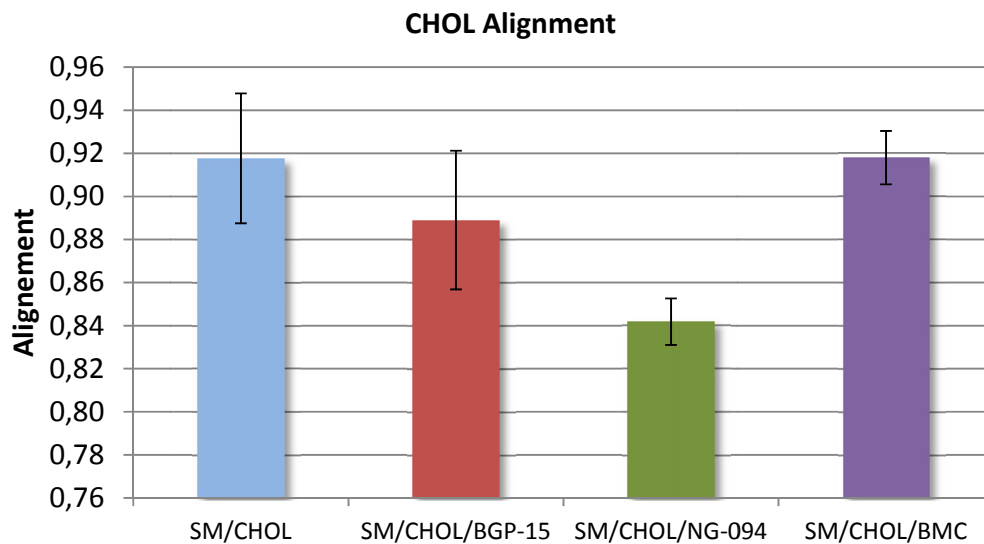


Figure 19: Orientation of cholesterol molecules respect of the normal to the membrane surface. 1 corresponds to perfect alignment. The error bars were calculated on 20 snapshots over the last 5 ns of simulation.

4.2.1 Radial distribution function

The radial distribution function (RDF), $g(r)$, is a useful tool to describe the structure of a system. Specifically, it is a measure of, on average, the probability of finding an atom in a shell dr at the distance r of another atom chosen as a reference point (Fig. 20) [112]. Interacting systems are characterized by RDFs that express peaks and valleys, which describe regions of high and low density, respectively.

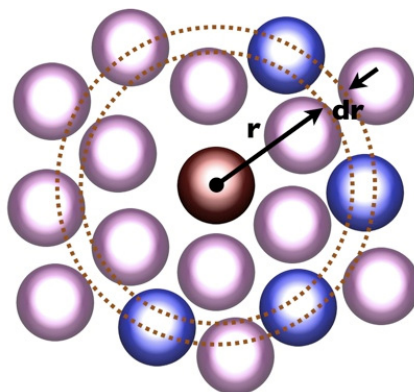


Figure 20: Space discretization for the evaluation of the radial distribution function.

The RDF for the pair O_{ch} and the BSM phosphorous (P) (Fig. 21a) is a measure of the lateral packing of the membrane. Compared with the pure BSM/CHOL membrane, the bilayer doped with BGP-15 shows a reduced packing, whereas NG-094 and BMC increase the O_{ch}-P coordination.

In BSM/CHOL membranes, the cholesterol tend to limit the interaction with water. The first peak at 3.4 Å indicates that the O_{Ch} has enough space to form hydrogen bond with one water molecule. The large hydrophobic body of the cholesterol is covered by the head groups of neighboring BSMs (see Figure 17b) according to the Umbrella model [113].

The RDF for the cholesterol oxygen (O_{ch}) and the water oxygen (O_{hh}) shows the typical distribution with the first water shell at 2.3 Å and the second water shell at 3.4 Å around the cholesterol (Fig. 21b). At larger distances no peaks are detectable as expected in systems with low order. The O_{ch}-O_{hh} distance is shorter than a normal hydrogen bond, because the water can hardly penetrate the BSM head groups and there is no space enough to place O_{hh} at 2.6 Å, that is

the minimum required for H-bonding. The penetration of water is increased by the addition of hydroxylamines that expose cholesterols to the medium.

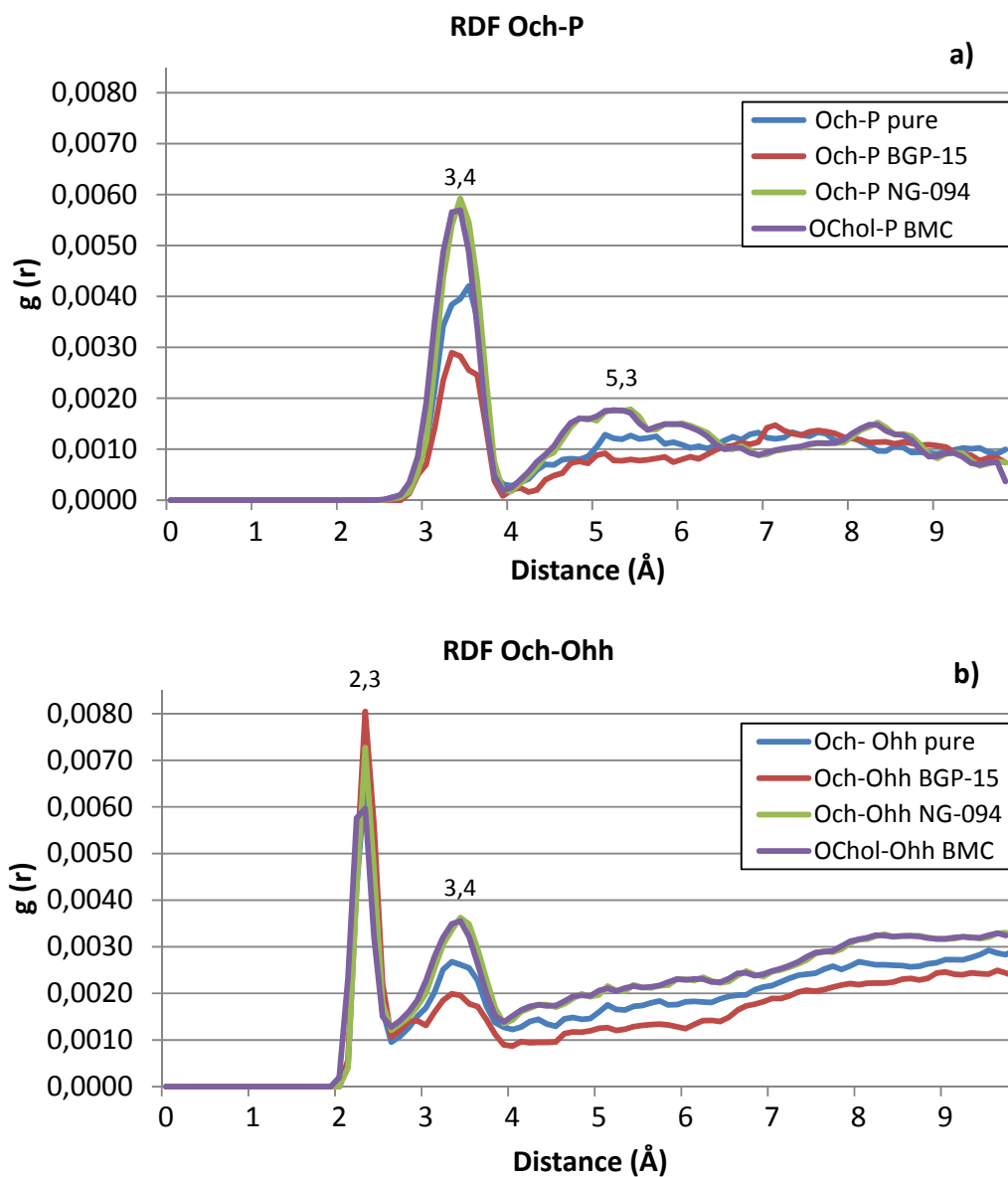


Figure 21: Comparison among the radial distribution function for the pair cholesterol oxygen (Och) and the BSM phosphorous (P) (a), and for the pair Och and the water oxygen (Ohh) (b).

4.2.2 Charge distribution

In pure BSM/CHOL membrane it is possible to measure a positive charge deep inside the membrane and two charged regions near the membrane surface. These two regions correspond to the NH_3^+ and to PO_4^{2-} groups of the BSM head. The outer region of membranes is positively charged and is counterbalanced by the presence of Cl^- ions in solution. The region occupied by phosphate groups represents the main barrier to the diffusion of apolar molecules through the membrane. The charge distribution of the solvent (not represented) shows a fraction of Na^+ ions closely interacting with this region.

BGP-15 and NG-094 show an opposite behavior in the charge distribution of the membrane. In fact, BGP-15 induces a protrusion of the NH_3^+ group from the membrane surface, whereas NG-094 induces a folding of the NH_3^+ groups toward cholesterol oxygens. The reorganization of the surface is not directly evident from the thickness values, since the thickness is usually calculated from the position of phosphates. BGP-15 and NG-094 modify the charge distribution across BSM/CHOL membranes and, consequently, may alter the free energy of binding of a protein inserted in a membrane. The variation of the free energy has also consequences in the kinetic of the passive transport of water and other little molecules across the membrane. The experiments clearly indicate that the three hydroxylamines are capable to radically alter the charge distribution of the membrane.

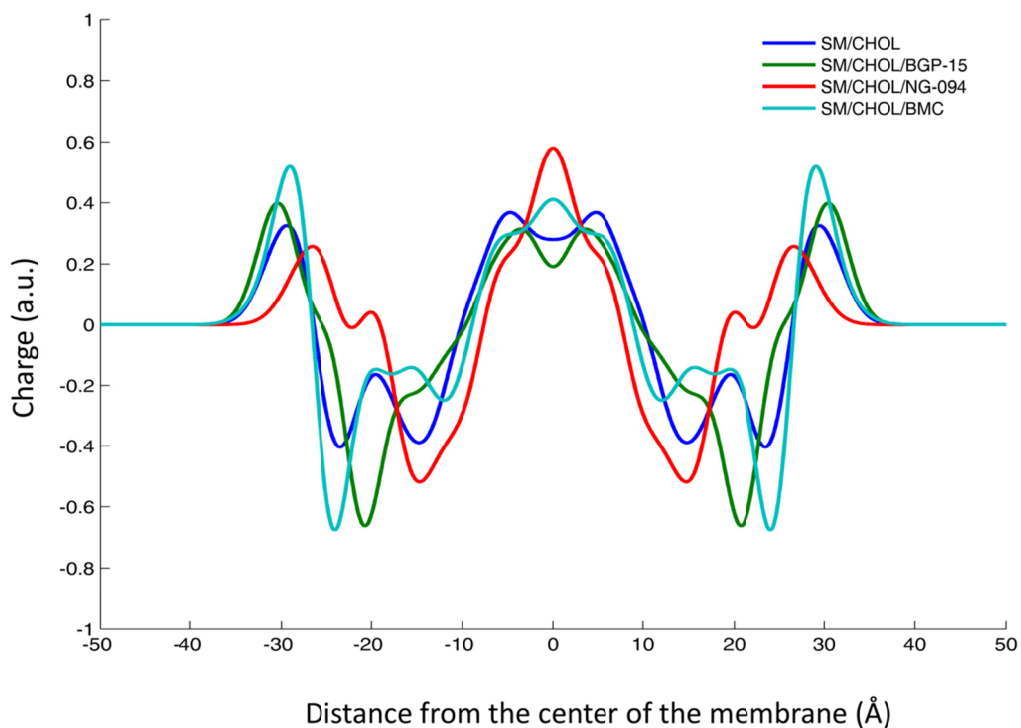


Figure 22: Charge profile of the BSM/CHOL membranes. The blue line represents the charge of the pure membrane. Solvent and hydroxylamines charges are not represented.

4.2.3 Density profile

The density profiles (Fig. 23) permit to compare the effect of hydroxylamines on the distribution and the orientation of BSM, CHOL and water in the membrane. NG-094 induces a thinning of the membrane (see also Figure 23a) triggered by a higher interdigitation of BSMs and a slight movement of CHOLs away from the center of the membrane (data not shown).

BMC and BGP-15 have a soft impact on the membrane, without substantial alteration of the lipophilic core. BMC and BGP-15 induce a protrusion of the head groups of BSMs (see also Fig 18a), which lead to a higher solvation of the CHOL

oxygens. Density profiles reveal that the interdigitation in these bilayers is directed by the long chains of BSM and that CHOL does not take part in it.

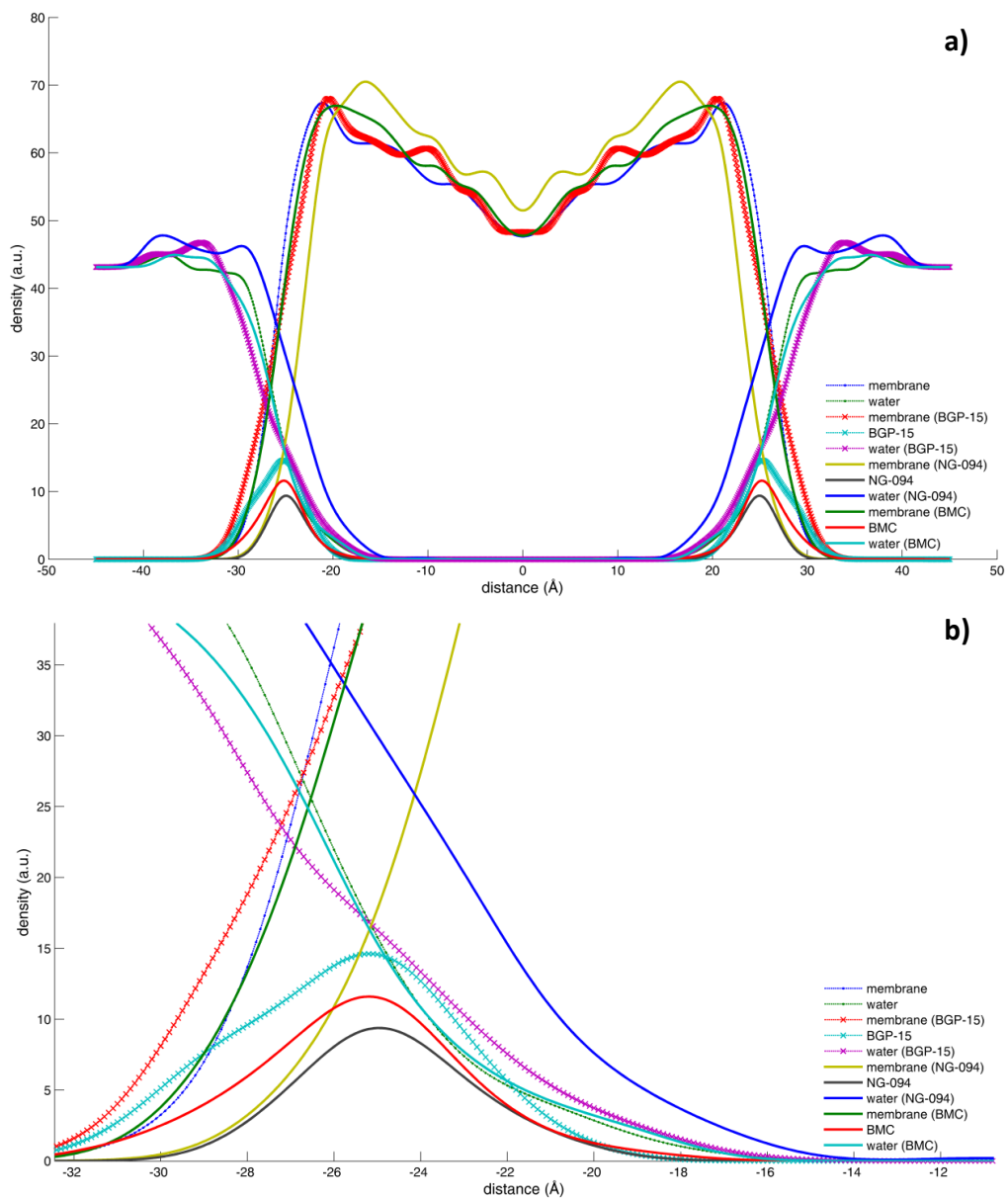


Figure 23: Comparison among density profiles for BSM/CHOL membranes (a). Figure (b) represents a close up of the region centered at 20 Å from the center of the membrane.

4.3 Conclusions

Taking together, the aim of this MD study was to explore the ability of HA derivatives to modify the physical state of model membranes of BSM/CHOL. The concept of fluidity is far too simplistic to suit HA derivatives. In fact, due the inhomogeneous nature of membranes, a drug can limit its effect on a narrow part or on the whole membrane. As such, I have discussed the action of BGP-15, NG-094 and BMC on the model membrane in terms of sterol tilting, charge, spatial distribution and lateral packing. The results demonstrate their ability to alter the physical state of model membranes while preserving the integrity.

5. Cholesterol removal upregulates specific HSP's

In the last two years, several evidences accumulated showing upregulation of specific heat shock proteins as consequence of cholesterol depletion.

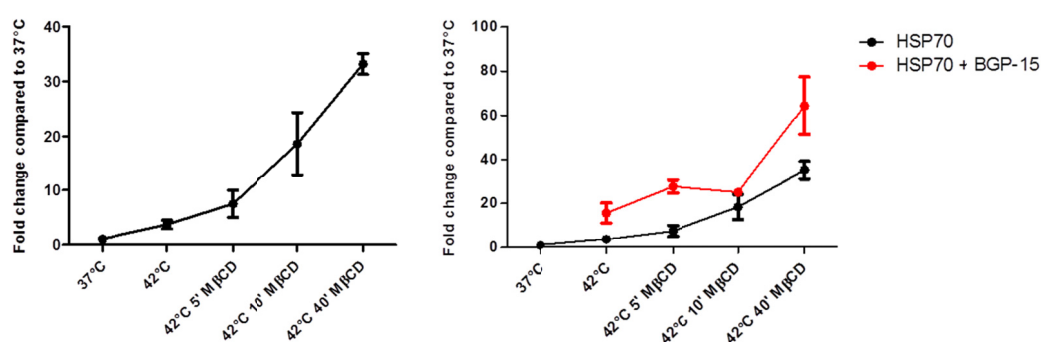


Figure 24: Effect of cholesterol removal in HEK293 lines (Crul et al, unpublished results).

Cholesterol depletion with methyl- β -cyclodextrin (MBCD) is commonly employed to establish the involvement of lipid rafts in a cellular process. A strongly reduced rate of CHOL depletion by MBCD caused by BGP-15 addition was documented *in vitro*.

Following the track of the previous study, I investigated the effect of different cholesterol concentration on the physical state of raft, and the synergic effect of hydroxylamines on raft domains.

5.1 Systems construction

Four all-atom lipid bilayer were used for models membranes made of BSM and CHOL at different concentrations (20, 30, 40 and 50%). BGP-15 and NG-094 were

added to each membrane to obtain a total of 12 membranes: 4 without drugs, 4 with NG, and 4 with BGP.

The 20% membrane consisted of 78 molecules of BSM and 20 of CHOL. The simulation box dimensions were X=145,61 Å, Y=47,54 Å and Z=46,01 Å. 20 Na⁺, 20 Cl⁻ counter ions and 7364 water molecules were added.

The 30% membrane was composed by 70 BSM and 28 CHOL, 21 Na⁺, 21 Cl⁻ counter ions and 7374 water molecules. The simulation box dimensions were X=145,56 Å, Y=47,10 Å and Z=46,21 Å.

The 40% membrane was composed by 60 BSM and 38 CHOL molecules. The simulation box dimensions were X=149,40 Å, Y=40,92 Å and Z=43,14 Å. I added 16 Na⁺, 16 Cl⁻ counter ions and 5778 water molecules.

The 50% membrane was composed by 50 BSM and 48 CHOL molecules. The simulation box dimensions were X=150,90 Å, Y=46,09 Å and Z=45,75 Å. 21 Na⁺, 21 Cl⁻ counter ions and 7053 water molecules were added.

Membranes were built and equilibrated as described in Paragraph 2.4.1.

The simulations were carried out with the program YASARA at pH 7.4.

5.2 Results and discussion

5.2.1 Binding energy

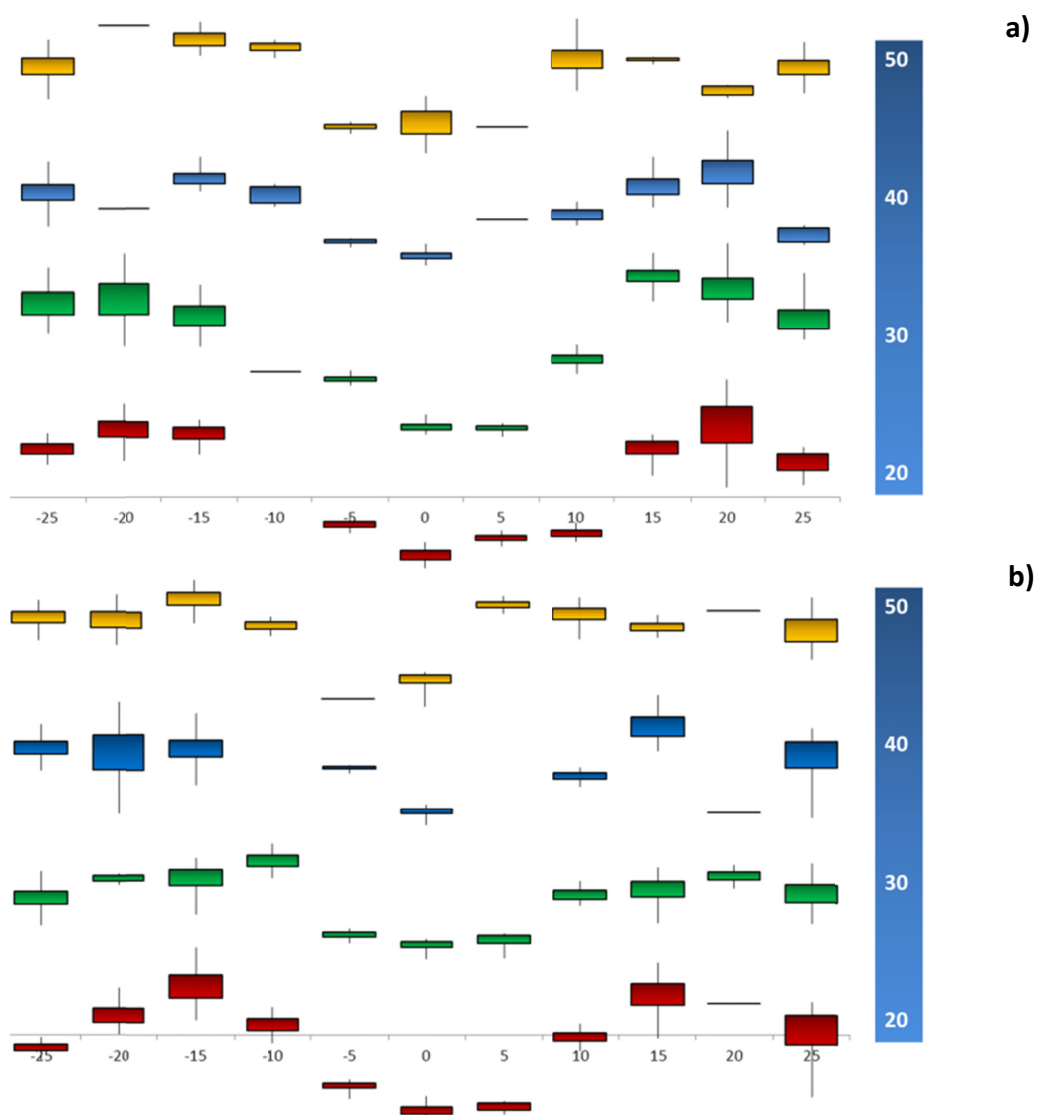


Figure 25: Binding energies calculated for BGP-15 (a) and NG-094 (b) interacting with BSM/CHOL membranes of different composition. 160 initial conformations have been generated for each membrane. On x-axis is reported the distance in nm from the center of the membrane. The y-axis (without scale)

represents the binding energies. On the right, the cholesterol content of membranes is indicated (20% corresponds to red candles, 30, 40 and 50% correspond to green, blue and yellow, respectively).

The binding energies are represented with candle stick diagram. Diagrams in Fig. 25 provide two kind of information: the position on the y-axis represents the strength of the drug-membrane interaction. Higher the value, better the binding. Secondly, the width of candle reflects the size of the conformational space available for the drug. Small candles mean that the drugs have few allowed conformations in a given portion of the membrane, whereas big candles indicate that the drug can explore more conformations. Though the hydroxylamines were uniformly placed in the membrane, the inner part of the membranes is clearly unfavorable for the drugs. The negative values of binding for both BGP-15 and NG-094, and the thickness of the candles in the inner part of the membranes, indicate that hydroxylamines cannot reach the middle point of the membrane. The structures with the highest values of binding energies, along with the 4 membranes at different cholesterol ratio without drugs, were chosen to run a full 50 ns molecular dynamics.

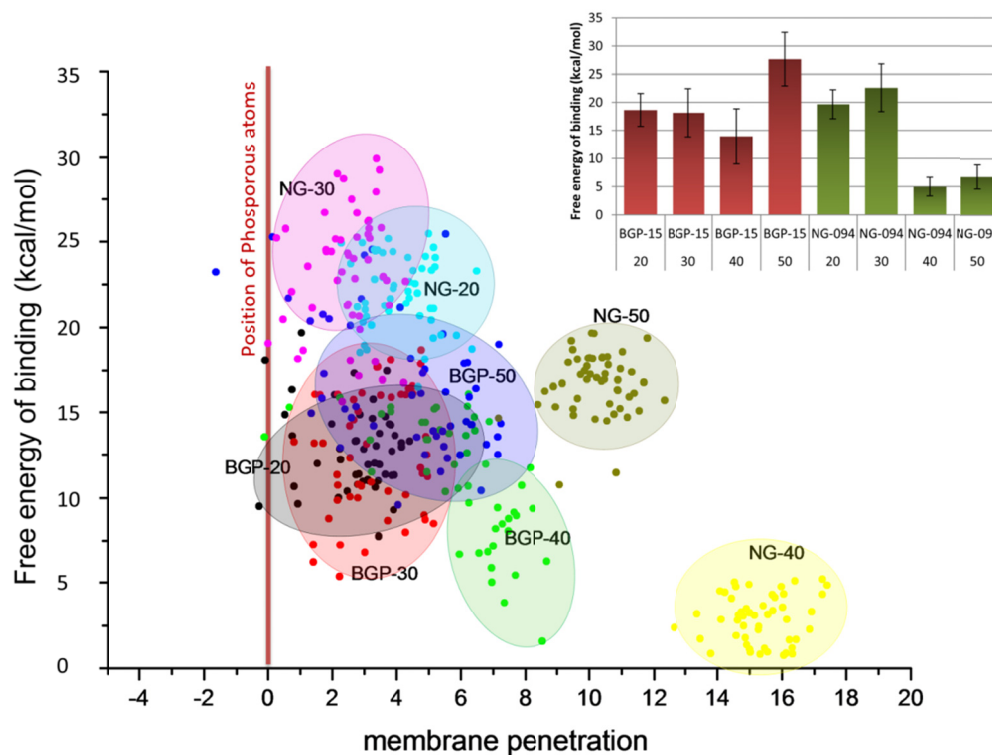


Figure 26: Calculation of free energy of binding of BGP-15 and NG-094 with model membranes. For each trajectory, the last 15 ns were analyzed and a snapshot was taken every 300 ps. Each dot represents the position of the drug baricenter through the membrane and the energy of binding. The averaged position of phosphorus atoms was taken as reference.

The trajectories have been analyzed over the last 15 ns. It was also taken a snapshot of the systems every 300 ps. The 50 snapshots were subsequently annealed and the binding energies calculated.

The results are shown in Fig. 26. The x-axis represents the position of the barycenter of the drug inside the membrane. The zero on the x-axis represents the position of the phosphorus atoms of the sphingomyelins. On y-axis is reported the binding energy in kcal/mol. With the exception of NG-094 in membrane with 40% and 50% cholesterol, the hydroxylamines penetrate the

membrane and remain just under the surface, behind the phosphorus atoms. Generally, NG-094 shows a better binding than BGP-15 with all membranes with exception of 40% cholesterol. This is related to the position of NG-094 inside the membranes. In fact, NG-094 induces a large perturbation in the 40% cholesterol membrane. This is also confirmed by the RDF of cholesterol oxygens-water oxygens of Fig. 29.

Both hydroxylamines can interact tightly with rafts: BGP-15 shows approximately the same binding with membranes of different composition. NG-094, which has overall a better binding than BGP-15, seems to prefer membranes with lower cholesterol content. This observation is consistent with preference of NG-094 for more fluid membranes.

5.2.2 Atomic energy contribution

The calculation of the contribution of each atom to the potential energies of BGP-15 and NG-094 can give some hints on the insertion mechanism. The contribution of an atom to the total potential energy is strongly influenced by the surrounding.

In Fig. 27 the 9 atoms with largest contribution to potential energy are listed. The nitrogen atom in the aliphatic ring, in both molecules, is responsible for large and positive interaction. This nitrogen atom appears capable to sense the cholesterol level in membrane.

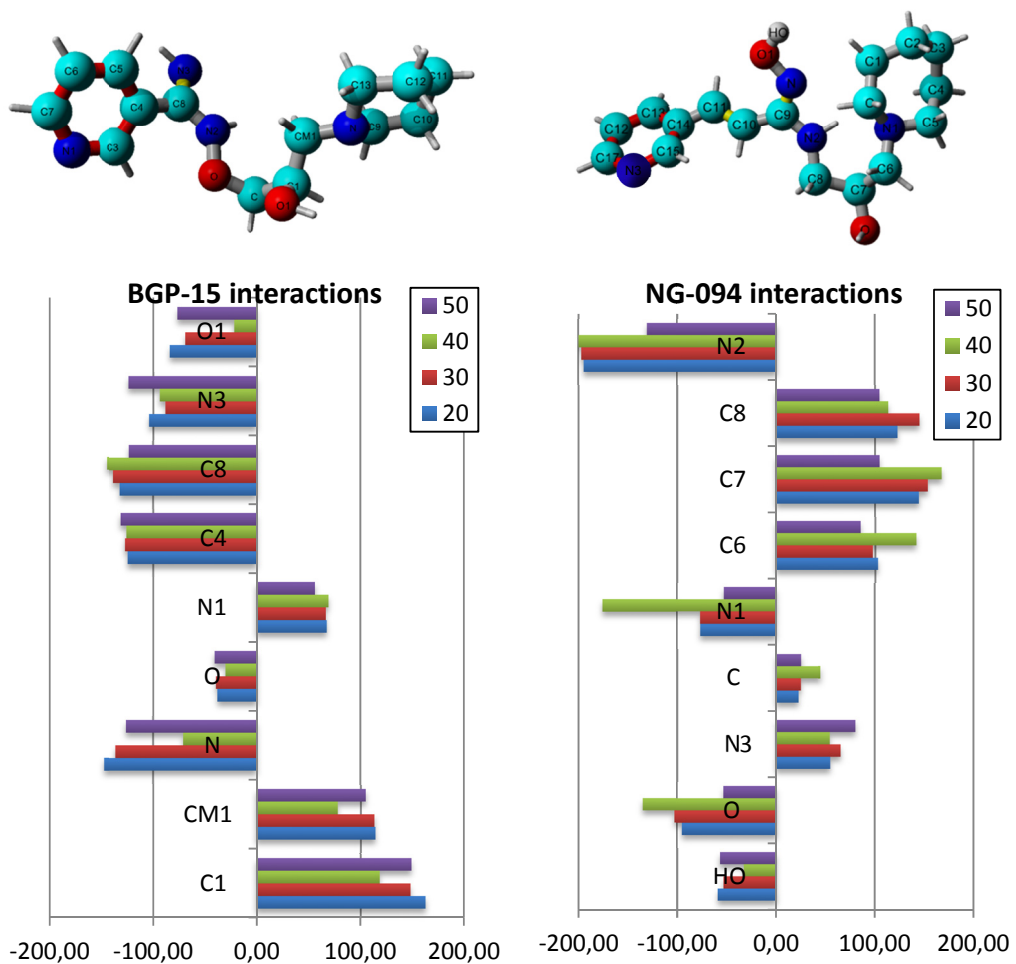


Figure 27: Potential energy decomposition. The atoms that mainly contribute to the potential energy of the drugs are indicated as colored bars. The labels are indicated in the ball and stick representations above.

5.2.3 Radial distribution function

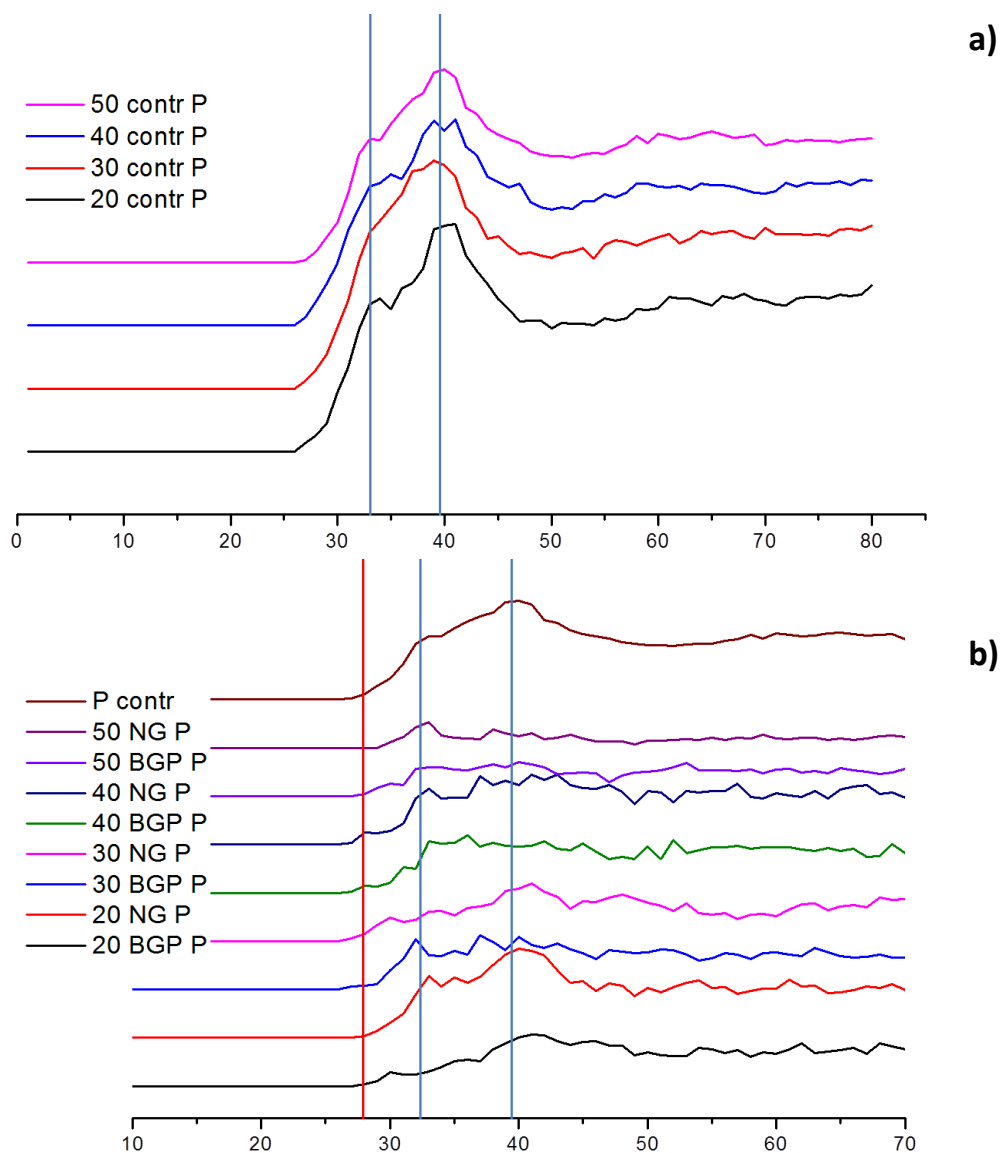


Figure 28: Radial distribution function. (a) Water organization around P atoms of sphingomyelin in membrane with 20, 30, 40 and 50% of cholesterol. (b) The upper curve of (a) representing the RDF of water-P in 50% cholesterol membrane is taken as control for water-P RDF in membranes after addition of BGP-15 and NG-094.

I have calculated RDF for water molecules around BSM phosphorus and cholesterol oxygen. Fig. 28 (a) shows the RDF for pure BSM/CHOL membranes at different composition. All membranes show the same organization with two peaks at around 3.3 and 3.9 Å, indicating two preferential orientation of water around P atoms. Since the profile is not significantly different for the four membranes, Fig. 28 (b) shows, as reference, the top line representing the RDF at 50% of cholesterol ratio. The addition of BGP-15 and NG-094 significantly alters the distribution. In fact, for 40% and 50% membranes, BGP-15 (and in minor extent NG-094) suppresses the water shell around P atoms. At 40% and 30%, the addition of these hydroxylamines allows water molecules to get closer, as indicated by an additional peak at around 2.8 Å. Surprisingly, for membranes with very low amount of cholesterol (20%), the addition of BGP-15 and NG-094 seems to have an opposite effect and, for the membrane 20% cholesterol doped with NG-094, the RDF profile is virtually identical to the unperturbed 50% cholesterol membrane.

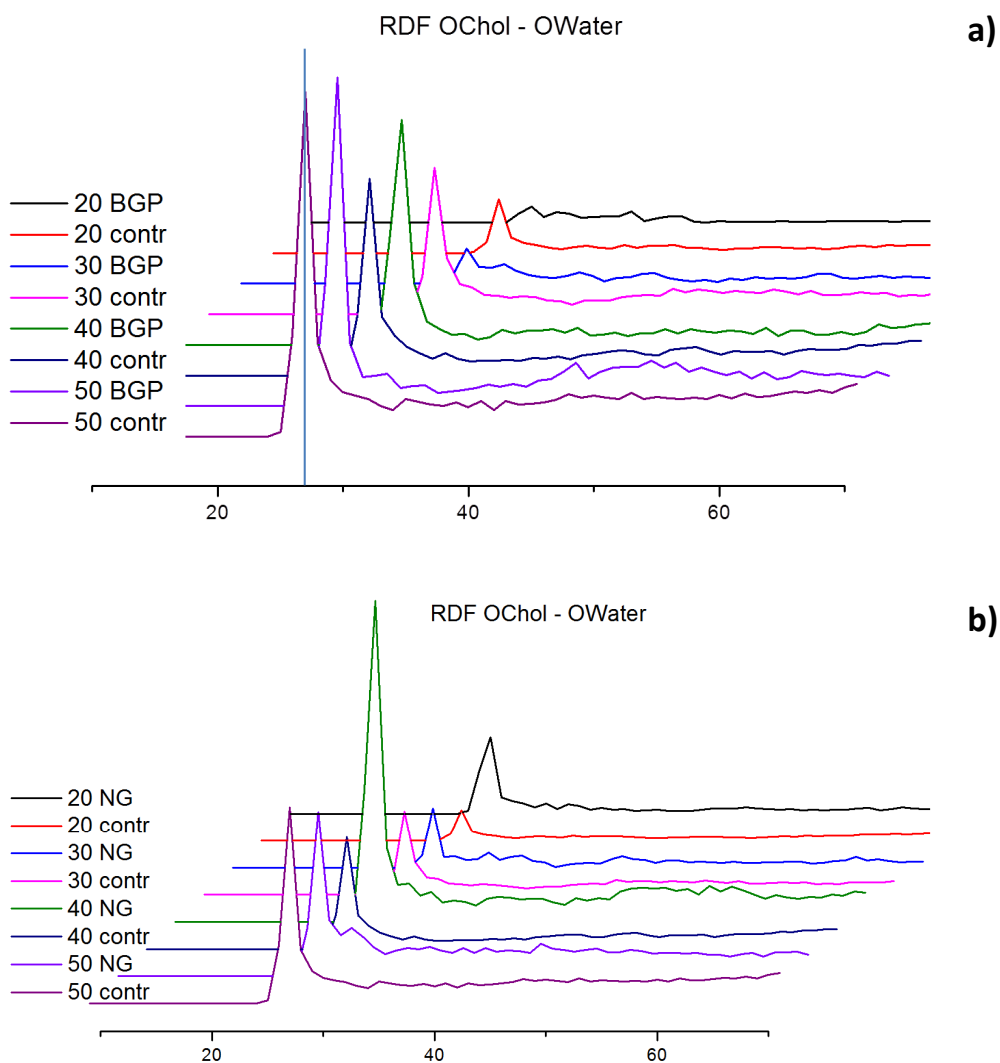


Figure 29: Radial distribution function of water molecules around cholesterol oxygens of membranes doped with BGP-15 (a) and NG-094 (b).

Fig. 29 shows the RDF of water molecules around the cholesterol oxygens. Since the number of cholesterol molecules is getting lower moving from 50% cholesterol to 20% cholesterol membranes, the height of the first peak at around 2.7 Å is reducing as well. In Fig. 29 (a) it is possible to see that, at low cholesterol

levels, BGP-15 is dramatically altering the water shell around cholesterol polar head. Fig. 29 (b) shows the effect of NG-094 on water distribution around cholesterol. Contrarily to BGP-15, NG-094 preserves the hydration of cholesterols. In 40% cholesterol membranes the addition of NG-094 improves the water organization around cholesterols.

5.2.4 Dynamical Cross-Correlation Matrix

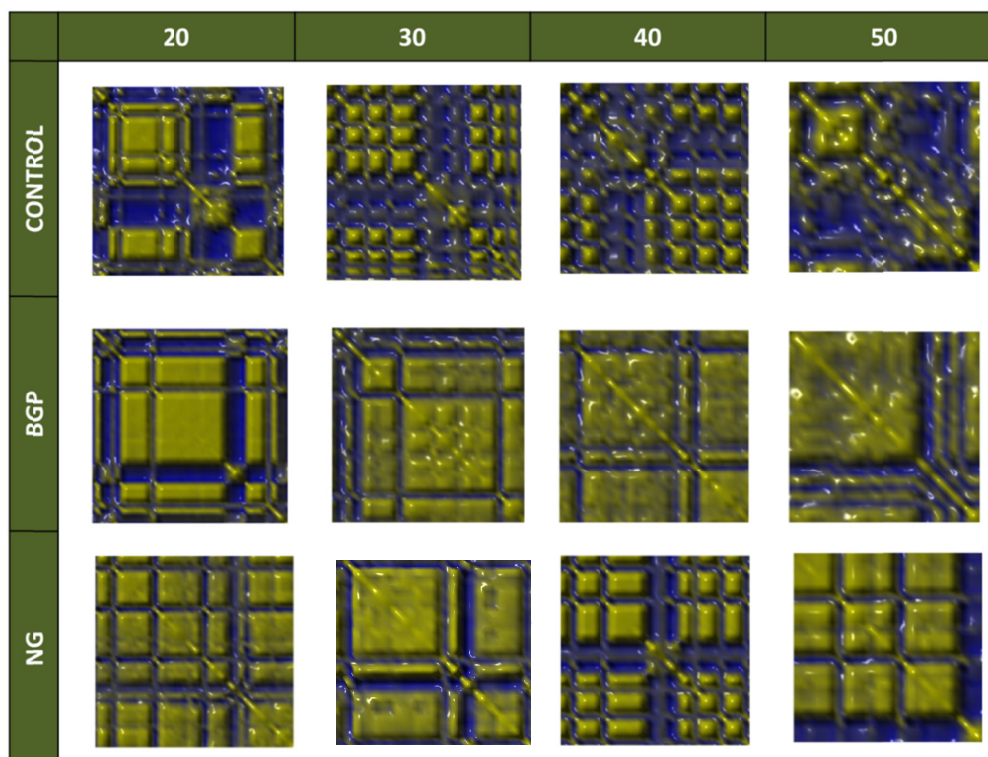


Figure 30: Dynamic cross correlation matrix of sphingomyelin phosphorous. The movement correlation of all P atoms of the layer interacting with drug, is analyzed. Yellow color corresponds to perfect correlation, blue corresponds to perfect anti-correlation.

The detection of transient rafts in simulated membranes remains an open issue, since the large time scale of raft formation usually precludes the molecular dynamics investigation. An imaging approach is often used to deduce the cluster formation. I have calculated the dynamic cross correlation matrix (DCCM) of sphingomyelin phosphorous, as in Fig. 30.

The DCCM shows how the movements of all selected pairs of phosphorous correlate. The values in the DCCM range from -1 (perfectly anti-correlated) to +1

(perfectly correlated). The values along the diagonal are always +1 (because the motion of an atom is perfectly correlated to itself). The highest correlations of the diagonal can indicate the presence of a cluster of sphingomyelins.

The DCCM between units i and j is obtained with the following formula:

$$DCCM_{ij} = \frac{\langle \vec{d}_i * \vec{d}_j \rangle}{\sqrt{\langle d_i^2 * d_j^2 \rangle}} \quad (\text{Eq. 1})$$

where d is the displacement between the current position and the position of P atoms in the membrane averaged during the last 10ns, and the angle brackets indicate the average over all samples.

The DCCM matrix for membranes of BSM/CHOL shows roughly a 60% of sphingomyelin phosphorous highly correlated. The data are compatible with existence of early stage of lipid cluster, in which a set of atoms starts a cooperative and coordinated motion. A high mobility could be easily associated to fluidity but the presence of cooperative and coordinated motion, even in the case of fast atom movements, can preserve important membrane properties such as stress profile.

The addition of both hydroxylamines reduce the coordination extent in sphingomyelin head groups, but BGP-15 shows a more evident effect.

5.2.5 Membrane fluidity

Membrane fluidity is an ill-defined and misleading concept. Since a lipid membrane is anisotropic, the “averaged” fluidity cannot capture the complex interactions inside the bilayer and how the physical properties of membranes are back regulated. The simplicity of the concept of fluidity is the reason for the popular use, though the use of a property that cannot be calculated, for its very nature, may mislead the investigator. For example, the addition of a fluidizer, as well as a temperature increase, certainly induce an increase in the mobility of lipid chains, but it is hard to predict which part, or section, of a membrane is affected most. Even more important, membranes have nonlinear response to heat stress and to the binding of drugs.

RDF and DCCM analysis helped to clarify the effect of BGP-15 and NG-094 on membrane structure. Both analysis indicate an increase in the hydration of sphingomyelin head groups and the losing of surface collective motion. However, the effect of hydroxylamines is not limited on altering the tightness of the membrane surface.

In Fig. 31, the overall mobility of all heavy atoms of the 20% and 40% cholesterol membranes is visualized in terms of B-factor.

The B-factor is defined as:

$$B = 8\pi^2\langle u^2 \rangle \quad (\text{Eq. 2})$$

Where $\langle u^2 \rangle$ is the mean squared displacement, the most common measure of the spatial extent of random motion. B-factor is measured in units of \AA^2 and can

be taken as indicating the relative vibrational motion of different parts of the structure. Atoms with low B-factors belong to a part of the structure that is well-ordered. Atoms with large B-factors generally belong to part of the structure that is very flexible.

The images are the result of 200 ps dynamics. The transparency, as well as the color of the atoms, depends on the root mean square displacement. Transparent atoms are more static, whereas more opaque atoms correspond to atoms that, during the short interval of 200 ps, are more mobile.

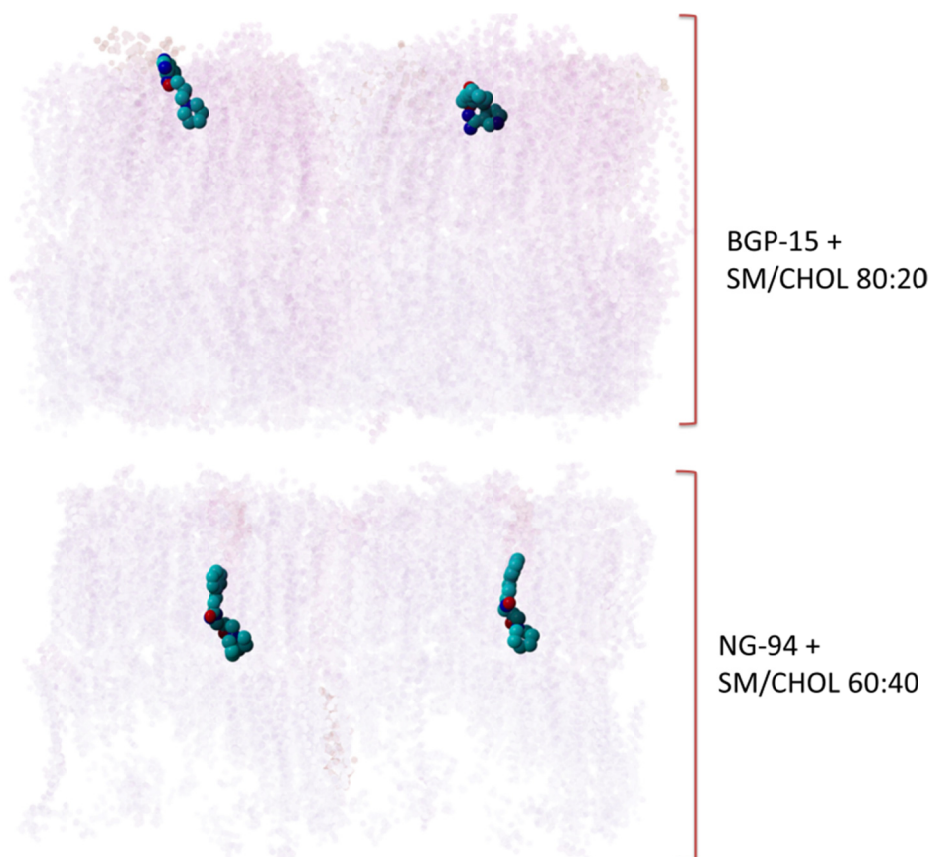


Figure 31: Mobility of heavy atoms indicated with transparency.

In Fig. 31 two typical situations are shown. The addition of BGP-15 to a membrane of BSM-CHOL with 20% in cholesterol induce an increase in the mobility of the whole membrane. The addition of NG-094 to a membrane containing 40% in cholesterol has a more localized effect and an increase of fluidity is observed only in the surrounding of NG-094. The localization of NG-094 may have a role in controlling the activity of membrane proteins.

A consequence of the higher layer mobility can be an altered propensity of the membrane to interact with the transmembrane portion of protein receptors.

5.3 Conclusions

Molecular dynamics investigation on BGP-15 and NG-094 on membranes of BSM/CHOL at different composition was extremely useful to understand some aspects of membrane functioning.

The present work was aimed to elucidate how, and to what extent, hydroxylamines are capable to mimic a heat shock stress in raft of sphingomyelin/cholesterol. I have found that BGP-15 and NG-094 can induce in membranes an alteration in fluidity similar to those induced by heat. The calculations revealed that the alteration in atoms mobility in rafts is of several angstroms and that BGP-15 and NG-094 affect differently the surface and the inner part of the membranes. The analysis of the surface structure shows a strong reorganization of BSM head groups and an increased penetration of water under the level of phosphorous atoms. The analysis of results indicates that NG-094 has a better penetration of the raft possibilities compared with BGP-15. Furthermore, these simulations suggest a critical role in the aliphatic ring of both

hydroxylamines. Moreover, I have observed that the effect of BGP-15 and NG-094 is limited to the outer layer but the effect in fluidity can interest tens of molecules surrounding the drug on the same layer. Since these drugs are capable to reduce the collective motion on the surface, hydroxylamines have a potential strong effect on microdomains reorganization. Finally, the sphingomyelin/cholesterol ratio in raft models is critical to shape the interaction of the drug and that a threshold concentration of cholesterol (around 40%) might separate two different interaction mechanisms.

6 Hydroxy arachidonic acid, a new potential non steroidal anti-inflammatory drug

The most part of my work focused on the interaction of fatty acids with cell membranes. Many of these molecules, in fact, have proven to be active against certain types of cancers and other diseases.

Among these molecules it is worth to mention the Minerval® [114-118], an analogue of oleic acid synthesized in the laboratory of Prof. Escribà, which shows a powerful anti-cancer effect coupled with absence of toxicity or side effects. Minerval regulates cellular activity by modulating the membrane lipid structure of cancer cells and leads to a reduction of up to 80% in the development of lung cancer and glioma cells.

Another promising fatty acid, which showed high anti-inflammatory activity, is a modification of arachidonic acid: the 2-hydroxy arachidonic acid (AAOH).

Due to the similarity with arachidonic acid (AA), that is the natural substrate of cyclooxygenase (COX), it was important to investigate the binding of AAxOH with COX-1 and COX-2, compared to that of AA.

The docking study was performed considering flexible both ligand and receptor. In the first part of this chapter I will briefly introduce the COX system, then I will describe the work and I will discuss the results.

6.1 The COX system

The cyclooxygenase (COX) functions as a membrane-associated homodimer, catalyzing the committed step in the conversion of AA to prostaglandin H₂

(PGH₂), following AA's release from membrane phospholipids. An overview of this reaction is depicted in the figure below:

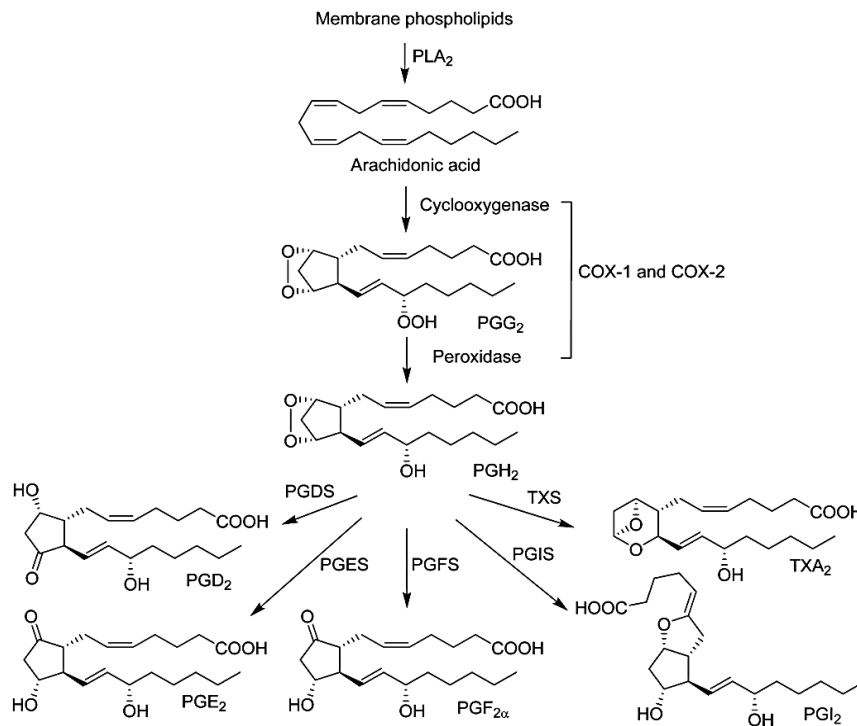


Figure 32: Prostaglandin biosynthetic pathway. PLA₂, phospholipase A₂; COX, cyclooxygenase; PG, prostaglandin; PGDS, prostaglandin D₂ synthase; PGES, prostaglandin E₂ synthase; PGFS, prostaglandin F₂ synthase; PGIS, prostaglandin I₂ synthase; TXS, thromboxane A₂ synthase, TXA₂, thromboxane A₂ [119].

COX is a bifunctional enzyme with two active sites. At the cyclooxygenase active site, COX controls the regio and stereo-selective bis-dioxygenation and cyclization of AA to form PGG₂. The reaction concludes at the entirely distinct peroxidase site, where intermediate PGG₂'s C15 hydroperoxide is reduced to an alcohol to form PGH₂.

The genome codes two 60% sequence-identical isoforms of COX. Both COX-1 and COX-2 catalyze the same reaction, and the discussion which follows applies to both.

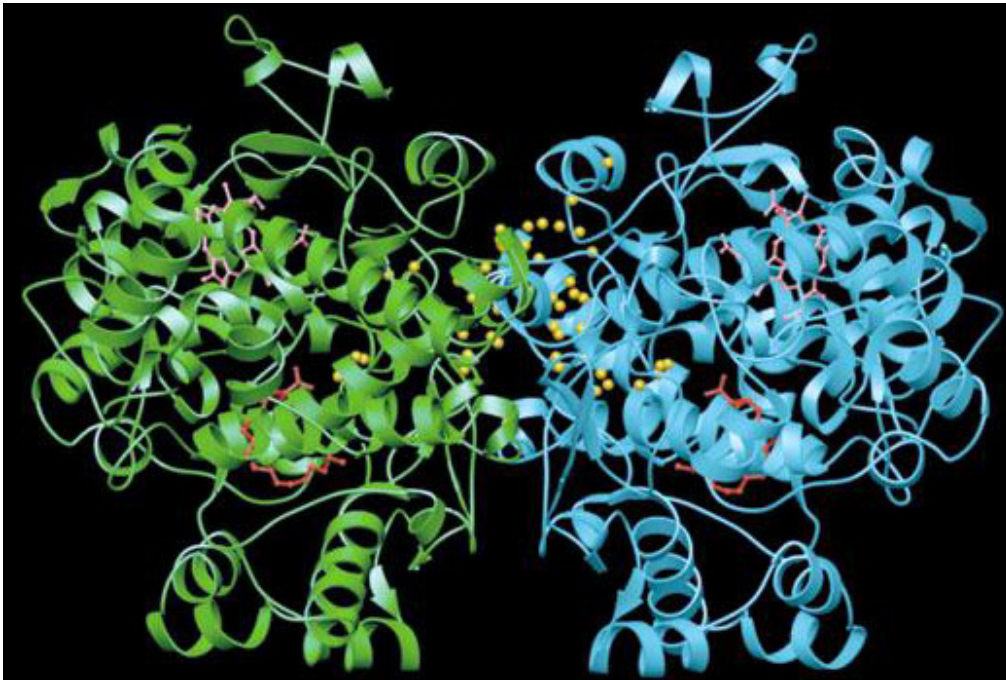


Figure 33: The two monomers (coloured green and blue) of the COX-2 dimer shown from the side. Cyclooxygenase and peroxidase active sites are marked by AA (red) and heme molecules (orange), respectively. Solvent molecules are shown as yellow spheres [120].

The COX reaction product PGH_2 is unstable [121, 122] and its bioactivity is imparted downstream by tissue-specific synthases which swiftly convert PGH_2 to other bioactive prostaglandins, as shown in Fig. 32. These prostaglandins, in turn, bind to G-protein-coupled receptors and effect diverse biological responses [123].

COX inhibitors (Aspirin being most famous) are therapeutically useful as antiinflammatory, analgesic, anti-pyretic, and anti-coagulant agents. As a group, these inhibitors are commonly known as non-steroidal anti-inflammatory drugs (NSAIDs). The physiological impacts of NSAIDs result from the drop in downstream prostaglandin concentrations which follows COX inhibition. To understand how COX inhibitors bind to the enzyme active site, it is helpful to review both the reactions catalyzed by cyclooxygenase, and the features that nature has evolved in the cyclooxygenase active site to bind arachidonic acid and tightly control its conversion to PGG₂.

Arachidonic acid (5,8,11,14-eicosatetraenoic acid or AA) has three bis-allylic methylene carbons (C7, C10, and C13, located between the cis double bonds). These carbons are readily oxidized non-enzymatically and the abstraction of a hydrogen atom at any of these positions yields a planar pentadienyl radical. In solution, O₂ molecules can add to either face of this radical, at the first, third, or fifth carbon which bear the unpaired electron spin density. Moreover, oxygen additions at the first or fifth carbon result in a final conjugated product which can be configured Z,E or E,E [124, 125]. Thus, for each of the three bis-allylic methylene carbons in arachidonic acid, an initial oxygenation can yield any one of 10 possible hydroperoxide products.

Oxygenation is only one possible fate for pentadienyl radicals, which can also propagate through intramolecular abstraction of other labile hydrogens, forming rings. Alternately, pentadienyl radicals can be quenched upon reaction with non-oxygen radical traps [126].

In contrast to these combinatorially diverse AA radical reaction products in solution, the enzymatic bis-dioxygenation and cyclization of AA at the

cyclooxygenase active site is strikingly specific, yielding (nearly) exclusively PGG₂. Impressively, key details of the cyclooxygenase reaction were unveiled by Samuelsson's radio-labeling experiments in the 1960s - long before the enzyme's isolation from tissue homogenates [127]. In part because of this work, he shared the 1982 Nobel Prize in Medicine. Our current understanding of the mechanism is shown in the figure below. In the following section, the mechanism will be discussed in greater detail, in the context of COX active site structural features.

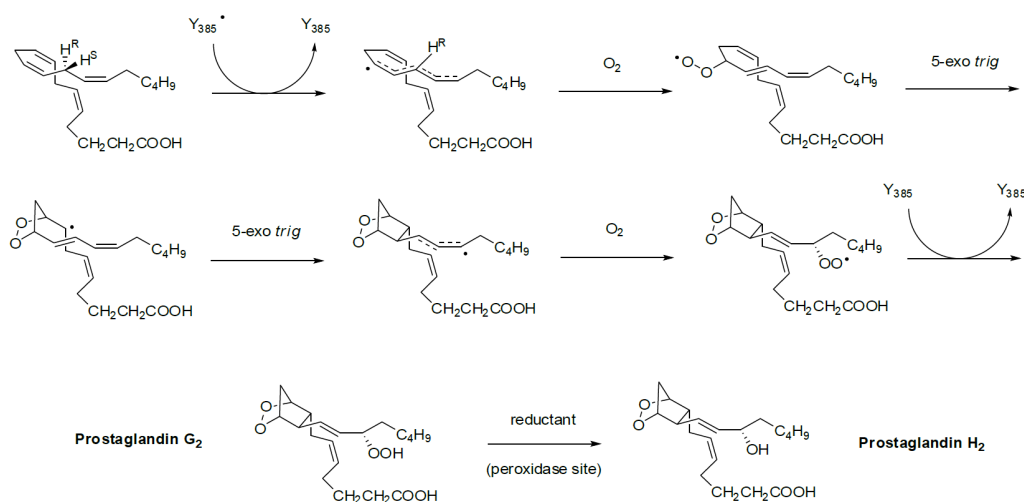


Figure 34: Mechanism of action of COX enzyme. PGG₂ is synthesized at the cyclooxygenase site through a free radical mechanism, in which two molecules of oxygen are added to arachidonic acid. The final product, PGH₂ is the result of a reduction at the distinct peroxidase site.

A tour of the enzyme active site aids a rationalization of the COX reaction mechanism. As suggested by Fig. 34, the first requirement for catalysis is a long, hydrophobic cavity to bind and anchor arachidonic acid in a bent conformation [128].

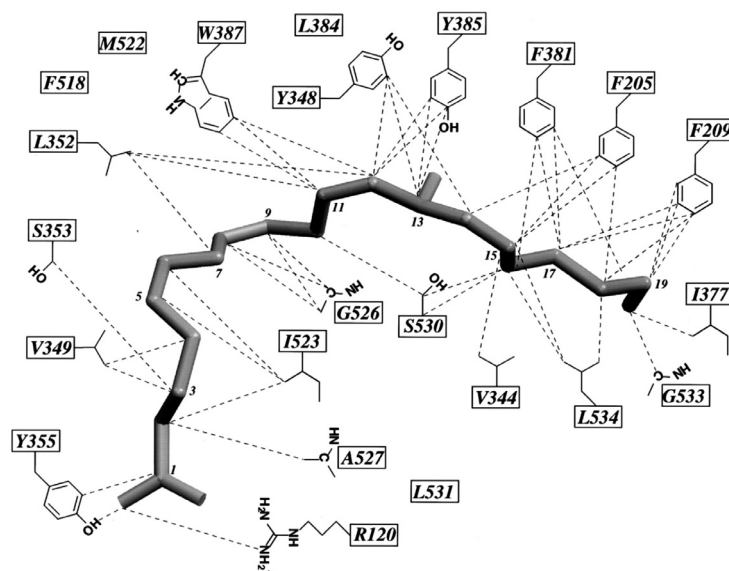


Figure 35: Schematic representation of interactions between arachidonic acid and amino acid residues lining the cyclooxygenase active site channel. All dashed lines represent interactions of ≤ 4.0 Å between specific side chain atoms of the protein and carbon or oxygen atoms of AA [129].

Gly-533 frames the “top” of the cavity. Mutations to bulkier residues at position 533 render COX inactive against arachidonate, though mutant COX will still oxygenate shorter fatty acid molecules [130]. At the “bottom” of the AA binding cavity is the constriction site - a hydrogen bonding network consisting of Arg-120, Tyr-355, and Glu-524. Structural and functional studies suggest that Arg-120 forms a bidentate, charge-reinforced hydrogen bond with the AA carboxyl group, anchoring it for catalysis [131]. To accomplish specific radical-mediated cyclization, the enzyme binds arachidonate in a bent “L shaped” conformation that favors cyclization as an intermediate radical propagation step. In radical form, Tyr-385 specifically abstracts the pro-S hydrogen atom from C13 to begin the cyclooxygenase reaction. Tyr-385 is ideally positioned for this, near the kink in the bound arachidonate [130]. The cyclization step is accomplished in a region

of the binding site that includes a number of hydrophobic residues. Most notably, mutation of Leu-384 (or Gly-526) in this region of the binding site impedes the ability of COX to complete cyclization [132].

Binding AA in a catalytically competent orientation is necessary, but insufficient to explain the reaction mechanism. Tyrosine must be oxidized to a free radical before catalysis can begin. The initiation of the tyrosyl radical begins at the heme group bound near the COX peroxidase site. There, cleavage of hydroperoxides activates COX via a two electron oxidation of the resting Fe^{3+} heme. The resulting cationic, radical porphyrin binds Fe^{4+} coordinated to the freed atom of oxygen. This radical system has significant oxidizing potential and removes one electron from Tyr-385 to yield a tyrosyl radical.

Abstraction of the AA 13-pro-S hydrogen by Tyr-385 results in a pentadienyl radical, centered on C11, C13, and C15. Next, oxygen adds to the pro-R face of C11.

The oxygen's preference for the pro-R face of C11 is not only attributable to steric crowding of the other five possible reaction sites - but that it is also conferred by the specific channeling of oxygen to this reaction site. Once a dioxygen radical has added to C11, its subsequent attack of the C8-C9 double bond is kinetically favorable [133]. C8 then attacks C12, closing the endoperoxide ring and forming an allylic radical centered on C13, C14, and C15. The second oxygen is added at C15 with S stereochemistry. The phenolic Tyr-385 hydrogen is abstracted by the oxygen radical, completing the synthesis of PGG_2 , and regenerating the Tyr-385 radical for another cycle of catalysis [126].

Mutagenesis implicates Ser-530 and Val-349 in the stereochemistry of the second oxygenation, as certain mutations at these positions strongly shift the

COX product profile from 15S to 15R PGG₂ [134]. A model derived from a crystal structure suggests that Tyr-348, Phe-381, Tyr-385, and Ser-530 all work to sterically block oxygen addition to the opposite face of the allyl radical [135].

6.2 Molecular Docking on COX enzymes

In order to avoid the search through the entire flexible conformational space of two proteins during the docking or refinement process, I have used the ensemble docking approach, which samples an ensemble of different feasible conformations prior to docking.

Generally, the ensemble may include different crystal structures and NMR conformers of the protein; in this specific work, structures were calculated using molecular dynamics simulations.

The preparation of the structure of COX-1 and COX-2 followed the protocol of Furse et al [136]. Crystal structures for COX-1 (pdb entry 2OYE) and COX-2 enzymes (pdb entry 1CVU) were used to generate the initial models. Since in the crystal structure of 1CVU AA is bound in a catalytically unproductive inverted orientation, a previous theoretical model for COX-2 with a properly oriented AA molecule was used (pdb entry 1DCX). Unfortunately, in the latter case, the docked conformation of AA in this complex appears to be inconsistent with the proposed reaction mechanism. The final conformation of COX-2 was used to reorient the COX-1 structure. This operation permitted to superpose the binding box and to easily automatize the docking screening.

The COX-2 construct used to obtain the 1CVU crystal structure has a point mutation, His-207-Ala, which was incorporated to prevent heme binding and

thus inactivate the enzyme. A BOG detergent molecule occupies the peroxidase active site in this crystal structure in the absence of the heme cofactor. To create a “catalytically competent” COX-2 homodimer model, the detergent molecule was removed from the peroxidase active site, the His-207 residue and heme groups were restored, and AA was repositioned in the cyclooxygenase active site in a catalytically viable orientation. To facilitate positioning of the heme group and substrate molecule in the COX-2 complex, the COX-2 active site region was superimposed to a COX-1 structure. The 3.0 Å resolution X-ray crystal structure of the ovine COX-1/AA complex [131], pdb entry 1DIY, was used to generate the initial model. Both heme and AA in the COX-2 model were overlaid on their corresponding positions in the COX-1 complex to generate the final COX-2 substrate complex. The reorientation of AA in the COX-2 active site and reinsertion of the heme group were quite simple and straightforward procedures. Neither generated any unfavorable steric interactions with protein residues, and the only structural modification necessary during the entire model-building procedure was adjustment of the reintroduced His-207 side chain so as to ligate the heme iron atom.

One of the four BOG detergents surrounding the membrane binding domain in the COX-1 crystal structure is also present in the COX-2 crystal structure; the other three detergent molecules were added to the COX-2 model to insure that differing numbers of detergent molecules in the two complexes did not induce different structural fluctuations during the simulations.

The COX-2 system consisted of the homodimer, two hemes, two AA molecules, eight detergent molecules, 32776 waters and 12 sodium counterions, for a total of 118858 atoms. Each homodimer complex was then energy minimized using a

steepest decent gradient method to relieve any residual unfavorable steric interaction introduced during the model building and solvation procedures. First, the protein, substrates, heme cofactors and detergent molecules were minimized for 300 steps while water molecules and sodium ions were held fixed. Then, the water and ion positions were minimized for 1000 steps while the protein-substrate complex was restrained. Finally, the full system was minimized for an additional 300 steps. Next, each enzyme-substrate complex was restrained during a 20 ps constant volume MD simulation, while water and sodium ions were allowed to move freely to relax the protein hydration shell. A thermalization procedure was then used to prepare each full system for equilibrium MD simulation. Initial velocities for each atom were assigned from a Boltzmann distribution at 298 K, followed by a 0.2 ps constant pressure dynamics simulation. This procedure was repeated ten times with a different Boltzmann velocity distribution in each cycle. This thermalization procedure serves to distribute atomic velocities more uniformly, eliminating potential “hot” and “cold” zones in the system. Isothermal-isobaric ensemble MD simulations were then run for 10 ns for each complex. An additional 10 ns MD simulation was run for AA in a periodic water box with a sodium counterion, to establish baseline equilibrium behavior for the substrate molecule free in solution. All covalent bonds containing hydrogen were fixed at equilibrium lengths using the SHAKE algorithm [137]. A 1 fs integration time step was used for all simulations, and conformations were collected every 1 ps for subsequent analysis. Constant temperature and pressure were maintained via weak coupling to a thermal reservoir ($\tau_{\text{autp}} = 1.0$ ps) and Berendsen piston ($\tau_{\text{aup}} = 1.0$ ps) [138]. A 9 Å real-space nonbonded cutoff was used in all simulations, and a particle-mesh Ewald

summation method was used to compute long-range electrostatic energy and force corrections [139].

The MD calculations were carried out with the YASARA program running on quad core Intel processors. The simulation box was of 107.11 Å, 75.44 Å, 85.73 Å respectively for the X, Y, and Z axis under periodic boundary conditions.

The simulations were carried out under the NPT ensemble at 310K and 1 atm by coupling the system with a Berendsen thermostat and by controlling the pressure in the in the manometer pressure control mode.

The AMBER03 force field was used for R and S isomers, and new force fields parameters were generated using the Autosmiles method. Briefly, the geometry of monomers was optimized by semi-empirical AM1 method using the COSMO solvation model. Partial atomic charges were calculated using the same level of theory by the Mulliken point charge approach, and were then improved by applying the 'AM1 Bond Charge Correction'.

Electrostatic interactions were calculated with a cutoff of 7.86 Å, and the long-range electrostatic interactions were handled by the particle mesh Ewald (PME) algorithm using a sixth-order B-spline interpolation and a grid spacing of 1 Å. After removal of conformational stress by a short steepest descent minimization, the procedure continued by simulated annealing (time step 1 fs, atom velocities scaled down by 0.9 every 10 steps) until convergence was reached, i.e. the energy improved by less than 0.0002 kcal/mol per atom during 200 steps.

In order to consider the flexibility of COX receptors, I have run docking experiments onto 10 structures obtained sampling every 1ns a 10 ns MD full atoms, keeping the ligands flexible. The calculation of binding energies was performed with the program Autodock 4 with the AMBER03 force field.

6.3 Results and discussion

In vivo studies carried out in the laboratory of Professor Escribà showed that AArOH and AAsOH had different activities on the two isoforms of COX, while showing similar binding energy.

In particular, pretreatment with AAxOH inhibited of about 90% the binding of AA to the COX-1 and of about 50% that to the COX-2.

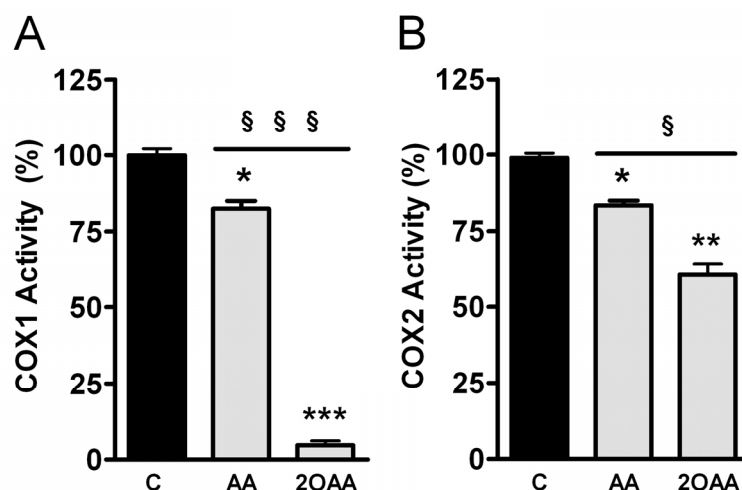


Figure 36: COX-1 and COX-2 activity with its natural substrate, AA, in the presence or absence of AAxOH. The control is COX + AA. The second bar is: pretreatment with AA (5 minutes) to study the natural substrate as inhibitor and after the AA was added. The third bar is: pretreatment with 2OHAA (5 minutes) and after the AA was added.

For this reason, I have performed an extended computational investigation to understand the mechanisms underlying a biological activity so different of the two molecules.

6.3.1 Binding energy

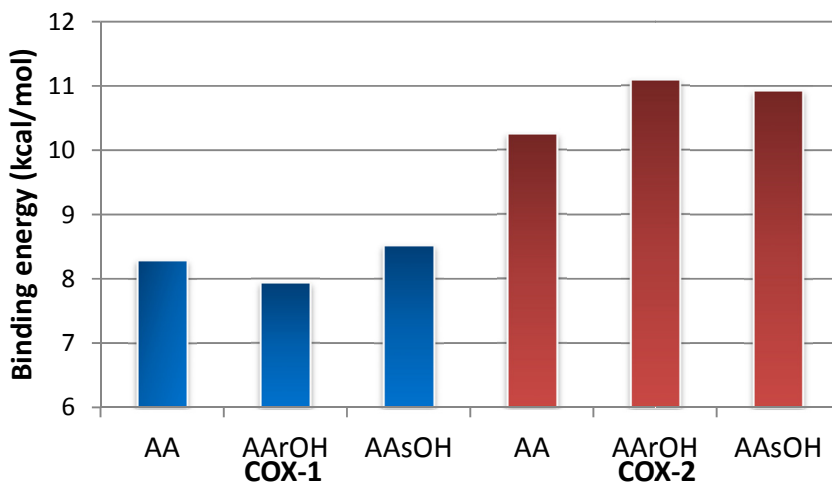


Figure 37: Binding energy of AA and AArOH molecules with the two COX isoforms.

TABLE 2: VALUES OF THE BINDING ENERGIES OF AA AND AAXOH MOLECULES WITH THE TWO COX ISOFORMS.

Receptor	Ligand	Binding energy (kcal/mol)
COX-1	AA	8.29
	AArOH	7.94
	AAsOH	8.52
COX-2	AA	10.25
	AArOH	11.09
	AAsOH	10.93

In COX-1 the binding of AA and derivatives is very similar. The two carboxyl oxygens (O1 and O2) of AA establish hydrogen bonds with Arg-120 and have close hydrophobic contacts with Phe-205, Val-344, Tyr-348. The orientation of AArOH (as well as AAsOH, not represented in Fig. 38) is very similar to AA and

the oxygens O1 and O2 occupy the same positions. The hydroxyl oxygen (O*) of AArOH and AAsOH is hydrogen bonded with Glu-524, but this favorable interaction is counterbalanced by a distortion of the carbon backbone (the RMSD between AA and AArOH is 1.39 Å). The S enantiomer has a better global interaction with the binding site and the binding energy is slightly higher than AA as shown in Fig. 37. Summarizing, the carboxylate groups of the inhibitors are essentially superimposable and the differences in the binding of the three arachidonic acids are not significant.

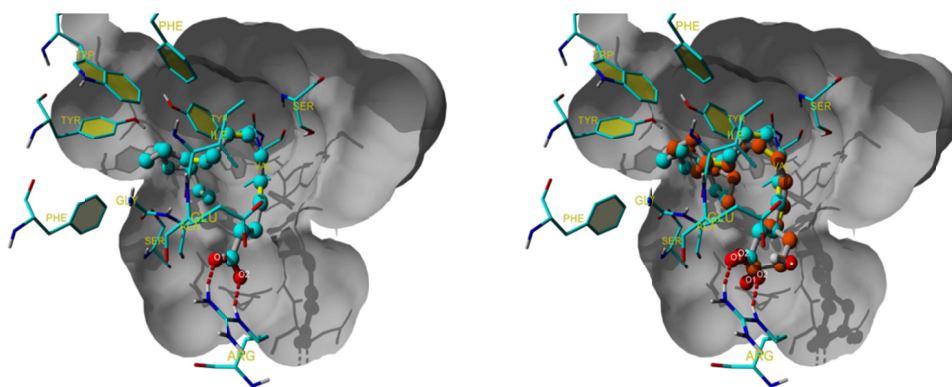


Figure 38: (Left) Arachidonic acid (AA) in the binding site of COX-1. (Right) AA and AArOH are shown simultaneously in the binding pocket for comparison. The two carboxyl oxygens (O1 and O2) of AA establish hydrogen bonds with Arg-120 and have close hydrophobic contacts with Phe-205, Val-344, Tyr-348. The orientation of AArOH is very similar to AA and the oxygens O1 and O2 occupy the same positions. The hydroxyl oxygen (O*) of AArOH is hydrogen bonded with Glu-524, but this favorable interaction is counterbalanced by a distortion of the carbon backbone. To facilitate the visual inspection of the interactions, the binding site is grey shaded, the fatty acids are represented in ball and stick, and only the aminoacids closer than 3Å are shown.

In COX-2 has been observed a higher binding energy value and, especially, a higher degree of hydrogen bondings among the arachidonic acids and the receptor. In fact, the carboxylate groups of AA is coordinated with Arg-120 with

one hydrogen bond while AArOH and AAsOH establish 5 hydrogen bonds as shown in Fig. 39.

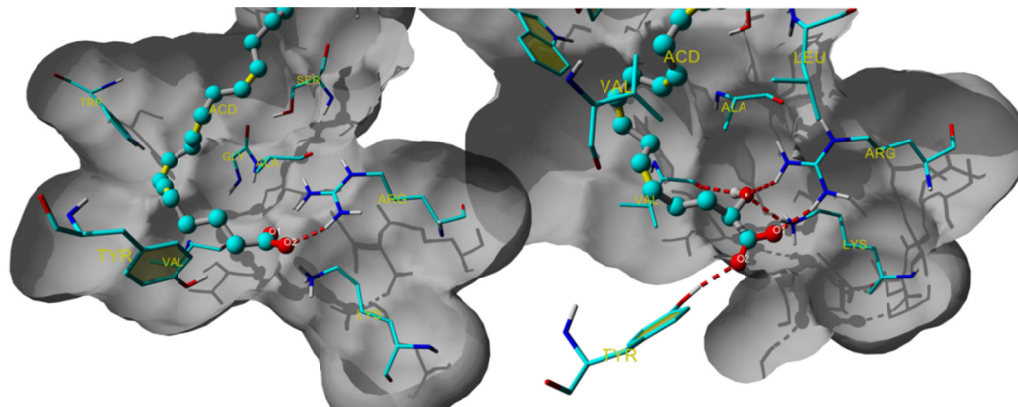


Figure 39: (Left) Arachidonic acid (AA) in the binding site of COX-2. (Right) AArOH in the binding site of COX-2. AA and AArOH are shown simultaneously in the binding pocket for comparison. The carboxylate groups of AA is coordinated with Arg-120 with one hydrogen bond, whereas AArOH have 5 hydrogen bonds. The O* oxygen occupies the position of O1 of AA. Analogously, O1 of AArOH takes the position of the AA O2. Finally, O2 of substituted arachidonic acids is free to hydrogen bond to Tyr-355. To facilitate the visual inspection of the interactions, the binding site is grey shaded, the fatty acids are represented in ball and stick, and only the aminoacids closer than 3Å are shown.

It is worth to notice that in COX-2 the O* oxygen occupies the position of O1 of AA. Analogously, O1 of AArOH (or AAsOH) takes the position of the AA O2. Finally, O2 of substituted arachidonic acids is free to hydrogen bond to Tyr-355.

6.3.2 The Fukui analysis

Binding a ligand in a catalytically competent orientation is necessary, but not sufficient to explain the reaction mechanism in COX. The initial steps for the formation of PGG₂ involve cleavage of hydroperoxides and the consequent formation of a cationic, radical heme group binding Fe⁴⁺. Tyrosine is then oxidized to a free radical before catalysis can begin. The subsequent abstraction

of the AA 13-pro-S hydrogen by Tyr-385 results in a pentadienyl radical, centered on C11, C13, and C15.

The multistep reaction of AA in COX is summarized in the following figure:

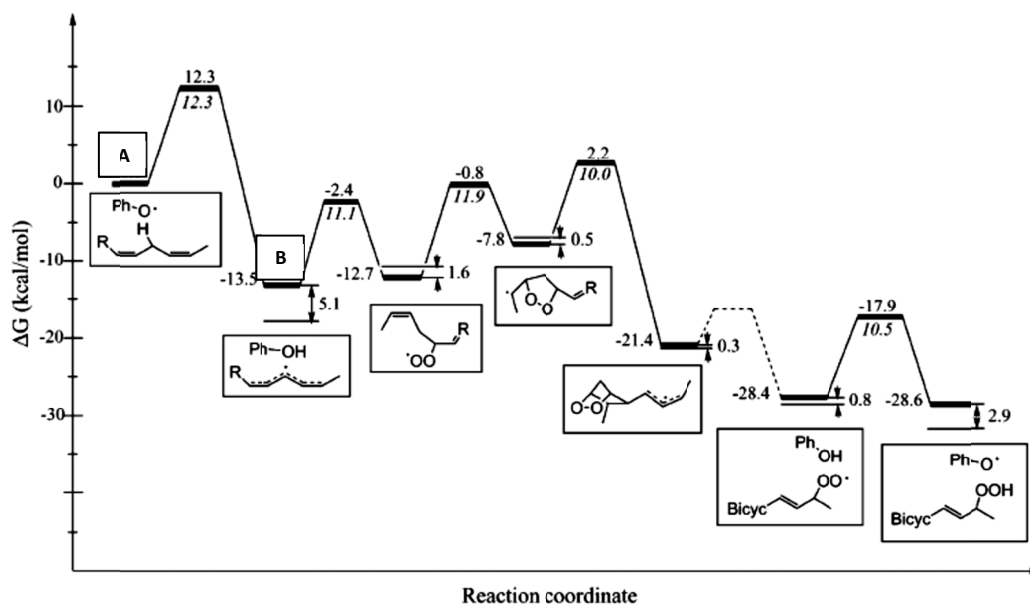


Figure 40: Calculated free-energy surface for the synthesis of PGG₂ [140].

The binding energy is a measure of the interaction of the ligand in the binding pocket, namely the energy of the system in (A).

I have used the Fukui analysis (see Appendix) to calculate the reactivity of AA and AAxOH molecules during the interaction with the COX.

The calculation was performed with the program DMol3 [141] with functional pwc, TNP basis set, Fermi occupation, and a global cutoff of 3 Å. The grid resolution was set to 0.15 Å.

The map of the Fukui radical function on the total electron density (Fig. 41) indicates clearly the sites more favorable for radical attack. The arrows indicate the C13, which is the carbon interested of H* abstraction in COX. It is evident that –OH group in alpha reduce the chance of AAxOH to react.

From this analysis AAxOH has a better interaction with COX-2 than AA, whereas AAxOH and AA have roughly the same interaction with COX-1. The good interaction of AAxOH is mainly due to hydrogen bond network, as indicated in Fig. 38 and 39. This excellent binding induces a distortion of the carbon chain, and the position of C13, the first carbon to react, is circa 0.3 Å farther by the Tyrosine residue. This distance is responsible, presumably, for an increasing of the activation energy and therefore for the slowdown of the reaction. The analysis of frontier orbitals at stage (A) and (B), i.e. non radical and radical form respectively, goes in the same direction and seems to suggest a lower capability to react of the C13 of AAxOH compared with the corresponding carbon of AA.

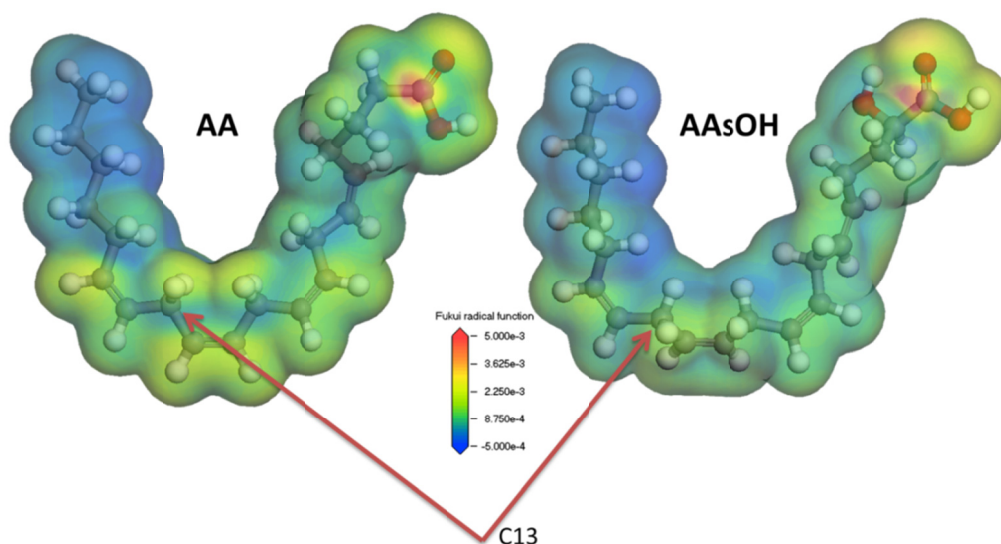


Figure 41: Map of the Fukui radical function on the total electron density. The Fukui function $f^0(r)$ is color mapped onto the electron density isosurface with isovalue equals. The map indicates clearly the sites

more favorable for radical attack. The arrows indicate the C13, which is the carbon interested of H* abstraction in COX. It is evident that –OH group in alpha reduce the chance to react of AAxOH.

The surfaces correspond to total density, the colors correspond to Fukui function. The higher the value, the greater the possibility of having a radical attack on C13. The Fukui function calculated on the density surface in correspondence to hydrogen atoms bond to C13 dropped from 2.5 meV to 0.7 meV, indicating a reduced availability of H13 hydrogens to radical extraction.

This result indicates a possible mechanism to explain the inhibitory capabilities of AAxOH: the binding energy of AAxOH is similar to that of AA, but the presence of a hydroxyl group reduce the chances of a radical extraction in the early stage of COX activity.

7 Appendix – Computational methods

7.1 Introduction to molecular dynamics

Molecular dynamics (MD), first developed in the late 1970s [142], uses simple approximations based on Newtonian physics to simulate atomic and molecular interactions, thus reducing the computational complexity. The general process of approximation used is showed in Fig. 42.

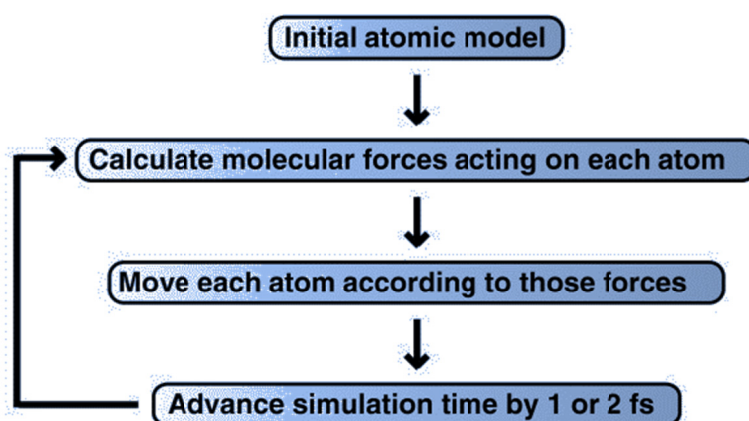


Figure 42: A schematic showing how a molecular dynamics simulation is performed. First, a computer model of the receptor-ligand system is prepared. An equation like that shown below is used to estimate the forces acting on each of the system atoms. The positions of the atoms are moved according to Newton's laws of motion. The simulation time is advanced, and the process is repeated many times [143]. This figure was adapted from a version originally created by Kai Nordlund.

The forces acting on each atom of the system are then estimated from an equation like that shown in Eq. 3 [144].

$$\begin{aligned}
 E_{total} = & \overbrace{\sum_{bonds} K_r (r - r_{eq})^2 + \sum_{angles} K_\theta (\theta - \theta_{eq})^2 + \sum_{dihedrals} \frac{V_n}{2} [1 + \cos(n\phi - \gamma)]}^{\text{Bonded}} \\
 & + \sum_{i < j} \left[\frac{A_{ij}}{R_{ij}^{12}} - \frac{B_{ij}}{R_{ij}^6} + \frac{q_i q_j}{\epsilon R_{ij}^{12}} \right] \\
 & \underbrace{\left[\text{Diagram of bond length } r, \text{ angle } \theta, \text{ dihedral } \phi, \text{ and non-bonded interaction } R_{ij} \right]}_{\text{Non-bonded}}
 \end{aligned}
 \tag{Eq. 3}$$

The atomic forces that govern molecular movement can be divided into those caused by interactions between atoms that are chemically bonded to one another and those caused by interactions between atoms that are not bonded. Chemical bonds and atomic angles are modeled using simple springs, and dihedral angles (that is, rotations about a bond) are modeled using a sinusoidal function that approximates the energy differences between eclipsed and staggered conformations. Non-bonded forces arise due to van der Waals interactions, modeled using the Lennard-Jones potential, and charged (electrostatic) interactions, modeled using Coulomb's law.

In order to reproduce the actual behavior of real molecules in motion, the energy terms described above are parameterized to fit quantum-mechanical calculations and experimental (for example, spectroscopic) data. This parameterization includes identifying the ideal stiffness and lengths of the springs that describe chemical bonding and atomic angles, determining the best

partial atomic charges used for calculating electrostatic-interaction energies, identifying the proper van der Waals atomic radii, and so on. Collectively, these parameters are called a 'force field' because they describe the contributions of the various atomic forces that govern molecular dynamics. Several force fields are commonly used in molecular dynamics simulations, including AMBER [144, 145], CHARMM [146] and GROMOS [147]. They differ principally in the way they are parameterized but generally give similar results.

7.1.1 Minimization

Using the force field that has been assigned to the atoms in the system it is essential to find a stable point or a minimum on the potential energy surface in order to begin dynamics. At a minimum on the potential energy surface the net force on each atom vanishes. There will be more than one minimum for a system under periodic boundary conditions. In principle there may be a global minimum, but this will not likely be found without a conformational search.

Minimization provides information that is complementary to molecular dynamics. Ensembles of structures are useful for calculating thermodynamic averages and estimating entropy, but the large number of structures makes detailed microscopic analysis difficult. Minimized structures represent the underlying conformations about which fluctuations occur during dynamics. The use of a force field to define structure is often called molecular mechanics.

Constraints may be imposed during minimization, as well as during dynamics. These constraints may be based on data such as NOEs from an NMR experiment

or they may be imposed by a template such that we force a ligand to find the minimum closest in structure to a target molecule.

To minimize we need a function (provided by the force field) and a starting guess or set of coordinates. The magnitude of the first derivative can be used to determine the direction and magnitude of a step (i.e. change in the coordinates) required to approach a minimum configuration. The magnitude of the first derivative is also a rigorous way to characterize convergence. A minimum has converged when the derivatives are close to zero. Usually the typical tolerance is 0.001 kcal/mole. To reach the minimum the structure must be successively updated by changing the coordinates (taking a step) and checking for convergence. Each complete cycle of differentiation and stepping is known as a minimization iteration. Typically thousands of minimization iterations are required for large macromolecules to reach convergence.

There are two major protocols for minimization:

- Simulated Annealing (SA)
- Steepest descent (SD)

Simulated annealing

Simulated annealing (SA) is a generic algorithm to locate the global minimum of a target function [148].

This protocol minimizes (to relax any "hot spots" in the molecule), heats to a set temperature, then slowly cools and finally minimizes the molecule. This procedure is repeated again and again to generate a large ensemble of

conformations which represents the possible energy minima, assuming that the dynamics is performed long enough to sample the entire range of conformations.

If the simulation cell contains a lot of potential energy (e.g. huge atom overlaps), the standard time step is usually too large to simulate the system reliably, the numerical error accumulates, the simulation cell overheats and 'explodes'. A steepest descent minimization avoids this problem by automatically choosing very small time steps and keeping the temperature at 0 K.

A SA minimization usually follows an initial short steepest descent minimization (to remove bumps), since it's much faster at finding the energy minimum. SA is more secure but much slower than a steepest descent minimization and should be used for a few hundred steps to remove bumps when importing a new protein structure.

Steepest descent

Steepest descent method [149] is an optimization algorithm that approaches a local minimum of a function by taking steps proportional to the negative of the gradient (or the approximate gradient) of the function at the current point. Simply put, steepest descent uses the gradient to determine the direction and move down in one dimension parallel to the net force. Steepest descent will lead directly to the nearest local minimum by following a path that is determined by moving from the previous value to a new value (at some constant times) in the directions in which the energy is decreasing. If the new movement decreases the energy, the new structure is accepted, and the process is repeated. If, on the

other hand, the energy increases, the previous structure is restored. This algorithm converges fast in a steep place for correcting “bad” initial geometry, especially when systems are far from harmonic. It has poor convergence properties, however, and often jitters around the minimum area, because the gradient approaches zero near the minimum.

7.2 Production

MD has been used to compute the dynamics of the molecular system, including time-averaged structural and energetic properties, structural fluctuations and conformational transitions. The dynamics of a system may be simplified as the movements of each of its atoms. If the velocities and the forces acting on atoms can be quantified, then their movement may be simulated. During the molecular dynamics process, the initial condition is specified by the analytical expression for the potential energy of a molecular system that includes coordinates, energies and a set of velocities for each atom. Then, a force is applied on each atom, which is described by Newton’s equation of motion:

$$F = m * a \tag{Eq. 4}$$

Where F is the force on an atom, m is the atom’s mass and a is the acceleration. Because the negative of the first derivative of the potential energy (E) with respect to the coordinates (r) gives the force on each atom, Newton’s equation can be used to describe the motion of a particular molecule:

$$F = m * a = -\frac{dE}{dr} = -m \frac{d^2r}{dt^2}$$

(Eq. 5)

Where t is the time and r represents the Cartesian coordinates of the atom. The forces are obtained from the energy expression by calculation of the analytical derivatives. The forces are applied for a small time step ($\sim 10^{-15}$ seconds), and the acceleration is calculated from Newton's law (Eq. 5). Then, the velocity and position of each atom is updated to a new velocity and position using an integration algorithm, and the forces and accelerations are calculated once again at the new atomic positions. Next, this process is repeated to produce a trajectory. The positions of each atom in the system are recorded in the dynamics history file. The structures are retreated and then minimized with molecular mechanics and analyzed later. Above all, the solution of Eq. 5 using an empirical fit to the potential energy surface is known as molecular dynamics simulation.

In molecular dynamics Newtonian equations of motion are solved numerically for all atoms as a function of time. A statistical average with time is obtained by applying initial velocities (i.e. kinetic energy), which allows the system to pass the energy barriers and sample all the local minima. An energy calculation, however, has to be carried out for each of a very large number of configurations. Only molecular mechanics can provide the necessary computational speed. So, molecular mechanics and molecular dynamics often are used together to achieve the target conformers with lowest energy configurations.

7.3 Principles of flexible docking

Most cellular processes are carried out by protein-protein interactions. Predicting the three dimensional structures of protein-protein complexes (docking) can shed light on their functional mechanisms and roles in the cell. Understanding and modeling the bound configuration are the major scientific challenges. The structures of the complexes provide information regarding the interfaces of the proteins and assist in drug design.

Docking can assist in predicting protein-protein interactions, in understanding signaling pathways and in evaluating the affinity of complexes.

Upon binding, proteins undergo conformational changes that include both backbone and side chain movements [150]. The first docking methods treated proteins as rigid bodies in order to reduce the search space for optimal structures of the complexes [151, 152]. However, ignoring flexibility could prevent docking algorithms from recovering native associations.

Accounting for flexibility is also essential for the accuracy of the solutions. In addition, flexibility must also be taken into account if the docked structures were determined by homology modeling [153] or if loop conformations were modeled [154].

Incorporating flexibility in a docking algorithm is much more difficult than performing rigid body docking. The high number of degrees of freedom not only significantly increases the running time, but also results in a higher rate of false-positive solutions. These must be scored correctly in order to identify near-native results [155]. Consequently, existing docking methods limit the flexibility to

certain types of motions allowing only one of the proteins in the complex to be flexible.

Using different solved 3D structures (by X-ray and NMR) of diverse conformations of the same protein, or of homologous proteins, is probably the most convenient way to obtain information relating to protein flexibility. Using such conformers, one can generate new viable conformations which might exist during the transition between one given conformation to another. These new conformations can be generated by “morphing” techniques [156, 157] which implement linear interpolations, but have limited biological relevance.

7.4 Fukui function

The behavior of an atom or a molecule often is characterized by some parameters that chemists have extracted from their experience and used for the prediction of chemical reactivity.

Density functional theory (DFT) [158-160] has extraordinary potential for quantifying chemical concepts and providing them with a theoretical basis. Among these DFT-derived concepts, the Fukui function, as derived by Parr and Yang [161, 162], is related to the electron density in the frontier molecular orbitals (FMO) and thus plays a vital role in chemical selectivity [163, 164].

The Fukui function, denoted by $f(r)$, is defined as the differential change in electron density due to an infinitesimal change in the number of electrons under the constraint of a constant external potential (v) [161]. That is,

$$f(\mathbf{r}) = \left(\frac{\partial \rho(\mathbf{r})}{\partial N} \right)_{v(\mathbf{r})} \quad (\text{Eq. 6})$$

where $\rho(\mathbf{r})$ is the electron density and

$$N = \int \rho(\mathbf{r}) d\mathbf{r} \quad (\text{Eq. 7})$$

is the total number of electrons in the system.

Fukui functions are defined using the one-sided derivatives:

$$f^+(\mathbf{r}) = \left(\frac{\partial \rho(\mathbf{r})}{\partial N} \right)_{v(\mathbf{r})}^+ = \lim_{\varepsilon \rightarrow 0^+} \frac{\rho_{N+\varepsilon}(\mathbf{r}) - \rho_N(\mathbf{r})}{\varepsilon} \quad (\text{Eq. 8})$$

$$f^-(\mathbf{r}) = \left(\frac{\partial \rho(\mathbf{r})}{\partial N} \right)_{v(\mathbf{r})}^- = \lim_{\varepsilon \rightarrow 0^+} \frac{\rho_N(\mathbf{r}) - \rho_{N-\varepsilon}(\mathbf{r})}{\varepsilon} \quad (\text{Eq. 9})$$

When a molecule accepts electrons, the electrons tend to go to places where $f^+(\mathbf{r})$ is large because it is at these locations that the molecule is most able to stabilize additional electrons. Therefore a molecule is susceptible to nucleophilic attack at sites where $f^+(\mathbf{r})$ is large. Similarly, a molecule is susceptible to electrophilic attack at sites where $f^-(\mathbf{r})$ is large, because these are the regions where electron removal destabilizes the molecule the least. In DFT, the Fukui functions are the key regioselectivity indicators for electron-transfer controlled

reactions. A large change in the chemical potential should be favorable and so molecules should be most reactive where $f(\mathbf{r})$ is large.

$F(\mathbf{r})$ is related to the change in density in response to changes in the number of electrons, N in the valence region, and therefore it is intimately related to the frontier orbital [165].

In the frozen orbital approximation, these derivatives can be approximated with the squares of the lowest unoccupied (LUMO) and highest occupied molecular orbitals (HOMO):

$$f_{v,N}^+(\mathbf{r}) = |\varphi_{v,N}^{LUMO}(\mathbf{r})|^2 = \rho_{v,N}^{LUMO}(\mathbf{r}) \quad (\text{Eq. 10})$$

$$f_{v,N}^-(\mathbf{r}) = |\varphi_{v,N}^{HOMO}(\mathbf{r})|^2 = \rho_{v,N}^{HOMO}(\mathbf{r}) \quad (\text{Eq. 11})$$

Based on the orbital approximations, it is clear that $f(\mathbf{r})$ is the DFT analog of the frontier orbital regioselectivity for nucleophilic ($f_{v,N}^+(\mathbf{r})$) and electrophilic ($f_{v,N}^-(\mathbf{r})$) attack. It is then reasonable to define a reactivity indicator for radical attack by analogy to the corresponding orbital indicator:

$$f_{v,N}^0(\mathbf{r}) \approx \frac{1}{2} \left(\rho_{v,N}^{HOMO}(\mathbf{r}) + \rho_{v,N}^{LUMO}(\mathbf{r}) \right) \quad (\text{Eq. 12})$$

The Fukui function includes effects - notably electron correlation and orbital relaxation - that are a priori neglected in a frontier molecular orbital (FMO)

approach. In most cases, the orbital relaxation contribution is negligible and the Fukui function and the FMO reactivity indicators give the same results.

In chemistry, one is rarely interested in which “point” in a molecule is most reactive; rather one wishes to identify the atom in a molecule is most likely to react with an attacking electrophile or nucleophiles. This suggests that a coarse-grained atom-by-atom representation of the Fukui function would suffice for chemical purposes. Such a representation is called a condensed reactivity indicator [166].

There are four strategies for computing the Fukui function. The first is to use the result of an orbital-based method (Hartree-Fock or Kohn-Sham DFT) on the N -electron system to evaluate the FMO approximation in Equations 10 and 11. This approach cannot be recommended (it neglects the effects of orbital relaxation), but neither should it be denigrated (it is one of the easiest ways to compute the Fukui function, and it is usually effective). The second approach gives accurate results and uses single-point calculations to calculate the density of the $N-1$ and $N+1$ electron systems and then computes the Fukui function using the equations for the Fukui function from exact theory. The third approach features mathematical constructions that allow one to exactly [167] or approximately [168] compute the derivatives in Equations 8 and 9. This approach is conceptually satisfying and generally reliable, but it is more difficult (it requires computer programming to implement) and computationally expensive. A fourth approach, which has been proposed but not yet implemented, would compute Fukui functions at the ab initio level using electron propagator theory [169, 170] or the closely related extended Koopmans’ theorem [171-175]. These

approaches are computational costly and difficult to implement, but potentially valuable for benchmarking.

The utility of the Fukui function for predicting chemical reactivity can also be described using the variational principle for the Fukui function [176, 177]. The Fukui function from the above discussion, $f_{v,N}^+(r)$, represents the “best” way to add an infinitesimal fraction of an electron to a system in the sense that the electron density $\rho_{v,N}(r) + \varepsilon f_{v,N}^+(r)$ has lower energy than any other $N + \varepsilon$ -electron density for this system. A Lewis base (also known as reducing agent, nucleophile, etc.) will attack the system in the place where it is most able to accept additional electrons. Thus, the Lewis base will attack the system where $f_{v,N}^+(r)$ is the largest. Similarly, the Fukui function below, $f_{v,N}^-(r)$, is the “least bad” way to remove an infinitesimal fraction of an electron from a system. A Lewis acid (also called oxidizing agent, electrophiles, etc.) will attack the system in the place where it is most willing to donate electrons. Thus the Lewis acid will attack the system where $f_{v,N}^-(r)$ is the largest. Although the mathematical details for this explanation of the Fukui function’s predictive power are relatively modern (from 2000) [176], the basic ideas described date back to the first papers on the Fukui function [161, 162].

Bibliography

1. de Kruijff, B., *Lipids beyond the bilayer*. Nature, 1997. **386**(6621): p. 129-30.
2. Tate, M.W., E.F. Eikenberry, D.C. Turner, E. Shyamsunder, and S.M. Gruner, *Nonbilayer phases of membrane lipids*. Chem Phys Lipids, 1991. **57**: p. 147-64.
3. Gil, T., J.H. Ipsen, O.G. Mouritsen, M.C. Sabra, M.M. Sperotto, and M.J. Zuckermann, *Biochem Biophys Acta*. Theoretical analysis of protein organization in lipid membranes, 1998. **1376**: p. 245-66.
4. Mouritsen, O.G., *Self-assembly and organization of lipid-protein membranes*. Curr Opin Coll Int Sci, 1998. **3**(78-87).
5. Hazel, J.R., *Thermal Adaptation in Biological Membranes: Is Homeoviscous Adaptation the Explanation?* Ann Rev Physiol, 1995. **57**: p. 19-42.
6. Quinn, P.J., F. Joo, and L. Vigh, *The role of unsaturated lipids in membrane structure and stability*. Prog Biophys Mol Biol, 1989. **53**(2): p. 71-103.
7. Cossins, A.R., *Temperature Adaptations of Biological Membranes*. 1994: London and Chapel Hill: Portland Press.
8. Fermor, B.F., J.R. Masters, C.B. Wood, J. Miller, K. Apostolov, and N.A. Habib, *Fatty acid composition of normal and malignant cells and cytotoxicity of stearic, oleic and sterculic acids in vitro*. Eur J Cancer, 1992. **28A**(6-7): p. 1143-7.
9. Nakada, T., I.L. Kwee, and W.G. Ellis, *Membrane fatty acid composition shows $\Delta 6$ -desaturase abnormalities in Alzheimer's disease*. NeuroReport, 1990. **1**: p. 153-5.
10. Daveloose, D., A. Linard, T. Arfi, J. Viret, and R. Christon, *Simultaneous changes in lipid composition, fluidity and enzyme activity in piglet intestinal brush border membrane as affected by dietary polyunsaturated fatty acid deficiency*. Biochim Biophys Acta, 1993. **1166**: p. 229-37.
11. Alvarez, E., V. Ruiz-Gutiérrez, C. Santa María, and A. Machado, *Age-dependent modification of lipid composition and lipid structural order parameter of rat peritoneal macrophage membranes*. Mech Ageing Dev, 1993. **71**: p. 1-12.
12. Parasassi, T., M. Di Stefano, G. Ravagnan, O. Sapora, and E. Gratton, *Membrane aging during cell growth ascertained by Laurdan generalized polarization*. Exp Cell Res, 1992. **202**: p. 432-9
13. Avery, S.V., D. Lloyd, and J.L. Harwood, *Temperature-dependent changes in plasma-membrane lipid order and the phagocytotic activity of the amoeba *Acanthamoeba castellanii* are closely correlated*. Biochem J, 1995. **312**: p. 811-6.
14. Hu, Q., E.J. Moerman, and S. Goldstein, *Altered Expression and Regulation of the $\alpha 5\beta 1$ Integrin-Fibronectin Receptor Lead to Reduced Amounts of Functional $\alpha 5\beta 1$ Heterodimer on the Plasma Membrane of Senescent Human Diploid Fibroblasts* Exp Cell Res, 1996. **224**: p. 251-63.
15. Shmeeda, H.R., E.B. Golden, and Y. Barenholz, *Membrane lipids and aging*, in *Handbook of Biomembranes. Mammalian Membrane, Structure and Function*, M.e. Shinitzky, Editor. 1994, Balaban VCH, New York: Weinheim. p. 1-82.
16. Escribà, P.V. and P. Bean, *Basic principles underlying the emerging field of lipid therapy*. Am Clin Lab, 2002. **21**: p. 29-31.
17. Voet, D. and J.G. Voet, eds. *Biochemistry* 3rd ed. 2004, John Wiley & Sons.

18. Gorter, E. and F. Grendel, *On Bimolecular Layers of Lipoids on the Chromocytes of the Blood*. J Exp Med, 1925. **41**(4): p. 439-43.
19. Singer, S.J. and G.L. Nicolson, *The fluid mosaic model of the structure of cell membranes*. Science, 1972. **175**: p. 720-31.
20. Engelman, D.M., *Membranes are more mosaic than fluid*. Nature, 2005. **438**(7068): p. 578-80.
21. Vereb, G., J. Szöllosi, J. Matkó, P. Nagy, T. Farkas, L. Vigh, L. Mátyus, T. Waldmann, and S. Damjanovich, *Dynamic, yet structured: The cell membrane three decades after the Singer-Nicolson model*. Proc Natl Acad Sci U S A, 2003. **100**(14): p. 8053-8.
22. Bretscher, M.S., *Phosphatidyl-ethanolamine: differential labelling in intact cells and cell ghosts of human erythrocytes by a membrane-impermeable reagent*. J Mol Biol, 1972. **71**(3): p. 523-28.
23. Op den Kamp, J.A.F., *Lipid asymmetry in membranes*. Annual Review of Biochemistry, 1979. **48**: p. 47-71.
24. Rothman, J.E. and J. Lenard, *Membrane Asymmetry. The nature of membrane asymmetry provides clues to the puzzle of how membranes are assembled*. Science, 1977. **195**: p. 743-53.
25. van Meer, G., D.R. Voelker, and G.W. Feigenson, *Membrane lipids: where they are and how they behave*. Nat Rev Mol Cell Biol, 2008. **9**(2): p. 112-24.
26. Verkleij, A.J., R.F. Zwaal, B. Roelofsen, P. Comfurius, D. Kastelijn, and L.L. van Deenen, *The asymmetric distribution of phospholipids in the human red cell membrane. A combined study using phospholipases and freeze-etch electron microscopy*. Biochim Biophys Acta, 1973. **323**(2): p. 178-93.
27. Li, Z., T.K. Hailemariam, H. Zhou, Y. Li, D.C. Duckworth, D.A. Peake, Y. Zhang, M.S. Kuo, G. Cao, and X.C. Jiang, *Inhibition of sphingomyelin synthase (SMS) affects intracellular sphingomyelin accumulation and plasma membrane lipid organization*. Biochim Biophys Acta, 2007. **1771**: p. 1186-94.
28. Simons, K. and W.L. Vaz, *Model systems, lipid rafts, and cell membranes*. Annu Rev Biophys Biomol Struct, 2004. **33**: p. 269-95.
29. Simons, K. and E. Ikonen, *Functional rafts in cell membranes*. Nature, 1997. **387**(6633): p. 569-72.
30. Cullis, P.R. and B. de Kruijff, *Lipid polymorphism and the functional roles of lipids in biological membranes*. Biochim Biophys Acta, 1979. **559**(4): p. 399-420.
31. Gruner, S.M., P.R. Cullis, M.J. Hope, and C.P. Tilcock, *Lipid polymorphism: the molecular basis of nonbilayer phases*. Annu Rev Biophys Chem, 1985. **14**: p. 211-38.
32. Basañez, G., *Membrane fusion: The process and its energy suppliers*. Cell Mol Life Sci, 2002. **59**(9): p. 1478-90.
33. Cullis, P.R., M.J. Hope, and C.P.S. Tilcock, *Lipid polymorphism and the roles of lipids in membranes*. Chemistry and Physics of Lipids, 1986. **40**: p. 127-44.
34. Epand, R., *Lipid polymorphism and protein-lipid interactions*. Biochim Biophys Acta, 1998. **1376**: p. 353-68.
35. Vögler, O., J.M. Barcelò, C. Ribas, and P.V. Escribà, *Membrane interactions of G proteins and other related proteins*. Biochim Biophys Acta, 2008. **1778**: p. 1640-52.
36. Luzzati, V., *Biological Membranes*, ed. D. Chapman. 1968, London: Academic Press. 77-123.

37. Lee, D.B.N., N. Jamgotchian, S.G. Allen, M.B. Abeles, and H.J. Ward, *A lipid-protein hybrid model for tight junction*. *Am J Physiol Renal Physiol*, 2008. **295**(6): p. F1601-12.
38. Israelachvili, J.N., S. Marcelja, and R.G. Horn, *Physical principles of membrane organization*. *Q. Rev. Biophys.*, 1980. **13**: p. 121–200.
39. Nieva, J.L., A. Alonso, G. Basanez, F.M. Goni, A. Gulik, R. Vargas, and V. Luzzati, *Topological properties of two cubic phases of a phospholipid:cholesterol:diacylglycerol aqueous system and their possible implications in the phospholipase C-induced liposome fusion*. *FEBS Lett*, 1995. **368**(1): p. 143-7.
40. Terrones, O., B. Antonsson, H. Yamaguchi, H.G. Wang, J. Liu, R.M. Lee, A. Herrmann, and G. Basanez, *Lipidic pore formation by the concerted action of proapoptotic BAX and tBID*. *J Biol Chem*, 2004. **279**(29): p. 30081-91.
41. Escribà, P.V., P.B. Wedegaertner, F.M. Goni, and O. Vögler, *Lipid-protein interactions in GPCR-associated signaling*. *Biochim Biophys Acta*, 2007. **1768**(4): p. 836-52.
42. Stevens, T.J. and I.T. Arkin, *Do more complex organisms have a greater proportion of membrane proteins in their genomes?* *Proteins*, 2000. **39**(4): p. 417-20.
43. Takeda, S., S. Kadowaki, T. Haga, H. Takaesu, and S. Mitaku, *Identification of G protein-coupled receptor genes from the human genome sequence*. *FEBS Lett.*, 2002. **520**(1-3): p. 97-101.
44. Filmore, D., *It's a GPCR world*. *Mod Drug Discov*, 2004. **7**: p. 24-6.
45. Palczewski, K., T. Kumasaka, T. Hori, C.A. Behnke, H. Motoshima, B.A. Fox, I. Le Trong, D.C. Teller, T. Okada, R.E. Stenkamp, M. Yamamoto, and M. Miyano, *Crystal structure of rhodopsin: a G protein-coupled receptor*. *Science*, 2000. **289**(5480): p. 739-45.
46. Rasmussen, S.G., H.J. Choi, R.D. M., K.T. S., T.F. S., E.P. C., B. M., R.V. R., S. R., F.R. F., S.G. F., W.W. I., and K.B. K., *Crystal structure of the human beta2 adrenergic G-protein-coupled receptor*. *Nature*, 2007. **450**(7168): p. 383-7.
47. Cabrera-Vera, T.M., J. Vanhauwe, T.O. Thomas, M. Medkova, A. Preininger, M.R. Mazzoni, and H.E. Hamm, *Insights into G protein structure, function, and regulation*. *Endocr Rev*, 2003. **24**(6): p. 765-81.
48. Malbon, C.C., *G proteins in development*. *Nat Rev Mol Cell Biol*, 2005. **6**(9): p. 689-701.
49. Melien, O., *Heterotrimeric G proteins and disease*. *Methods Mol Biol*, 2007. **361**: p. 119-44.
50. Spiegel, A.M. and L.S. Weinstein, *Inherited diseases involving G proteins and G protein-coupled receptors*. *Annu Rev Med*, 2004. **55**: p. 27-39.
51. Spiegelberg, B.D. and H.E. Hamm, *Roles of G protein-coupled receptor signaling in cancer biology and gene transcription*. *Curr Opin Genet Dev*, 2007. **17**(1): p. 40-4.
52. Sondek, J. and D.P. Siderovski, *Ggamma-like (GGL) domains: new frontiers in G-protein signaling and beta-propeller scaffolding*. *Biochem Pharmacol*, 2001. **61**(11): p. 1329-37.
53. Pierce, K.L., R.T. Premont, and R.J. Lefkowitz, *Seven-transmembrane receptors*. *Nature Rev Mol Cell Biol*, 2002. **3**: p. 639-50.
54. Neves, S.R., P.T. Ram, and R. Iyengar, *G protein pathways*. *Science* 2002. **296**: p. 1636-9.
55. Marinissen, M.J. and J.S. Gutkind, *G-protein-coupled receptors and signaling networks: emerging paradigms*. *Trends Pharmacol Sci*, 2001. **22**: p. 368-76.
56. Mills, G.B. and W.H. Moolenaar, *The emerging role of lysophosphatidic acid in cancer*. *Nature Rev Cancer*, 2003. **3**: p. 582-91.

57. Dorsam, R.T. and J.S. Gutkind, *G-protein-coupled receptors and cancer*. Nat Rev Cancer, 2007. **7**(2): p. 79-94.
58. O'Brien, P.J. and M. Zatz, *Acylation of bovine rhodopsin by [3H]palmitic acid*. J Biol Chem, 1984. **259**(8): p. 5054-7.
59. Buss, J.E., S.M. Mumby, P.J. Casey, A.G. Gilman, and B.M. Sefton, *Myristoylated alpha subunits of guanine nucleotide-binding regulatory proteins*. Proc Natl Acad Sci U S A, 1987. **84**(21): p. 7493-7.
60. Sugars, J.M., S. Celtek, M. Manifava, J. Coadwell, and N.T. Ktistakis, *Fatty acylation of phospholipase D1 on cysteine residues 240 and 241 determines localization on intracellular membranes*. J Biol Chem, 1999. **274**(42): p. 30023-7.
61. Stoffel, R.H., R.R. Randall, R.T. Premont, R.J. Lefkowitz, and J. Inglese, *Palmitoylation of G protein-coupled receptor kinase, GRK6. Lipid modification diversity in the GRK family*. J Biol Chem, 1994. **269**(45): p. 27791-4.
62. Brown, D.A. and E. London, *Functions of lipid rafts in biological membranes*. Annu Rev Cell Dev Biol, 1998. **14**: p. 111-36.
63. Simons, K. and D. Toomre, *Lipid rafts and signal transduction*. Nat Rev Mol Cell Biol, 2000. **2**(3): p. 216.
64. Janosch, S., C. Nicolini, L. B., C. Peters, M. Völkert, T.L. Hazlet, E. Gratton, H. Waldmann, and R. Winter, *Partitioning of dual-lipidated peptides into membrane microdomains: lipid sorting vs peptide aggregation*. J Am Chem Soc, 2004. **126**(24): p. 7496-503.
65. Rowat, A.C., J. Brask, T. Sparrman, K.J. Jensen, G. Lindblom, and J.H. Ipsen, *Farnesylated peptides in model membranes: a biophysical investigation*. Eur Biophys J, 2004. **33**(4): p. 300-9.
66. Farazi, T.A., G. Waksman, and J.I. Gordon, *The biology and enzymology of protein N-myristoylation*. J Biol Chem, 2001. **276**(43): p. 39501-4.
67. Maurer-Stroh, S., B. Eisenhaber, and F. Eisenhaber, *N-terminal N-myristoylation of proteins: refinement of the sequence motif and its taxon-specific differences*. J Mol Biol, 2002. **317**: p. 523-40.
68. Peitzsch, R.M. and S. McLaughlin, *Binding of acylated peptides and fatty acids to phospholipid vesicles: pertinence to myristoylated proteins*. Biochemistry, 1993. **32**: p. 10436-43.
69. Galbiati, F., D. Volonte, D. Meani, G. Milligan, D.M. Lublin, M.P. Lisanti, and M. Parenti, *The dually acylated NH2-terminal domain of G_{i1}alpha is sufficient to target a green fluorescent protein reporter to caveolin-enriched plasma membrane domains. Palmitoylation of caveolin-1 is required for the recognition of dually acylated G-protein alpha subunits in vivo*. J Biol Chem, 1999. **274**: p. 5843-50.
70. Mumby, S.M., C. Kleuss, and A.G. Gilman, *Receptor regulation of G-protein palmitoylation*. Proc Natl Acad Sci U S A, 1994. **91**: p. 2800-4.
71. Mitchell, D.A., A. Vasudevan, M.E. Linder, and R.J. Deschenes, *Protein palmitoylation by a family of DHHC protein S-acyltransferases*. J Lipid Res, 2006. **47**(6): p. 1118-27.
72. Degtyarev, M.Y., A.M. Spiegel, and T.L. Jones, *Increased palmitoylation of the Gs protein alpha subunit after activation by the beta-adrenergic receptor or cholera toxin*. J Biol Chem, 1993. **268**(32): p. 23769-72.

73. Loisel, T.P., L. Adam, T.E. Hebert, and M. Bouvier, *Agonist stimulation increases the turnover rate of beta 2AR-bound palmitate and promotes receptor depalmitoylation*. *Biochemistry*, 1996. **35**(49): p. 15923-32.
74. Kleuss, C. and E. Krause, *Galpha(s) is palmitoylated at the N-terminal glycine*. *EMBO J*, 2003 **22**(4): p. 826-32.
75. Boyartchuk, V.L., M.N. Ashby, and J. Rine, *Modulation of Ras and α -factor function by carboxyl-terminal proteolysis*. *Science*, 1997. **275**: p. 1796-800.
76. Dai, Q., E. Choy, V. Chiu, J. Romano, S.R. Slivka, S.A. Steitz, S. Michaelis, and M.R. Philips, *Mammalian prenylcysteine carboxyl methyltransferase is in the endoplasmic reticulum*. *J Biol Chem*, 1998. **273**: p. 15030-4.
77. Takida, S. and P.B. Wedegaertner, *Heterotrimer formation, together with isoprenylation, is required for plasma membrane targeting of Gbetagamma*. *J Biol Chem*, 2003. **278**: p. 17284-90.
78. Evanko, D.S., M.M. Thiyagarajan, and P.B. Wedegaertner, *Interaction with Gbetagamma is required for membrane targeting and palmitoylation of Galpha(s) and Galpha(q)*. *J Biol Chem*, 2000. **275**(2): p. 1327-36.
79. Lòpez, D.J., R. Alvarez, and P.V. Escribà, *G Protein-Coupled Receptors: From Structure to Function*, ed. J. Giraldo and J.P. Pin. 2011.
80. Barceló, F., J. Prades, J.A. Encinar, S.S. Funari, O. Vögler, J.M. González-Ros, and P.V. Escribà, *Interaction of the C-terminal region of the Ggamma protein with model membranes*. *Biophys J*, 2007. **93**(7): p. 2530-41.
81. Epand, R.M., R.F. Epand, N. Ahmed, and R. Chen, *Promotion of hexagonal phase formation and lipid mixing by fatty acids with varying degrees of unsaturation*. *Chem Phys Lipids*, 1991. **57**(1): p. 75-80.
82. Funari, S.S., J. Prades, P.V. Escribà, and F. Barceló, *Farnesol and geranylgeraniol modulate the structural properties of phosphatidylethanolamine model membranes*. *Mol Membr Biol*, 2005. **22**(4): p. 303-11.
83. Yang, Q., R. Alemany, J. Casas, K. Kitajka, S.M. Lanier, and P.V. Escribà, *Influence of the Membrane Lipid Structure on Signal Processing via G Protein-Coupled Receptors*. *Mol Pharmacol*, 2005. **68**: p. 210-17.
84. Krieger, E., T. Darden, S.B. Nabuurs, A. Finkelstein, and G. Vriend, *Making optimal use of empirical energy functions: force-field parameterization in crystal space*. *Proteins*, 2004. **57**(4): p. 678-83.
85. Berendsen, H.J.C., J.P.M. Postma, W.F. van Gunsteren, A. Di Nola, and J.R. Haak, *Molecular dynamics with coupling to an external bath*. *J Phys Chem* 1984. **81**: p. 3684-9.
86. Klamt, A., *Conductor-like Screening Model for Real Solvents: A New Approach to the Quantitative Calculation of Solvation Phenomena*. *J Phys Chem*, 1995. **99**(7): p. 2224-35.
87. Stewart, J.J.P., *MOPAC: A semiempirical molecular orbital program*. *J Comput Aided Mol Des*, 1990. **4**: p. 1-103.
88. Essmann, U., L. Perera, M.L. Berkowitz, T. Darden, H. Lee, and L. Pederson, *A smooth particle mesh Ewald method*. *J Chem Phys*, 1995. **103**: p. 8577-93.
89. Kucerka, N., S. Tristram-Nagle, and J.F. Nagle, *J Membr Biol*, 2005. **208**: p. 193-202.
90. Cantor, R.S., *Lateral pressures in cell membranes: a mechanism for modulation of protein function*. *J Phys Chem*, 1997. **101**: p. 1723-5.

91. Vögler, O., J. Casas, D. Capò, T. Nagy, G. Borchert, and G.e.a. Martorell, *The Gbetagamma dimer drives the interaction of heterotrimeric Gi proteins with nonlamellar membrane structures*. J Biol Chem, 2004. **279**: p. 36540-5.
92. Melkonian, K.A., A.G. Ostermeyer, J.Z. Chen, M.G. Roth, and D.A. Brown, *Role of lipid modifications in targeting proteins to detergent-resistant membrane rafts. Many raft proteins are acylated, while few are prenylated*. J Biol Chem, 1999. **274**: p. 3910-7.
93. Moffett, S., D.A. Brown, and M.E. Linder, *Lipid-dependent targeting of G proteins into rafts*. J Biol Chem, 2000. **275**: p. 2191-8.
94. Escribà, P.V., *Membrane-lipid therapy: a new approach in molecular medicine*. Trends in Molecular Medicine, 2006. **12**(1): p. 34-43.
95. Escribà, P.V., J.M. González-Ros, F.M. Goñi, P.K. Kinnunen, L. Vigh, L. Sánchez-Magraner, A.M. Fernández, B. X., I. Horváth, and G. Barceló-Coblijn, *Membranes: a meeting point for lipids, proteins and therapies*. J Cell Mol Med, 2008. **12**(3): p. 829-75.
96. Voellmy, R. and F. Boellmann, *Chaperone regulation of the heat shock protein response*. Adv Exp Mol Biol, 2007. **594**: p. 89-99.
97. Maula, T., B. Westerlund, and J.P. Slotte, *Differential ability of cholesterol-enriched and gel phase domains to resist benzyl alcohol-induced fluidization in multilamellar lipid vesicles*. Biochim Biophys Acta, 2009. **1788**: p. 2454-61.
98. Nagy, E., Z. Balogi, I. Gombos, M. Akerfelt, A. Björkbom, G. Balogh, Z. Török, A. Maslyanko, A. Fiszler-Kierzkowska, K. Lisowska, P.J. Slotte, L. Sistonen, I. Horváth, and L. Vigh, *Hyperfluidization-coupled membrane microdomain reorganization is linked to activation of the heat shock response in a murine melanoma cell line*. Proc Natl Acad Sci U S A, 2007. **104**(19): p. 7945-50.
99. Sharp, K.A., B. Madan, E. Manas, and J.M. Vanderkooi, *Water structure changes induced by hydrophobic and polar solutes revealed by simulations and infrared spectroscopy*. J Chem Phys, 2001. **114**: p. 1791-6.
100. Van der Brink-Van der Laan, E., J.A. Killian, and B. De Kruijff, *Nonbilayer lipids affect peripheral and integral membrane proteins via changes in the lateral pressure profile*. Biochim Biophys Acta, 2004. **1666**: p. 275-88.
101. Vigh, L., P.V. Escribà, A. Sonnleitner, M. Sonnleitner, S. Piotto, M. B., I. Horváth, and J.L. Harwood, *The significance of lipid composition for membrane activity: New concepts and ways of assessing function*. Progress in Lipid Research, 2005. **44**: p. 303-44.
102. Vigh, L., Z. Torok, G. Balogh, A. Glatz, S. Piotto, and I. Horvath, *Membrane-regulated stress response: a theoretical and practical approach*. Adv Exp Med Biol, 2007. **594**: p. 114-31.
103. Cantor, R.S., *The lateral pressure profile in membranes: a physical mechanism of general anesthesia* Biochemistry, 1997. **36**: p. 2339-44.
104. Balogh, G., I. Horváth, E. Nagy, Z. Hoyk, S. Benkő, O. Bensaude, and L. Vigh, *The hyperfluidization of mammalian cell membranes acts as a signal to initiate the heat shock protein response*. FEBS J, 2005. **272**: p. 6077-86.
105. Balogh, G., M. Péter, G. Liebisch, I. Horvath, Z. Torok, E. Nagy, A. Maslyanko, S. Benko, G. Schmitz, J.L. Harwood, and L. Vigh, *Lipidomics reveals membrane lipid remodelling and release of potential lipid mediators during early stress responses in a murine melanoma cell line*. Biochim Biophys Acta, 2010. **1801**(9): p. 1036-47.

106. Vigh, L., B. Maresca, and J.L. Harwood, *Does the membrane's physical state control the expression of heat shock and other genes?* TIBS, 1998. **23**: p. 369-374.
107. Vigh, L., I. Horvath, B. Maresca, and J.L. Harwood, *Can the stress protein response be controlled by "membrane-lipid therapy"?* Trends Biochem Sci, 2007. **32**: p. 357-63.
108. Horvath, I., G. Multhoff, A. Sonnleitner, and L. Vigh, *Membrane-associated stress proteins: more than simply chaperones.* Biochim Biophys Acta, 2008. **1778**: p. 1653-64.
109. Akiyama, H., T. Hamada, Y. Nagatsuka, S. Kobayashi, Y. Hirabayashi, and K. Murakami-Murofushi, *A Possible Mechanism of Cholesteryl Glucoside Formation Involved in Heat Shock Response in the Animal Cell Membrane.* Cutologia, 2011. **76**: p. 19-25.
110. Vigh, L., N.P. Literati, I. Horvath, Z. Torok, G. Balogh, A. Glatz, E. Kovacs, I. Boros, P. Ferdinandy, B. Farkas, L. Jaszlits, A. Jednakovits, L. Koranyi, and B. Maresca, *Bimoclomol: a nontoxic, hydroxylamine derivative with stress protein-inducing activity and cytoprotective effects.* Nature Med, 1997. **3**: p. 1150-4.
111. Rinia, H.A., M.M. Snel, J.P. van der Eerden, and B. de Kruijff, *Visualizing detergent resistant domains in model membranes with atomic force microscopy.* FEBS Lett, 2001. **501**: p. 92-6.
112. Allen, M.P., D.J. Tildesley, and N.A.T.A.S.A. Division., *Computer simulation in chemical physics.* NATO ASI series. Series C, Mathematical and physical sciences. 1993, Dordrecht ; Boston: Kluwer Academic Publishers. xii, 519 p.
113. Huang, J. and G.W. Feigenson, *A microscopic interaction model of maximum solubility of cholesterol in lipid bilayers.* Biophys J, 1999. **76**(4): p. 2142-57.
114. Llado, V., A. Gutierrez, J. Martínez, J. Casas, S. Terés, M. Higuera, A. Galmés, C. Saus, J. Besalduch, X. Busquets, and P.V. Escriba, *Minerval induces apoptosis in Jurkat and other cancer cells.* J Cell Mol Med, 2010. **14**(3): p. 659-70.
115. Martínez, J., A. Gutierrez, J. Casas, V. Lladó, A. López-Bellan, J. Besalduch, A. Dopazo, and P.V. Escribá, *The repression of E2F-1 is critical for the activity of Minerval against cancer.* J Pharmacol Exp Ther, 2005. **315**(1): p. 466-74.
116. Llado, V., S. Terés, M. Higuera, R. Alvarez, M.A. Noguera-Salva, J.E. Halverc, P.V. Escriba, and X. Busquets, *Pivotal role of dihydrofolate reductase knockdown in the anticancer activity of 2-hydroxyoleic acid.* PNAS, 2009. **106**(33): p. 13754-8.
117. Barceló-Coblijn, G., M.L. Martin, R.F.M. de Almeida, M.A. Noguera-Salvà, A. Marcilla-Etxenike, F. Guardiola-Serrano, A. Lüth, B. Kleuser, J.E. Halver, and P.V. Escribá, *Sphingomyelin and sphingomyelin synthase (SMS) in the malignant transformation of glioma cells and in 2-hydroxyoleic acid therapy.* PNAS, PNAS. **108**(49): p. 19569-74.
118. Terés, S., V. Lladó, M. Higuera, G. Barceló-Coblijn, M.L. Martin, M.A. Noguera-Salvà, A. Marcilla-Etxenike, J.M. García-Verdugo, M. Soriano-Navarro, C. Saus, U. Gómez-Pinedo, X. Busquets, and P.V. Escribá, *2-Hydroxyoleate, a nontoxic membrane binding anticancer drug, induces glioma cell differentiation and autophagy.* PNAS, 2012. **109** (22): p. 8489-94.
119. Waltenberger, B., K. Wiechmann, J. Bauer, P. Markt, S.M. Noha, G. Wolber, J.M. Rollinger, O. Werz, D. Schuster, and H. Stuppner, *Pharmacophore Modeling and Virtual Screening for Novel Acidic Inhibitors of Microsomal Prostaglandin E2 Synthase-1 (mPGES-1).* J Med Chem, 2011. **54**: p. 3163-74.
120. Kiefer, J.R., J.L. Pawlitz, K.T. Moreland, R.A. Stegeman, W.F. Hood, J.K. Gierse, A.M. Stevens, D.C. Goodwin, S.W. Rowlinson, L.J. Marnett, W.C. Stallings, and R.G. Kurumbail,

- Structural insights into the stereochemistry of the cyclooxygenase reaction.* Nature, 2000. **405**(6782): p. 97-101.
121. Andersen, N.H. and C.J. Hartzell, *High Field 1H NMR Studies of Prostaglandin H2 and its Decomposition Pathways.* Biochem. Biophys. Res. Comm. , 1984. **120**: p. 512-519.
 122. Hamberg, M. and B. Samuelsson, *Detection and Isolation of an Endoperoxide Intermediate in Prostaglandin Biosynthesis.* Proc. Natl. Acad. Sci. U.S.A., 1973. **70**: p. 899-903.
 123. Funk, C.D., *Prostaglandins and Leukotrienes: Advances in Eicosonoid Biology.* Science, 2001. **294**: p. 1871-1875.
 124. Porter, N.A., *Mechanisms for the autoxidation of polyunsaturated lipids.* Acc. Chem. Res. , 1986. **19**: p. 262-268.
 125. Porter, N.A., B.A. Weber, H. Weenen, and J.A. Khan, *Autoxidation of Polyunsaturated Lipids. Factors Controlling the Stereochemistry of Product Hydroperoxides.* J. Am. Chem. Soc., 1980. **102**: p. 5597-5601.
 126. Rouzer, C.A. and L.J. Marnett, *Mechanism of Free Radical Oxygenation of Polyunsaturated Fatty Acids by Cyclooxygenases.* Chem. Rev. , 2003. **103**: p. 2239-2304.
 127. Samuelsson, B., *On the Incorporation of Oxygen in the Conversion of 8,11,14-Eicosatrienoic Acid to Prostaglandin E1.* J. Am. Chem. Soc. , 1965. **87**: p. 3011-3013.
 128. Marnett, L.J. and K.R. Maddipati, *Prostaglandin H synthase*, in *Peroxidase in Biology*, J. Everse, K.E. Everse, and M.B. Grisham, Editors. 1991, CRC Press: Boca Raton. p. 293-334.
 129. Malkowski, M.G., S.L. Ginell, W.L. Smith, and R.M. Garavito, *The Productive Conformation of Arachidonic Acid Bound to Prostaglandin Synthase.* Science 2000. **289**: p. 1933-7.
 130. Rowlinson, S.W., B.C. Crews, C.A. Lanzo, and L.J. Marnett, *The binding of arachidonic acid in the cyclooxygenase active site of mouse prostaglandin endoperoxide synthase-2 (COX-2). A putative L-shaped binding conformation utilizing the top channel region.* J Biol Chem. , 1999. **274**: p. 23305-23310.
 131. Malkowski, M.G., S.L. Ginell, W.L. Smith, and R.M. Garavito, *The Productive Conformation of Arachidonic Acid Bound to Prostaglandin Synthase.* Science 2000. **289**: p. 1933-1937.
 132. Schneider, C., W.E. Boeglin, and A.R. Brash, *Identification of Two Cyclooxygenase Active Site Residues, Leucine 384 and Glycine 526, That Control Carbon Ring Cyclization in Prostaglandin Biosynthesis.* J. Biol. Chem. , 2004. **279**: p. 4404-4414.
 133. Furse, K.E., D.A. Pratt, N.A. Porter, and T.P. Lybrand, *Molecular Dynamics Simulations of Arachidonic Acid-Derived Pentadienyl Radical Intermediate Complexes with COX-1 and COX-2: Insights into Oxygenation Regioand Stereoselectivity.* Biochemistry, 2006. **45**(10): p. 3189-3205.
 134. Schneider, C., W.E. Boeglin, J.J. Prusakiewicz, S.W. Rowlinson, L.J. Marnett, N. Samel, and A.R. Brash, *Control of prostaglandin stereochemistry at the 15-carbon by cyclooxygenases-1 and 2. A critical role for serine 530 and valine 349.* J. Biol. Chem., 2002. **277**: p. 478-485.
 135. Kiefer, J.R., J.L. Pawlitz, K.T. Moreland, R.A. Stegeman, W.F. Hood, J.K. Gierse, A.M. Stevens, D.C. Goodwin, S.W. Rowlinson, L.J. Marnett, W.C. Stallings, and R.G. Kurumbail, *Structural insights into the stereochemistry of the cyclooxygenase reaction.* Nature 2000. **405**: p. 97-101.

136. Furse, K.E., D.A. Pratt, N.A. Porter, and T.P. Lybrand, *Molecular Dynamics Simulations of Arachidonic Acid-Derived Pentadienyl Radical Intermediate Complexes with COX-1 and COX-2: Insights into Oxygenation Regioand Stereoselectivity*. *Biochemistry*, 2006. **45**(10): p. 3189-205.
137. Miyamoto, S. and P.A. Kollman, *SETTLE: an analytical version of the SHAKE and RATTLE algorithm for rigid water models*. *J.Comp.Chem.* , 1992. **13**: p. 952-962.
138. Berendsen, H.J.C., J.P.M. Postma, W.F. van Gunsteren, A. Di Nola, and J.R. Haak, *Molecular dynamics with coupling to an external bath*. *J. Chem. Phys.*, 1984. **81**: p. 3684–3689.
139. Essmann, U., L. Perera, M.L. Berkowitz, T. Darden, H. Lee, and L.G. Pedersen, *A smooth particle mesh Ewald routine*. *J. Chem. Phys.*, 1995. **103**: p. 8577-8593.
140. Blomberg, L.M., M.R.A. Blomberg, and P.E.M. Siegbahn, *A Quantum Chemical Study of the Synthesis of Prostaglandin G2 by the Cyclooxygenase Active Site in Prostaglandin Endoperoxide H Synthase 1*. *J Phys Chem B*, 2003. **107**: p. 3297-308.
141. Delley, B., *From molecules to solids with the DMol3 approach*. *J. Chem. Phys.* , 2000. **113**: p. 7756-7764.
142. McCammon, J.A., B.R. Gelin, and M. Karplus, *Dynamics of folded proteins*. *Nature*, 1977. **267**: p. 585-90.
143. Durrant, J.D. and J.A. McCammon, *Molecular dynamics simulations and drug discovery*. *BMC Biol.* **9**: p. 71.
144. Cornell, W.D., P. Cieplak, C.I. Bayly, I.R. Gould, K.M. Merz, D.M. Ferguson, D.C. Spellmeyer, T. Fox, J.W. Caldwell, and P.A. Kollman, *A second generation force field for the simulation of proteins, nucleic acids, and organic molecules*. *J Am Chem Soc*, 1995. **117**: p. 5179-97.
145. Wang, J., R.M. Wolf, J.W. Caldwell, P.A. Kollman, and D.A. Case, *Development and testing of a general amber force field*. *J Comput Chem*, 2004. **25**: p. 1157-74.
146. Brooks, B.R., R.E. Bruccoleri, B.D. Olafson, D.J. States, S. Swaminathan, and M. Karplus, *CHARMM - a program for macromolecular energy, minimization, and dynamics calculations*. *J Comput Chem*, 1983. **4**: p. 187-217.
147. Christen, M., P.H. Hünenberger, D. Bakowies, R. Baron, R. Bürgi, D.P. Geerke, T.N. Heinz, M.A. Kastenholtz, V. Kräutler, C. Oostenbrink, C. Peter, D. Trzesniak, and W.F. van Gunsteren, *The GROMOS software for biomolecular simulation: GROMOS05*. *J Comput Chem*, 2005,. **26**: p. 1719-51.
148. Kirkpatrick, S., J.C.D. Gelatt, and M.P. Vecchi, *Optimization by simulated annealing*. *Science*, 1983. **220**: p. 671-80.
149. Burt, S.K., D. Mackay, and A.T. Hagler, *Theoretical Aspects of Drug Design. Molecular Mechanics and Molecular Dynamics*, in *Computer-Aided Drug Design. Methods and Applications*. 1989, Perun, T. J., Propst, C. I., New York and Basel: Marcel Dekker Inc. p. 55-92.
150. Betts, M.J. and M.J. Sternberg, *An analysis of conformational changes on protein-protein association: implications for predictive docking*. *Protein Eng* 1999. **12**(4): p. 271-283.
151. Wodak, S.J. and J. Janin, *Computer analysis of protein-protein interactions*. *J. Mol. Biol* 1978. **124**: p. 323-342.
152. Halperin, I., B. Ma, H.J. Wolfson, and R. Nussinov, *Principles of docking: an overview of search algorithms and a guide to scoring functions*. *Proteins* 2002. **47**: p. 409-442.

153. Marti-Renom, M.A., A.C. Stuart, R. Sanchez, A. Fiser, F. Melo, and A. Sali, *Comparative protein structure modeling of genes and genomes*. Annu Rev Biophys Biomol Struct, 2000. **29**: p. 291-325.
154. Soto, C.S., M. Fasnacht, J. Zhu, L. Forrest, and B. Honig, *Loop modeling: sampling, filtering, and scoring*. Proteins, 2007. **70**: p. 834-843
155. Grunberg, R., J. Leckner, and M. Nilges, *Complementarity of structure ensembles in protein-protein binding*. Structure, 2004. **12**(12): p. 2125-36.
156. Zeev-Ben-Mordehai, T. and I. Silman, Sussman, J.L., *Acetylcholinesterase in motion: visualizing conformational changes in crystal structures by a morphing procedure*. Biopolymers 2003. **68**(3): p. 395-406.
157. Franklin, J., P. Koehl, S. Doniach, and M. Delarue, *MinActionPath: maximum likelihood trajectory for large-scale structural transitions in a coarse-grained locally harmonic energy landscape*. Nucleic Acids Res 2007. **35**(Web Server issue): p. W477-W482.
158. Parr, R.G., *Density functional theory*. Annu Rev Phys Chem, 1983. **34**: p. 631-56.
159. Pearson, R.G., *Hard and Soft Acids and Bases*. J Am Chem Soc, 1963. **85**: p. 3533-9.
160. Pearson, R.G., *Acids and Bases*. Science, 1966. **151**: p. 172-7.
161. Parr, R.G. and W. Yang, *Density functional approach to the frontier-electron theory of chemical reactivity*. J Am Chem Soc, 1984. **106**: p. 4049-50.
162. Yang, W.T., R.G. Parr, and R. Pucci, *Electron Density, Kohn-Sham Frontier Orbitals, and Fukui Functions*. J Chem Phys, 1984. **81**: p. 2862.
163. Berkowitz, M., *Density Functional Frontier Controlled Reactions*. J Am Chem Soc, 1987. **109**: p. 4823-5.
164. Fukui, K., *Recognition of stereochemical paths by orbital interaction*. Acc Chem Res, 1971. **4**: p. 57-64.
165. Méndez, F., M. Galván, A. Garritz, A. Vela, and J. Gàzquez, *Local softness and chemical reactivity of maleimide: nucleophilic addition*. Journal of Molecular Structure: THEOCHEM, 1992. **277**: p. 81-6.
166. Yang, W.T. and W.J. Mortier, *The use of global and local molecular parameters for the analysis of the gas-phase basicity of amines*. J Am Chem Soc, 1986. **108**: p. 5708.
167. Ayers, P.W., F. De Proft, A. Borgoo, and P. Geerlings, *Computing the Fukui Function Without Differentiation with Respect to Particle Number. I. Basic Theory*. J Chem Phys, 2007. **126**: p. 224107.
168. Michalak, A., F. De Proft, P. Geerlings, and R.F. Nalewajski, *Fukui Functions from the Relaxed Kohn-Sham Orbitals*. J Phys Chem A 1999. **103**(6): p. 762-71.
169. Melin, J., P.W. Ayers, and J.V. Ortiz, *J Chem Sci*. The electron-propagator approach to conceptual density-functional theory, 2005. **117**: p. 387.
170. Ohrn, Y. and G. Born, *Molecular electron propagator theory and calculations*. Adv Quantum Chem, 1981. **13**: p. 1-88.
171. Ayers, P.W. and J. Melin, *Computing the Fukui Function from Ab Initio Quantum Chemistry: Approaches Based on the Extended Koopmans Theorem*. Theor Chem Acc, 2007. **117**: p. 371-81.
172. Day, O.W., D.W. Smith, and R.C. Morrison, *Extension of Koopmans' theorem. II. Accurate ionization energies from correlated wavefunctions for closed-shell atoms*. J Chem Phys, 1975. **62**: p. 115.

173. Ellenbogen, J.C., O.W. Day, D.W. Smith, and R.C. Morrison, *Extension of Koopmans' theorem. IV. Ionization potentials from correlated wavefunctions for molecular fluorine*. J Chem Phys, 1977. **66**: p. 4795.
174. Morrell, M.M., R.G. Parr, and M. Levy, *Calculation of ionization potentials from density matrices and natural functions, and the long-range behavior of natural orbitals and electron density*. J Chem Phys, 1975. **62**: p. 549.
175. Smith, D.W. and O.W. Day, *Extension of Koopmans' theorem. I. Derivation*. J Chem Phys, 1975. **62**: p. 113.
176. Ayers, P.W. and R.G. Parr, *Variational Principles for Describing Chemical Reactions: The Fukui Function and Chemical Hardness Revisited*. J Am Chem Soc, 2000. **122**(9): p. 2010-8.
177. Chattaraj, P.K., A. Cedillo, and R.G. Parr, *Variational method for determining the Fukui function and chemical hardness of an electronic system*. J Chem Phys, 1995. **103**: p. 7645.